



**NLTERT – A Collisional-Radiative
Code for Computing the Radiative
Properties of Non-LTE Plasmas**

J.J. MacFarlane

August 1997

UWFDM-1050

FUSION TECHNOLOGY INSTITUTE

UNIVERSITY OF WISCONSIN

MADISON WISCONSIN

**NLTERT – A Collisional-Radiative Code for Computing
the Radiative Properties of Non-LTE Plasmas**

J. J. MacFarlane

Fusion Technology Institute
University of Wisconsin-Madison
1500 Engineering Drive
Madison, WI 53706

August 1997

UWFDM-1050

Contents

1. Introduction	1.1
2. Statistical Equilibrium Model	2.1
3. Time-Dependent Collisional-Radiative Model	3.1
4. Radiative Transfer Models	4.1
4.1. Escape Probability Model	4.1
4.2. Multifrequency, Multiangle Feautrier Radiative Transfer Model	4.10
4.3. Multifrequency, Multiangle Method of Short Characteristics	4.13
5. Atomic Physics Models	5.1
5.1. ATBASE Models	5.1
5.2. High-Z UTA Multigroup Opacities	5.1
5.3. Occupation Probability Continuum Lowering Model	5.2
6. Input/Output File Descriptions	6.1
7. Namelist Input Variables	7.1
8. Subroutines	8.1
9. Common Blocks	9.1
10. Sample Calculations	10.1
10.1. Example 1: Thermal Spectrum for Aluminum	10.1
10.2. Example 2: 2-Level Atom	10.1
10.3. Example 3: K_{α} Absorption Spectrum for Aluminum	10.1
10.4. Example 4: Time-Dependent Carbon Recombination	10.2
10.5. Example 5: Time-Dependent Argon Plasma With Hot Electrons	10.2

10.6. Example 6: A SiO₂ Cylindrical Plasma Surrounded by Tungsten 10.2

10.7. Example 7: Al K_α Satellite Emission and Absorption Spectra Based on
Radiation-Hydrodynamics Output 10.3

References **11.1**

1. Introduction

Emission and absorption spectroscopy are often used to determine the physical conditions of laboratory and astrophysical plasmas. Absorption spectroscopy has been utilized in determining plasma temperatures and densities, as well as measure opacities, in laser-produced plasma experiments [1-9]. Emission spectroscopy is often used to deduce plasma conditions in Z-pinch plasmas, laser-produced plasmas, and imploding inertial confinement fusion (ICF) targets [10-14]. In plasmas heated by intense light ion beams, x-ray emission lines arising from inner-shell transitions can be used to diagnose plasma conditions [15-19]. Proper interpretation of experimental spectra often requires detailed radiative and atomic physics models.

In this document, we describe the features of NLTERT — a code we have developed to investigate the radiative properties of high energy density plasmas. This is a non-LTE (LTE = local thermodynamic equilibrium) radiative transfer code, or collisional-radiative (C-R) code, which can be used to calculate emission and absorption spectra, including the effects radiative transport. The major features of the physics models have been described elsewhere [20-23], and only a brief overview of the models will be presented here. This report is intended to be a “users’ guide.” Thus, the focus here will be on the structure of the code and how to use it. A users’ guide for the atomic physics package which sets up atomic data files for NLTERT has been presented elsewhere [24].

Given a temperature and density distribution for a plasma, NLTERT computes atomic level populations and resultant spectra for single- or multi-component plasmas. The models are 1-D, and work for planar, cylindrical, and spherical geometries. Opacity effects are considered in computing both the atomic level populations (via photoexcitation and photoionization) and the spectra. In addition, hot electron and ion beam-induced ionization and excitation are considered in the atomic rate equations. This allows for the analysis of spectra obtained in intense light ion beam experiments.

This document is an update of the NLTERT Users Guide written in December 1993. Since that time, several modifications have been made to the code. These include:

- An option to perform time-dependent collisional-radiative modeling. The earlier version of NLTERT included a collisional-radiative equilibrium (CRE) model; thus, the atomic level populations were determined using a steady-state solution of the atomic rate equations.

- A continuum lowering model has been added based on the occupation probability model of Hummer and Mihalas [25,26].
- An algorithm for solving the radiative transfer equation based on the method of short characteristics [27] has been added. This can be used for both computing resultant spectra and computing photoexcitation and photoionization rates.
- A option has been added for including the effects of high-Z materials on photoexcitation and photoionization rates. In this model, multigroup UTA (unresolved transition array) opacities [28,29] are utilized for high-Z regions.
- An option has been added to model non-Maxwellian electron distributions.

Sections 2 through 5 of this report provide brief descriptions of the statistical equilibrium, time-dependent collisional-radiative, radiative transfer, and atomic physics models. Input and output files are described in Section 6, while the namelist input used to set up a calculation is detailed in Section 7. The subroutines and common block descriptions are provided in Sections 8 and 9, respectively. Finally, a series of sample calculations is shown in Section 10.

2. Statistical Equilibrium Model

In the collisional-radiative equilibrium (CRE model), atomic level populations are calculated by solving multilevel, steady-state atomic rate equations self-consistently with the radiation field. For multilevel systems, the rate equation for atomic level i can be written as:

$$\frac{dn_i}{dt} = -n_i \sum_{j \neq i}^{N_L} W_{ij} + \sum_{j \neq i}^{N_L} n_j W_{ji} = 0, \quad (2.1)$$

where W_{ij} and W_{ji} represent the depopulating and populating rates between levels i and j , n_i is the number density of level i , and N_L is the total number of levels in the system. For upward transitions ($i < j$),

$$\begin{aligned} W_{ij} = & B_{ij} \bar{J}_{ij} + n_e C_{ij} + H_{ij}^{\text{hot}} \\ & + \beta_{ij} + n_e \gamma_{ij} + \Gamma_{ij}^{\text{hot}} + \mathcal{R}_{ij}, \end{aligned} \quad (2.2)$$

while for downward transitions,

$$\begin{aligned} W_{ji} = & A_{ji} + B_{ji} \bar{J}_{ji} + n_e D_{ji} + K_{ij}^{\text{hot}} \\ & + n_e (\alpha_{ji}^{RR} + \alpha_{ji}^{DR}) + n_e^2 \delta_{ji} + \Delta_{ij}^{\text{hot}} + \Omega_{ji}, \end{aligned} \quad (2.3)$$

where n_e is the electron density and \bar{J}_{ij} ($\equiv \int \phi_{ij}(\nu) J_\nu d\nu$) is the frequency-averaged mean intensity of the radiation field for a bound-bound transition. The rate coefficients in the above equations are:

- A_{ij} = spontaneous emission
- B_{ij} = stimulated absorption ($i < j$) or emission ($i > j$)
- C_{ij} = collisional excitation due to thermal electrons
- D_{ij} = collisional deexcitation due to thermal electrons
- H_{ij}^{hot} = collisional excitation rate due to hot electrons
- K_{ij}^{hot} = collisional deexcitation rate due to hot electrons
- α_{ij}^{RR} = radiative recombination
- α_{ij}^{DR} = dielectronic recombination
- β_{ij} = photoionization plus stimulated recombination (defined in Sec. 4)
- γ_{ij} = collisional ionization

$$\begin{aligned}
\delta_{ij} &= \text{collisional recombination} \\
\Gamma_{ij}^{\text{hot}} &= \text{collisional ionization rate due to hot electrons} \\
\Delta_{ij}^{\text{hot}} &= \text{collisional recombination rate due to hot electrons} \\
\mathcal{R}_{ij} &= \text{ion beam impact ionization and excitation} \\
\Omega_{ij} &= \text{autoionization.}
\end{aligned}$$

Atomic cross sections for the above terms are described briefly in Section 5. The last two terms, \mathcal{R}_{ij} and Ω_{ij} , are relevant for problems involving inner-shell ionization by intense ion beams. The ion beam-impact ionization rate coefficient can be written as:

$$\mathcal{R}_{ij} = J_B \sigma_{S,ij}(E_B),$$

where J_B is the ion beam current density, E_B is the beam energy (per particle), and $\sigma_S(E_B)$ is the ion-impact ionization cross section for ejecting an electron out of subshell S . The autoionization rate coefficient out of autoionizing level i is:

$$\Omega_{ij} = \left(\frac{1 - Y_i}{Y_i} \right) \sum_{j'} A_{ij'},$$

where A_{ij} is the spontaneous emission rate and Y_i is the fluorescence yield. NLTERT uses energy level-dependent ion-impact ionization cross sections and autoionization rates (fluorescence yields) calculated by ATBASE [24]. Thus, it is not necessary to rely on configuration- or ion-averaged values as was done in early studies using NLTERT.

In this detailed configuration accounting model each atomic level of a given gas species can in principle be coupled to any other level in that gas. This allows for modelling plasmas in which multiple ionization processes are important (such as non-protonic ion beams or Auger ionization due to x-rays). The degree of coupling between levels depends on how the atomic data files are generated by ATBASE.

The statistical equilibrium equations (Eq. (2.1)) depend on the atomic level populations in a nonlinear fashion (through the radiation intensity and electron density). Because of this, an iterative procedure is used to obtain atomic level populations which are self-consistent with the radiation field. The coupled set of steady-state rate equations is solved using the LAPACK linear algebra package [30]. Besides inverting the statistical equilibrium equation matrix to obtain the level populations, LAPACK also contains algorithms for improving the condition of the matrix via scaling, as well as iterative refinement. The overall procedures for computing the level populations is as follows:

1. Make an initial guess for population distributions (e.g., LTE or optically thin plasma)
2. Compute radiative rate coefficients
3. Compute coefficients for statistical equilibrium matrix ($N_L \times N_L$)
4. Solve matrix for level populations
5. If new populations are consistent with previous iteration, calculation is complete; otherwise go back to step 2.

Steps 2 through 4 are performed one spatial zone at a time. This is possible because we employ an accelerated lambda iteration procedure (ALI) which utilizes the diagonal of the Λ -operator [31,32; see also Section 4].

To improve the rate of convergence for this iterative procedure we utilize an acceleration technique based on the work of Ng [33; see also 34,32]. The Ng acceleration method is applied every several (typically 2 to 6) iterations to obtain updated solutions to the solution vector \mathbf{x} . In our case, the solution vector is the level population of a spatial zone. The “accelerated” solution is calculated from solutions obtained during the previous several iterations — that is, the evolution, or history, of the convergence becomes important. The accelerated solution vector after the n 'th iteration can be written as:

$$\mathbf{x}^n = \left(1 - \sum_{m=1}^M \alpha_m\right) \mathbf{x}^{n-1} + \sum_{m=1}^M \alpha_m \mathbf{x}^{n-m-1}, \quad (2.4)$$

where \mathbf{x}^{m-n} is the solution vector of the $(n-m)$ 'th iteration. The acceleration coefficients, α , are determined from the solution

$$\mathbf{A}\alpha = \mathbf{b}, \quad (2.5)$$

where the elements of \mathbf{A} and \mathbf{b} are given by:

$$\begin{aligned} A_{ij} &= \sum_{d=1}^D (\Delta x_d^n - \Delta x_d^{n-i})(\Delta x_d^n - \Delta x_d^{n-j}), \\ b_i &= \sum_{d=1}^D \Delta x_d^n (\Delta x_d^n - \Delta x_d^{n-i}), \end{aligned} \quad (2.6)$$

and

$$\Delta x_d^k \equiv x_d^k - x_d^{k-i}.$$

The quantity x_d^k refers to the d 'th element of \mathbf{x} on iteration cycle k . The order of the acceleration method, M , represents the number of previous cycles used to compute the accelerated solution for \mathbf{x} .

In our radiative transfer code M can be chosen to have a value from 2 to 4. It is found that using $M = 2$ provides very good acceleration to the converged solution. This method has proven to be particularly valuable in improving the computational efficiency of our radiative transfer simulations.

3. Time-Dependent Collisional-Radiative Model

In the time-dependent collisional-radiative (C-R) model, atomic level populations are determined from the solution of multilevel atomic rate equations of the form:

$$\frac{dn_i}{dt} = -n_i \sum_{j \neq i}^{M_L} W_{ij} + \sum_{j \neq i}^{M_L} n_j W_{ji}. \quad (3.1)$$

Note that this has the same as Eq. (2.1), except that the assumption of steady-state ($\frac{dn_i}{dt} = 0$) is not made. The atomic processes which contribute to the populating (W_{ji}) and depopulating (W_{ij}) rates are the same as those described in Section 2.

In the time-dependent C-R calculation, the user must specify the initial populations and the time-dependent plasma conditions. This procedure is illustrated by example in Section 10.

In practice, after the populating and depopulating rates are calculated, the atomic level populations (n_i) are computed using the LSODE [35] ordinary differential equation solver. The user has the ability to specify the simulation time grid, as well as the relative and absolute tolerances used by LSODE. Example calculations are given in Section 10.

4. Radiative Transfer Models

NLTERT utilizes several radiative transfer models: (1) an angle- and frequency-averaged escape probability model [36-38]; (2) a multiangle, multifrequency model based on the second order form of the radiative transfer equation (Feautrier method) [39]; and (3) a multiangle, multifrequency integral (short characteristics) model [27]. The advantage of the escape probability model is that it is faster. This is especially true in spherical geometry, where the multiangle methods solve the radiative transfer equation along a large number of impact parameters (approximately equal to the number of spatial zones). The advantage of the multiangle methods is accuracy. In addition, the Feautrier method is second order accurate, while the escape probability model assumes the source function — and thereby the atomic level populations — are uniform throughout each spatial zone (this is sometimes referred to as the “flat flux approximation”). Also, because it utilizes a multifrequency grid for each bound-bound transition, the multiangle, multifrequency methods can more accurately treat line transport in problems with a significant background continuum. Below we describe each model separately.

4.1. Escape Probability Model

In the escape probability model, the stimulated absorption and emission rates in Eqs. (2.2) and (2.3) can be written in terms of zone-to-zone coupling coefficients:

$$n_j^a B_{ji} \bar{J}_{ij} - n_i^a B_{ij} \bar{J}_{ij} = \begin{cases} -A_{ji} \sum_{e=1}^{N_D} n_j^e Q_{ji}^{ea} & (i < j) \\ A_{ij} \sum_{e=1}^{N_D} n_i^e Q_{ij}^{ea} & (i > j) \end{cases}$$

where Q^{ea} is defined as the probability a photon emitted in zone e is absorbed in zone a , n_i is the population density of level i , the superscripts e and a denote the emitting and absorbing zones, respectively, and N_D is the number of spatial zones. Our model utilizes a computationally efficient method for computing angle- and frequency-averaged escape probability coupling coefficients in planar, cylindrical, and spherical geometries for Doppler, Lorentz, and Voigt line profiles. (This method is based largely on the work of J. Apruzese et al. [36-38].)

Consider first the 1-D planar geometry shown in Fig. 4.1. The distance traversed as a photon travels from point 1 to point 2 is z_{12}/μ , where $\mu \equiv \cos \theta$ and θ is the angle between the direction of propagation and the normal to the slab surface. In this geometry, the angle- and frequency-averaged escape probability, \bar{P}_e , can be computed directly:

$$\bar{P}_e(\tau_c) = \int_0^1 P_e(\tau_c/\mu) d\mu, \quad (4.1)$$

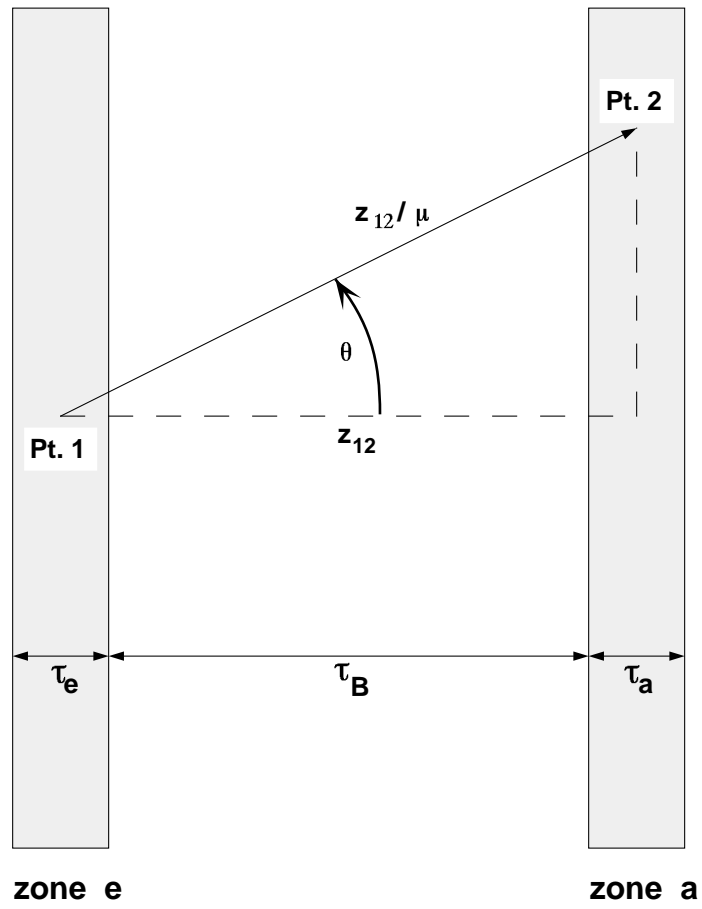


Figure 4.1. Schematic illustration of photon transport in planar geometry.

where P_e is the frequency-averaged escape probability (described below). The probability a photon emitted in zone e traverses a depth τ_B between zones e and a , and is then absorbed in zone a is

$$Q^{ea} = \frac{1}{2\tau_e} \int_0^{\tau_e} [\bar{P}_e(\tau_B + \tau) - \bar{P}_e(\tau_B + \tau_a + \tau)] d\tau. \quad (4.2)$$

Note that τ_e, τ_B , and τ_a are the optical depths in the direction normal to the slab surface. The first term within the integral represents the probability a photon will get to the nearer surface of zone a without being absorbed, while the second term represents the probability the photon is absorbed before exiting the surface farther from zone e . The coupling coefficients are efficiently computed using analytic expressions.

Evaluation of the coupling coefficients in cylindrical and spherical geometries is more difficult because Eq. (4.1) is not valid and angle-averaged escape probabilities cannot be computed directly. For these geometries, it was found [37] that introducing a “mean diffusivity angle,” $\bar{\theta} \equiv \cos^{-1} \bar{\mu}$, for which

$$P_e\left(\frac{\tau}{\bar{\mu}}\right) \cong \int_0^1 P_e\left(\frac{\tau}{\mu}\right) d\mu, \quad (4.3)$$

leads to solutions that compare reasonably well with exact solutions. The meaning of the mean diffusivity angle is clarified in Fig. 4.2. The quantities τ_e, τ_a , and τ_B again represent the line center optical depths of the emitting and absorbing zones and the depth between them, respectively. In this case, however, the optical depths are computed along the ray defined by $\bar{\theta}$ and the midpoint of the emitting zone.

It can also be seen from Fig. 4.2 that additional geometrical complications arise when the absorbing zone is inside the emitting zone. To overcome this, while at the same time maintaining computational efficiency, we take advantage of the reciprocity relation:

$$N^i Q^{ij} = N^j Q^{ji}, \quad (4.4)$$

where N^i and N^j are the total number of absorbing atoms in zones i and j , respectively. (A proof of this relation is given in Ref. [37].) Thus, in cylindrical and spherical geometries the coupling coefficients are given by:

$$Q^{ea} = \frac{1}{\tau_e} \int_0^{\tau_e} [P_e(\tau_B + \tau) - P_e(\tau_B + \tau_a + \tau)] d\tau, \quad (4.5)$$

where P_e is the non-angle-averaged escape probability. The Q^{ea} are calculated using Eq. (4.5) only for the cases when the absorbing zone is at a larger radius than the emitting zone. Otherwise, the reciprocity relation (Eq. (4.4)) is used. It has been shown

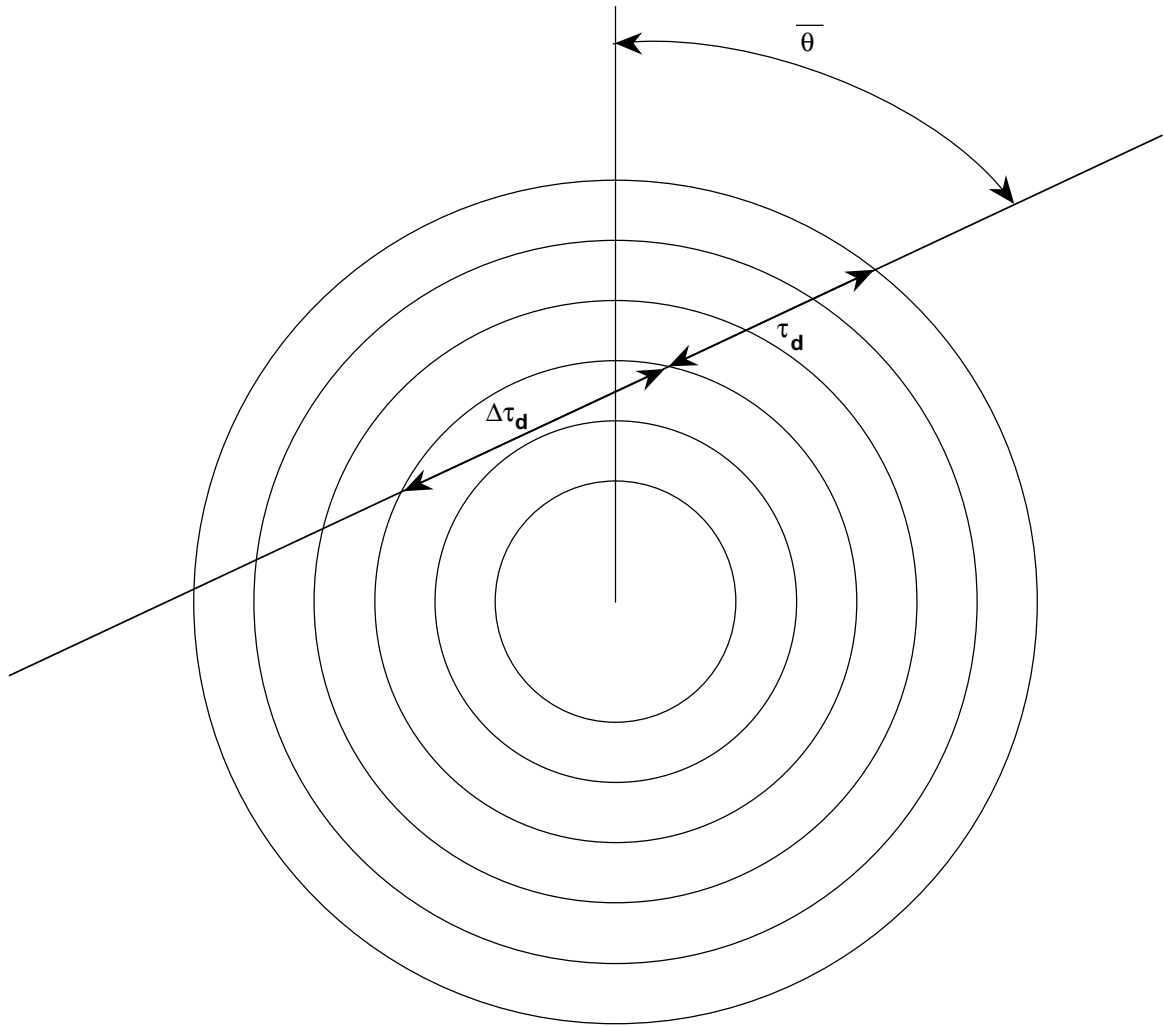


Figure 4.2. Schematic illustration of photon transport in cylindrical and spherical geometries.

[25] that using $\bar{\mu} = 0.51$ leads to solutions for 2-level atoms that are accurate to within 25% for a wide range of total optical depths.

The frequency-averaged probability a photon will traverse a distance equivalent to a line center optical depth τ_c is:

$$P_e(\tau_c) = \int_0^\infty \phi(\nu) e^{-\tau_\nu} d\nu, \quad (4.6)$$

where $\phi(\nu)$ is the normalized line profile ($\int \phi(\nu) d\nu = 1$), and

$$\tau_\nu = \tau_c \phi(\nu) / \phi(\nu_0).$$

The quantity ν_0 represents the frequency at line center.

The profiles considered for bound-bound transitions are:

$$\begin{aligned} \text{Doppler : } \phi(\nu) &= (\pi^{1/2} \Delta\nu_D)^{-1} e^{-x_D^2}, & x_D &= \frac{\nu - \nu_0}{\Delta\nu_D} \\ \text{Lorentz : } \phi(\nu) &= \frac{4}{\Gamma} \frac{1}{1+x_L^2}, & x_L &= \frac{4\pi}{\Gamma} (\nu - \nu_0) \\ \text{Voigt : } \phi(\nu) &= (\pi^{1/2} \Delta\nu_D)^{-1} H(a, x_D), & a &= \frac{\Gamma}{4\pi\Delta\nu_D}. \end{aligned} \quad (4.7)$$

The parameter Γ can be interpreted as the reciprocal of the mean lifetimes of the upper and lower states, $\Delta\nu_D$ is the Doppler width of the line, and

$$H(a, x_D) = \frac{a}{\pi} \int_{-\infty}^{\infty} \frac{e^{-y^2}}{(x_D - y)^2 + a^2} dy \quad (4.8)$$

is the Voigt function[39].

In evaluating the escape probability integrals we use an approach similar to that of Apruzese et al. Simple analytic fits to accurate numerical solutions to the frequency-averaged escape probabilities were obtained for each profile. For bound-bound transitions, complete frequency redistribution is assumed; i.e., the emission and absorption profiles are identical.

For Doppler profiles we use:

$$P_e(\tau_c) = \begin{cases} 2.329 [\tan^{-1}(0.675 \tau_c + 0.757) - \tan^{-1}(0.757)], & \tau_c \leq 5.18 \\ 0.209 + 1.094 [\ln \tau_c]^{1/2}, & \tau_c > 5.18, \end{cases} \quad (4.9)$$

while for Lorentz profiles we use:

$$P_e(\tau_c) = \begin{cases} 1.707 \ln(1 + 0.586 \tau_c), & \tau_c \leq 5.18 \\ -0.187 + 1.128 \tau_c^{1/2}, & \tau_c > 5.18. \end{cases} \quad (4.10)$$

For Voigt profiles, the escape probability integrals were fitted to two different regimes of the Voigt broadening parameter a . For $a < 0.49$,

$$P_e(\tau) = \begin{cases} (1 + 1.5 \tau)^{-1} & (\tau \leq 1), \\ 0.4 \tau^{-1} & (1 < \tau \leq \tau_c), \\ 0.4 (\tau_c \tau)^{-1/2} & (\tau > \tau_c), \end{cases} \quad (4.11)$$

where

$$\tau_c \equiv \frac{0.83}{a(1 + a^{1/2})}.$$

For $a \geq 0.49$,

$$P_e(\tau) = \begin{cases} (1 + \tau)^{-1} & (\tau \leq 1), \\ 0.5 \tau^{-1/2} & (\tau > 1). \end{cases} \quad (4.12)$$

The fits for Voigt profiles are typically accurate to about 20%, although errors of up to 40% can occur. Note, however, that in our model the frequency-averaged escape probability integrals are used only to compute the level populations self-consistently with the radiation field. The frequency-dependent spectral calculations do not directly use frequency-averaged escape probabilities.

We now discuss the transport of bound-free radiation in the context of the escape probability model. The frequency-averaged escape probability is obtained by averaging the attenuation factor, $e^{-\tau\nu}$, over the emission profile ϕ_E :

$$P_e(\tau_0, \alpha_0) = \int_{\nu_1}^{\infty} \phi_E(\nu, \alpha_0) \exp(-\tau\nu) d\nu, \quad (4.13)$$

where

$$\phi_E(\nu, \alpha_0) = \frac{\exp(-h\nu/kT_e)}{\nu E_1(\alpha_0)}$$

and

$$\alpha_0 \equiv h\nu_1/kT_e.$$

The optical depth and frequency at the photoionization edge are τ_0 and ν_1 , respectively, τ_ν is the optical depth at frequency ν , T_e is the electron temperature, and $E_1(x)$ represents the exponential integral of order 1. The quantities h and k as usual refer to the Planck constant and Boltzmann constant, respectively.

As in the case of line transport, frequency-averaged escape probabilities have been fitted to simple analytic functions to allow for computationally efficient solutions. The curve fits are given by:

$$P_e(\tau_0, \alpha_0) = \begin{cases} e^{-\gamma_1 t} & , \quad t \leq 1.0 \\ t^{-1/3} \exp[-\gamma_1 - \gamma_2(t^{1/3} - 1)] & , \quad t > 1.0 \end{cases} \quad (4.14)$$

where

$$\begin{aligned} \gamma_1(\alpha_0) &= 2.01 \alpha_0 - 1.23 \alpha_0^{3/2} + 0.210 \alpha_0^2, \\ \gamma_2(\alpha_0) &= 1.01 \alpha_0 + 0.0691 \alpha_0^{3/2} - 0.0462 \alpha_0^2, \end{aligned}$$

and $t \equiv \tau_0/3$. The fits are accurate to about 15% over a wide range of parameter space: $0.3 < \alpha_0 < 10$ and values of τ_0 such that $P_e(\tau_0, \alpha_0) \geq 10^{-5}$.

The photoionization rate in zone a is obtained by summing the recombinations over all emitting zones e . Thus, the photoionization rate (corrected for stimulated recombinations) from lower level ℓ to upper level u can be written as:

$$\begin{aligned} \beta_{\ell u} &= 4\pi \int_{\nu_0}^{\infty} \frac{\alpha_\nu^{bf}}{h\nu} J_\nu^a \left(1 - \left(\frac{n_u^a}{n_\ell^a} \right) \left(\frac{n_\ell^a}{n_u^a} \right)^* e^{-h\nu/kT_e} \right) d\nu \\ &= \sum_{e=1}^{N_D} N_u^e n_e^e \alpha_{rr}^e Q^{ea}, \end{aligned} \quad (4.15)$$

where α_ν^{bf} is the photoionization cross section, J_ν is the radiation mean intensity, $(n_\ell/n_u)^*$ refers to the LTE population ratio [39], α_{rr}^e is the radiative recombination rate coefficient for zone e , n_e^e is the electron density in zone e , and N_D is the total number of spatial zones in the plasma.

Frequency-dependent spectra are computed in the escape probability model as follows. We first compute the opacities and optical depths in each spatial zone from all possible sources and consider the contributions from free-free (Bremsstrahlung),

bound-free (photoabsorption), and bound-bound (line) transitions. The optical depth at frequency ν in zone d , is related to the opacity by:

$$\begin{aligned}\tau_{\nu,d} &= \int_{z_{min}}^{z_{max}} \chi_{\nu}(z) dz \\ &= \chi_{\nu,d} \Delta z_d,\end{aligned}\tag{4.16}$$

where the opacity in zone d , $\chi_{\nu,d}$, is assumed to be constant throughout the zone, and Δz_d is the zone thickness. The opacity can be written as [39]:

$$\begin{aligned}\chi_{\nu} &= \sum_j n_e n_{j+1} (1 - e^{h\nu/kT}) \alpha^{ff}(\nu) \\ &+ \sum_j \sum_n [n_{nj} - n_{nj}^* e^{-h\nu/kT}] \alpha_n^{bf}(\nu) \\ &+ \sum_j \sum_n \sum_{m>n} \left[n_{nj} - \left(\frac{g_{nj}}{g_{mj}} \right) n_{mj} \right] \alpha_{mn}^{bb}(\nu),\end{aligned}\tag{4.17}$$

where the index j refers to the ionization stage, n and m refer to the excitation levels, g_{nj} and g_{mj} are the statistical weights, n_{nj} is the number density of atoms in level n of ionization stage j , and n_{j+1} is the number density of atoms in ionization stage $j + 1$ summed over all excitation levels. The quantity n_{nj}^* is the LTE population of state n_{nj} computed using the actual ion density of the upper ionization stage. The first term in Eq. (4.17) is the contribution from free-free absorption, the second is from bound-free absorption, and the third is due to bound-bound absorption. The free-free cross section is given by

$$\alpha^{ff}(\nu) = \left(\frac{4e^6}{3ch} \right) \left(\frac{3\pi}{3km_e} \right)^{1/2} \overline{g}_{ff} Z_{eff}^2 T^{-1/2} \nu^{-3},\tag{4.18}$$

where e and m_e are the electron charge and mass, respectively, c is the speed of light, \overline{g}_{ff} is the free-free Gaunt factor [40], and Z_{eff} is the effective charge.

The bound-free cross section has the form:

$$\alpha^{bf}(\nu) = \alpha^{bf}(\nu_1) \left\{ \beta \left(\frac{\nu_1}{\nu} \right)^s + (1 - \beta) \left(\frac{\nu_1}{\nu} \right)^{s+1} \right\}, \quad \nu \geq \nu_1,\tag{4.19}$$

where ν_1 is the cutoff frequency, and β , s , and $\alpha^{bf}(\nu_1)$ are obtained by fitting to Hartree-Fock cross section for electrons in each subshell of each atomic level. The bound-bound cross section is given by

$$\alpha^{bb}(\nu) = \left(\frac{\pi e^2}{m_e c} \right) f_{nm} \phi_\nu, \quad (4.20)$$

where f_{nm} is the oscillator strength and ϕ_ν is the normalized line profile ($\int \phi_\nu d\nu = 1$).

After the total optical depth for each spatial zone is calculated, the frequency-dependent flux at the plasma boundary is computed as follows. The flux at the surface due to photons emitted in zone d , $F_{\nu,d}$, can be written in terms of the plasma emissivity of the zone, $\eta_{\nu,d}$:

$$F_{\nu,d} = \frac{4\pi\eta_{\nu,d}\Delta V_d}{A} \mathcal{A}_{\nu,d}, \quad (4.21)$$

where ΔV_d is the volume of zone d , and A is the area of the plasma boundary. The attenuation factor, $\mathcal{A}_{\nu,d}$, represents the attenuation due to all other zones along the path to the boundary. The path from the emitting zone to the boundary is defined by the mean diffusivity angle. The optical depths for each zone are computed along this path. The attenuation factor is then obtained by averaging over the emitting zone:

$$\mathcal{A}_{\nu,d} = \frac{1}{\Delta\tau_{\nu,d}} \int_{\tau_{\nu,d}}^{\tau_{\nu,d}+\Delta\tau_{\nu,d}} e^{-\tau_\nu} d\tau_\nu. \quad (4.22)$$

where τ_d is the optical depth from the plasma boundary to the closer boundary of zone d . The emissivity can be written as [39]:

$$\begin{aligned} \eta_\nu = & \left(\frac{2h\nu^3}{c^2} \right) \sum_j \left\{ n_e n_{j+1} e^{-h\nu/kT} \alpha^{ff}(\nu) \right. \\ & + \sum_n n_{nj}^* e^{-h\nu/kT} \alpha_n^{bf}(\nu) \\ & \left. + \sum_n \sum_{m>n} \left(\frac{g_{nj}}{g_{mj}} \right) n_{mj} \alpha_{mn}^{bb}(\nu) \right\}. \end{aligned} \quad (4.23)$$

Note that the radiation produced by one type of transition can be significantly attenuated by other types of transitions. For instance, continuum emission can decrease abruptly near the cores of optically thick lines and photoabsorption edges. We note,

however, that this interaction of the radiation field for different transitions is not fully accounted for when calculating the level populations. We do not expect this to be a serious deficiency in the model for many types of plasma diagnostics.

4.2. Multifrequency, Multiangle Feautrier Radiative Transfer Model

An alternative approach for computing radiative transfer in NLTE is a multifrequency, multiangle model based on the second order form of the transfer equation. The model, which has been developed for planar and spherical geometries, is more accurate and can better model a wider class of problems (e.g., line transport in the presence of a significant continuum background, or large density and/or temperature gradients). The trade-off is of course that the required computational time is greater. This is particularly true in the case of spherical geometry, where the tangent ray method employed requires that the number of angles for which the radiative transfer equation is solved is comparable to the number of spatial grid points.

The second order form of the radiative transfer equation in planar geometry can be written as [39]:

$$\mu^2 \frac{\partial^2 u_{\mu\nu}}{\partial \tau_\nu^2} = u_{\mu\nu} - S_\nu, \quad (4.24)$$

where

$$u(z, \mu, \nu) = \frac{1}{2} [I(z, \mu, \nu) + I(z, -\mu, \nu)]$$

is the average of the specific intensity in the positive and negative μ directions, μ is the cosine of the angle between the direction the photon propagates and the normal to the slab, τ_ν is the optical depth at frequency ν , and S_ν is the source function ($= \eta_\nu/\kappa_\nu$).

Discretizing Eq. (4.24) onto the optical depth grid τ_d ($d = 1, \dots, N_D$) leads to the tridiagonal system of equations [41]:

$$-A_d u_{d-1} + B_d u_d - C_d u_{d+1} = S_d, \quad (4.25)$$

where second-order differencing provides for $2 \leq d \leq N_D$:

$$A_d = \frac{2}{\Delta\tau_{d-1}(\Delta\tau_{d-1} + \Delta\tau_d)},$$

$$B_d = 1 + \frac{2}{\Delta\tau_d \Delta\tau_{d-1}},$$

$$C_d = \frac{2}{\Delta\tau_d(\Delta\tau_{d-1} + \Delta\tau_d)},$$

where $\Delta\tau_d = \tau_{d+1} - \tau_d$. The values of A_d , B_d , and C_d for $d = 1$ and N_D depend on boundary conditions.

A key point to note is that this approach is second-order accurate. The solution of u_d depends on the value of the source function at d and $d \pm 1$. By comparison, the escape probability model is numerically less accurate because the source function is assumed to be uniform within each zone.

The photoexcitation and photoionization rates used in the statistical equilibrium equations are obtained by integrating over angle and frequency. Expressions for these rates are given in Ref. [32]. In planar geometry the angle grid is defined by Gaussian integration abscissas and weights (see, e.g., [42]). In spherical geometry the transfer equation is solved along rays which are tangent to the radius of each zone of the spatial grid (see Fig. 4.3). This approach is commonly used to solve spherical radiative transfer problems [39,43].

The frequency grid for lines is set up so that there are equally-spaced points in each line core and logarithmically-spaced points in the line wings. Typically the core region has a frequency interval of several Doppler widths. About 5 frequency points are used for the core and 10-15 are used for the wings. These parameters can be adjusted by the user. For bound-free transitions we choose frequencies such that y -values ($y \equiv \nu_1/\nu$; $\nu_1 \equiv$ frequency of absorption edge) are evenly spaced.

To accelerate the convergence to a solution in which the statistical equilibrium and radiative transfer equations are simultaneously satisfied, we employ an accelerated lambda iteration procedure in which the diagonal of the “ Λ -operator” is included in an implicit fashion in the statistical equilibrium equations. The mean intensity \bar{J} can be expressed in terms of the Λ -operator in planar geometry as [39,41]:

$$\begin{aligned} \bar{J}(\vec{r}) &= \bar{\Lambda}[S(\vec{r}\vec{\nu})] = \frac{1}{2} \int_0^\infty d\nu \phi_\nu \left[\int_0^1 d\mu \int_{\tau_\nu}^{T_\nu} S_\nu(t) e^{-(t-\tau_\nu)/\mu} \frac{dt}{\mu} \right. \\ &\quad \left. + \int_{-1}^0 d\mu \int_0^{\tau_\nu} S_\nu(t) e^{-(\tau_\nu-t)/\mu} \frac{dt}{\mu} \right]. \end{aligned}$$

In the context of the escape probability model, the diagonal of the Λ -operator corresponds to the probability a photon emitted in a spatial zone is reabsorbed in the same zone before it escapes.

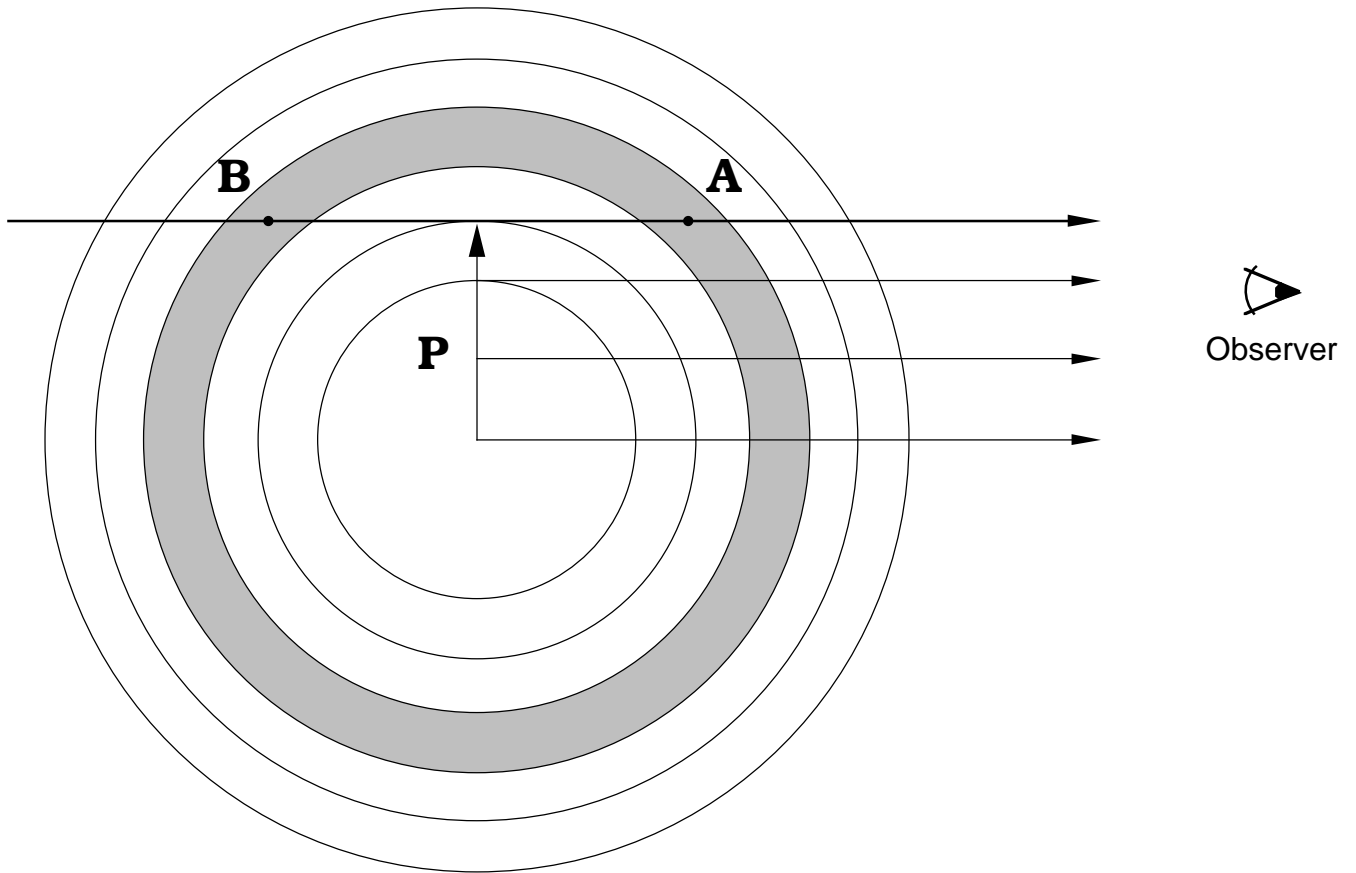


Figure 4.3. Illustration of spatial grid used to solve radiative transfer equation in spherical geometry. The impact parameters are tangent to the spherical shells. The radiation field is determined at points defined by the intersection of the rays and the spherical shells.

In the multifrequency radiation transport model of NLTERT, the matrix elements of the Λ -operator are calculated using the method recently proposed by Rybicki and Hummer [41], who showed that the diagonal elements of the Λ -operator can be calculated very efficiently using the matrix coefficients used to calculate the radiation intensity. A more detailed description of this technique is presented elsewhere [32].

4.3. Multifrequency, Multiangle Method of Short Characteristics

The short characteristics method of radiative transfer is based on the work of Olson and Kunasz [27]. This approach is based on the formal solution of the time-independent form of the transfer equation. The formal solution to the transfer equation in planar (slab) geometry can be written as:

$$I^+(\tau_\nu, \mu, \nu) = I^+(T_\nu, \mu, \nu) e^{[-(T_\nu - \tau_\nu)/\mu]} + \mu^{-1} \int_{\tau_\nu}^{T_\nu} dt S_\nu(t) e^{[-(t - \tau_\nu)/\mu]} \quad (4.26)$$

where $I^+(\tau_\nu, \mu, \nu)$ is the specific intensity in the “+”-direction ($0 \leq \mu \leq 1$) at frequency ν , at position τ_ν , and along a ray defined by the cosine angle $\mu = \cos \theta$ ($\mu = 1 \Rightarrow$ perpendicular to the slab). τ_ν is the frequency-dependent optical depth measured along a path normal to the slab boundary ($0 \leq \tau_\nu \leq T_\nu$), and S_ν is the source function. In the “-”-direction ($-1 \leq \mu \leq 0$), the specific intensity is:

$$I^-(\tau_\nu, \mu, \nu) = I^-(0, \mu, \nu) e^{\tau_\nu/\mu} + \mu^{-1} \int_0^{\tau_\nu} dt S_\nu(t) e^{[-(\tau_\nu - t)/\mu]}. \quad (4.27)$$

The flux at the boundaries is simply computed from the angle-average of the specific intensities:

$$\mathcal{F}_\nu(\tau_\nu) = 2\pi \int_{-1}^1 I(\tau_\nu, \mu, \nu) \mu d\mu. \quad (4.28)$$

In practice, Eqs. (4.26) and (4.27) are solved on a discretized optical depth grid τ_d , $d = 1, \dots, N_D$. Boundary conditions can readily be applied at $\tau_\nu = 0$ and $\tau_\nu = T_\nu$. In NLTERT, a Planckian (blackbody) flux can be applied to one or both sides of the plasma slab (using input variables TRADB1 and TRADBN).

As noted in Ref. [27], Eqs. (4.26) and (4.27) can also be rewritten for a discretized optical depth grid in a form in which the specific intensity at a point *appears* to depend only on the local source function $S_\nu(\tau_\nu)$ and the “local boundary conditions” for spatial zone d :

$$I^+(\tau_d, \mu, \nu) = I^+(\tau_{d+1}, \mu, \nu) e^{(-\Delta\tau_d)} + \Delta I_d^+(S, \mu, \nu) \quad (4.29)$$

$$I^-(\tau_d, \mu, \nu) = I^-(\tau_{d-1}, \mu, \nu) e^{(-\Delta\tau_{d-1})} + \Delta I_d^-(S, \mu, \nu) \quad (4.30)$$

where $\Delta\tau_{d-1} \equiv (\tau_d - \tau_{d-1}) / |\mu|$. Note that the local boundary conditions on each cell depend on the source function throughout the plasma. Thus, emission and absorption occurring in other zones is accounted for in this approach.

In Eqs. (4.29) and (4.30) the intensity increments, ΔI^\pm can be obtained using various approximations to the source function distribution about a spatial zone. Following Ref. [27], we assume the local source function to vary either linearly or quadratically. Then we can write:

$$\Delta I_d^+ = \alpha_d^+ S_{d-1} + \beta_d^+ S_d + \gamma_d^+ S_{d+1} \quad (4.31)$$

and

$$\Delta I_d^- = \alpha_d^- S_{d-1} + \beta_d^- S_d + \gamma_d^- S_{d+1} . \quad (4.32)$$

Integration of Eqs. (4.31) and (4.32) lead to, for a linear approximation of the spatial variation of S ,

$$\begin{aligned} \alpha_d^+ &= 0 & \alpha_d^- &= E_{0,d} - (\Delta\tau_{d-1})^{-1} E_{1,d} \\ \beta_d^+ &= (\Delta\tau_d)^{-1} E_{1,d+1} & \beta_d^- &= (\Delta\tau_{d-1})^{-1} E_{1,d} \\ \gamma_d^+ &= E_{0,d+1} - (\Delta\tau_d)^{-1} E_{1,d+1} & \gamma_d^- &= 0 \end{aligned}$$

where

$$\begin{aligned} E_{0,d} &\equiv 1 - \exp(-\Delta\tau_{d-1}) \\ E_{1,d} &\equiv \Delta\tau_{d-1} - E_{0,d} . \end{aligned}$$

For a quadratic approximation for S , the coefficients in Eqs. (4.31) and (4.32) are:

$$\begin{aligned} \alpha_d^- &= E_{0,d} + \frac{E_{2,d} - (\Delta\tau_d + 2\Delta\tau_{d-1}) E_{1,d}}{\Delta\tau_{d-1} (\Delta\tau_d + \Delta\tau_{d-1})} \\ \beta_d^- &= \frac{-E_{2,d} + (\Delta\tau_d + \Delta\tau_{d-1}) E_{1,d}}{(\Delta\tau_d + \Delta\tau_{d-1})} \\ \gamma_d^- &= \frac{E_{2,d} - (\Delta\tau_{d-1}) E_{1,d}}{\Delta\tau_d (\Delta\tau_d + \Delta\tau_{d-1})} \\ \alpha_d^+ &= \frac{E_{2,d+1} - (\Delta\tau_d) E_{1,d+1}}{\Delta\tau_{d-1} (\Delta\tau_d + \Delta\tau_{d-1})} \end{aligned}$$

$$\beta_d^+ = \frac{-E_{2,d+1} + (\Delta\tau_d + \Delta\tau_{d-1}) E_{1,d+1}}{(\Delta\tau_d + \Delta\tau_{d-1})}$$

$$\gamma_d^+ = E_{0,d+1} + \frac{E_{2,d+1} - (\Delta\tau_{d-1} + 2\Delta\tau_d) E_{1,d+1}}{\Delta\tau_d(\Delta\tau_d + \Delta\tau_{d-1})}$$

where

$$E_{2,d} \equiv (\Delta\tau_{d-1})^2 - 2E_{1,d}.$$

In practice, the above equations are solved by carrying out a sweep from zone 1 to zone N_D , and then sweeping in the opposite direction. The linear (first order) form of the calculation is performed if $\text{ISW}(71) = 0$ (default). If $\text{ISW}(71) = 1$, the quadratic (second order) form of the algorithm is invoked.

The short characteristics solution of the radiative transfer equation is utilized in subroutines SPECT4 and SPECT5 when computing the emergent spectrum, and in subroutine RRATE2 in computing photoexcitation and photoionization rates. RRATE2 allows for a more complete and accurate treatment of photoexcitation and photoionization in that it can include the contribution of all transitions on the radiation-induced transition rates (e.g., photo-pumping of one line by another), as well as the effects of radiation which originate from high-Z materials (e.g., photoexcitation of a low-Z tracer line by radiation from a high-Z medium modeled by UTA opacities.) An example of modeling high-Z materials is given in Section 10.

5. Atomic Physics Models

5.1. ATBASE Models

Atomic structure calculations for energy levels are performed using a configuration interaction (CI) model using Hartree-Fock wavefunctions [24,44]. An L-S coupling scheme is used to define the angular momentum coupling of electrons. Rate coefficients for collisional and radiative transitions are calculated as follows. Collisional excitation and ionization rates are computed using a combination of semiclassical impact parameter, Born-Oppenheimer, and distorted wave models [45-47]. The corresponding inverse processes were specified from detailed balance arguments. Rate coefficients for dielectronic recombination are computed using a Burgess-Mertz model [48] in conjunction with Hartree-Fock energies and oscillator strengths. Photoionization cross sections and radiative recombination rates are obtained from Hartree-Fock calculations. Ion beam impact ionization of target K -shell and L -shell electrons are calculated for each ionization stage using a plane wave Born approximation model with corrections for Coulomb deflection, perturbations to the binding energy due to the incident projectile, and relativistic effects for target wavefunctions [49,50]. Details of the atomic physics calculations are given elsewhere [24,44].

5.2. High-Z UTA Multigroup Opacities

When modeling high-Z materials, opacities are obtained from multigroup opacity tables computed using UTAOPA [28,29]. In this model, atomic configuration populations are calculated assuming local thermodynamic equilibrium (LTE). In the unresolved transition array (UTA) calculations, a detailed configuration accounting (DCA) method is used, but with term splitting effects included using a UTA model assuming $j - j$ coupling [29]. The UTA model treats the superposition of many overlapping, intrinsically broadened bound-bound transitions resulting from two electronic configurations as a single spectral feature. Each configuration-configuration transition array is then characterized by average quantifiers such as total intensity, average transition energy, and variance. In our calculations, the transition energies, oscillator strengths, and variances are evaluated using Dirac-Fock-Slater [51,52] self-consistent field potentials.

5.3. Occupation Probability Continuum Lowering Model

The occupation model of Hummer and Mihalas was originally implemented in the EOSOPA code of P. Wang [28]. The following description of the model is based on Ref. [44].

A procedure for treating pressure ionization effects has been suggested by Hummer and Mihalas [25,26] called the ‘‘occupation probability’’ formalism. In this procedure, an occupation probability, w_{ijk} ($0 \leq w_{ijk} \leq 1$), is introduced for each atomic level. The quantity w_{ijk} is the probability of finding the ion in state i relative to that of finding it in a similar ensemble of non-interacting ions. Alternatively, w_{ijk} can be considered as a factor expressing the survival probability of the level due to the perturbation of surrounding particles, neutral and charged. The survival probability has to be calculated directly from a physical description of interparticle interactions.

In the models suggested by Hummer et al., perturbations by neutral particles are based on an excluded volume treatment and perturbations by charges are calculated from a fit to a quantum mechanical Stark ionization theory. The level survival probability can then be expressed as

$$\begin{aligned} \ln w_{ijk} = & -\left(\frac{4\pi}{3}\right)\left\{\sum_{\nu'k'}[(r_{ijk} + r_{1\nu'k'})^3 + \beta(r_{1jk} + r_{1\nu'k'})^\gamma]\right. \\ & \left.+ 16\left[\frac{\sqrt{z_{jk} + 1}e^2}{\sqrt{K_{ijk}I_{ijk}}}\right]^3 \sum_{s \neq e} n_s z_s^{3/2}\right\}. \end{aligned} \quad (5.1)$$

Here, the index ν' runs over neutral particles, the index s runs over charged ions, r_{ijk} is the radius assigned to a particle in state i of ion j of species k , I_{ijk} is the ionization potential of such a particle, z_{jk} is the net charge of a particle of ion j of species k , β and γ are two empirical parameters, and

$$K_{ijk} = \begin{cases} 1 & p_i \leq 3 \\ \frac{16}{3} \left(\frac{p_i}{p_i+1} \right)^2 \frac{p_i+7/6}{p_i^2+p_i+1/2} & p_i > 3 \end{cases} \quad (5.2)$$

is a quantum mechanical correction and p_i is the effective quantum number of the state i .

The occupation probability formalism has several advantages. (1) The w_{ijk} decrease continuously and monotonically as the strength of the relevant interaction increases relative to the binding energy of a level. (2) The continuous state-by-state fadeout with decreasing w_{ijk} allows one to assure continuity of all material properties (pressure, internal energy, opacity, etc.). (3) The probabilistic interpretation of w_{ijk}

allows us to combine survival probabilities from statistically independent interactions. It is thus straightforward to allow for the simultaneous action of different mechanisms, as well as of several different species of perturbers by any one mechanism. Hence the method provides a scheme for treating partially ionized plasmas, and it goes smoothly to the limits of completely neutral or completely ionized gas.

A general rate equation for the population density in level j of ion z , $n_{z,j}$ can be written as

$$\begin{aligned}
\frac{dn_{z,j}}{dt} = & - \sum_k I(z, j; z+1, k) n_e n_{z,j} + \sum_k I(z-1, k; z, j) n_e n_{z-1,k} \\
& - \sum_k R(z, j; z-1, k) n_e n_{z,j} + \sum_k R(z+1, k; z, j) n_e n_{z+1,k} \\
& - \sum_{u>j} E(z, j; z, u) n_e n_{z,j} - \sum_{l<j} D(z, j; z, l) n_e n_{z,j} \\
& + \sum_{l<j} E(z, l; z, j) n_e n_{z,l} - \sum_{u>j} D(z, u; z, j) n_e n_{z,u}
\end{aligned} \tag{5.3}$$

where n_e is the density of electrons, $I(z, j; z+1, k)$ is the ionization rate coefficient for the ionization of ion z in level j to ion $z+1$ in level k , $R(z, j; z-1, k)$ is the recombination rate coefficient (radiative + collisional + dielectronic), $E(z, j; z, u)$ is the electron collisional excitation rate coefficient, and $D(z, j; z, l)$ is the deexcitation rate coefficient (spontaneous decay + collisional).

In plasmas with $n_e \leq 10^{22} \text{ cm}^{-3}$, the coupling between excited levels of neighboring ionization stages through ionization and recombination is, in general, negligible. Assuming that the residual ions (for ionization) and the target ions (for recombination) are in the ground state only, we have:

$$\begin{aligned}
\frac{dn_{z,j}}{dt} = & - I(z, j; z+1, 1) n_e n_{z,j} + [\sum_k I(z-1, k; z, j) n_e n_{z-1,k}] \delta_{j1} \\
& + R(z+1, 1; z, j) n_e n_{z+1,1} - [\sum_k R(z, j; z-1, k) n_e n_{z,j}] \delta_{j1} \\
& - \sum_{u>j} E(z, j; z, u) n_e n_{z,j} - \sum_{l<j} D(z, j; z, l) n_e n_{z,j} \\
& + \sum_{l<j} E(z, l; z, j) n_e n_{z,l} - \sum_{u>j} D(z, u; z, j) n_e n_{z,u}.
\end{aligned} \tag{5.4}$$

The ideal gas model, which assumes that interparticle interaction is negligible, leads to an infinite coupled set of the rate equations because of the infinite number of existing levels. In reality, however, the pressure ionization determines that there are only a finite number of levels for each ion and hence truncates the coupling rate equations to a finite set.

There are two factors affecting the atomic level occupation numbers: (1) does this level survive? (2) how is it occupied? If we assume the level survival probability is $w_{z,j}$ and the occupation probability is $p_{z,j}$, then the level occupation number density can be expressed as:

$$n_{z,j} = w_{z,j}p_{z,j}A_z \quad (5.5)$$

with

$$\sum_j n_{z,j} = \sum_j w_{z,j}p_{z,j}A_z = N_z \quad (5.6)$$

where N_z is the ion abundance of ion z . Now, the rate equation becomes

$$\begin{aligned} \frac{d(w_{z,j}p_{z,j})A_z}{dt} &= -I(z, j; z+1, 1)n_e(w_{z,j}p_{z,j})A_z \\ &+ \left[\sum_k I(z-1, k; z, j)n_e(w_{z-1,j}p_{z-1,j})A_{z-1} \right] \delta_{j1} \\ &+ R(z+1, 1; z, j)n_e w_{z,j}(w_{z+1,j}p_{z+1,j})A_{z+1} \\ &- \left[\sum_k R(z, j; z-1, k)n_e w_{z-1,k}(w_{z,j}p_{z,j})A_z \right] \delta_{j1} \\ &- \sum_{u>j} E(z, j; z, u)n_e(w_{z,j}p_{z,j})A_z \\ &- \sum_{l<j} D(z, j; z, l)n_e(w_{z,j}p_{z,j})A_z \\ &+ \sum_{l<j} E(z, l; z, j)n_e(w_{z,l}p_{z,l})A_z \\ &+ \sum_{u>j} D(z, u; z, j)n_e(w_{z,u}p_{z,u})A_z . \end{aligned} \quad (5.7)$$

Note that for the recombination processes we need to account for the survival probability of the final level. By summing over all levels of the ion, we have

$$\begin{aligned} \frac{d}{dt} \sum_j (w_{z,j}p_{z,j})A_z &= - \sum_j I(z, j; z+1, 1)n_e(w_{z,j}p_{z,j})A_z \\ &+ \left[\sum_{j,k} I(z-1, k'; z, j)n_e(w_{z-1,j}p_{z-1,j})A_{z-1} \right] \delta_{j1} \\ &+ \sum_j R(z+1, 1; z, j)n_e w_{z,j}(w_{z+1,j}p_{z+1,j})A_{z+1} \\ &- \left[\sum_{j,k} R(z, j; z-1, k)n_e w_{z-1,k}(w_{z,j}p_{z,j})A_z \right] \delta_{j1} . \end{aligned} \quad (5.8)$$

Defining the effective ionization rate coefficient for the ionization of ion $z-1$ to ion z as

$$\alpha_{z-1} = \sum_{j,k} I(z-1, k; z, j)w_{z-1,k}p_{z-1,k} \quad (5.9)$$

and the effective recombination rate coefficient for the recombination of ion z to ion $z-1$ as

$$\beta_z = \sum_{j,k} R(z, j; z-1, k) w_{z-1,k} w_{z,j} p_{z,j} , \quad (5.10)$$

then the equation for the proportional factor A_z becomes

$$\frac{dN_z}{dt} = -n_e(\alpha_z A_z + \beta_{z+1} A_{z+1} + \alpha_{z-1} A_{z-1} - \beta_z A_z) . \quad (5.11)$$

Assuming the plasma is in steady state, namely,

$$\begin{aligned} \frac{dN_z}{dt} &= 0 \\ z &= 0, 1, 2, 3, \dots, Z, \end{aligned} \quad (5.12)$$

we have a recursive equation

$$\frac{A_z}{A_{z-1}} = \frac{\alpha_{z-1}}{\beta_z} \quad (5.13)$$

$$z = 1, 2, 3, \dots, Z. \quad (5.14)$$

This recursive equation can be solved in the following way; set

$$\frac{\beta_z}{\alpha_{z-1}} = c_z. \quad (5.15)$$

Then

$$\begin{aligned} A_z &= c_{z+1} A_{z+1} \\ &= c_{z+1} \cdot c_{z+2} \cdot c_{z+3} \cdots c_Z \cdot A_Z \end{aligned} \quad (5.16)$$

$$z = 0, 1, 2, \dots, Z-1. \quad (5.17)$$

By using the particle conservation condition

$$\sum_z N_z = \sum_z \left(\sum_j w_{z,j} p_{z,j} \right) A_z = N_{total}, \quad (5.18)$$

we have

$$A_Z = \frac{N_{total}}{\sum_j w_{Z,j} p_{Z,j} + \sum_{z=0}^{Z-1} \left[\left(\sum_j w_{z,j} p_{z,j} \cdot c_{z+1} \cdot c_{z+2} \cdots c_Z \right) \right]}. \quad (5.19)$$

Finally, the ion abundances and the level number densities are given by

$$\begin{aligned} n_{z,j} &= w_{z,j} p_{z,j} A_z \\ N_z &= \sum_j w_{z,j} p_{z,j} A_z . \end{aligned} \quad (5.20)$$

This model has the advantage that by combining the general CRE model and the level survival probability formalism, the pressure ionization effects can be directly introduced in the calculations of ion abundances and level occupation numbers for a non-LTE plasma.

6. Input/Output File Descriptions

The NLTERT code uses up to 8 types of input files, 10 output files, and 2 scratch files. The files are listed in Table 6.1, along with their default logical unit numbers (LUN), names (for UNIX systems), types, and a brief description of their contents. (Note that the LUNs and most file names can be easily modified in the block data routine BDATA.) For each plasma species, up to four input files are required containing atomic data computed by the ATBASE suite of atomic physics codes [24]. Two of these files (LUNs 4 and 8) are required for all calculations. LUN 4 contains data for atomic level energies, oscillator strengths, collisional (electron impact) rate coefficients, and dielectronic recombination rate coefficients. LUN 8 contains photoionization cross section data. For calculations with ion beam-induced inner-shell ionization, an additional atomic data file is required for each target material (LUN 9). LUN 9 contains ion impact ionization and excitation cross sections.

Most parameters defining a problem are specified in the namelist input file (LUN 2). Details concerning variable names and definitions are given in Section 7. Example input files are shown in Section 10.

To set up the target plasma temperature and density distributions, the user has the option of: (1) using namelist input, or (2) using results from hydrodynamics output. The latter option is chosen by setting $ISW(44) \neq 0$, in which case the hydrodynamics output is read in from LUN 45 by subroutine DHYDRO, DHYDR1, or DHYDR2. The file name and current format options for reading the hydrodynamics data can be seen by examining these subroutines. These subroutines can be easily modified to read in other formatted data.

For a time-dependent collisional radiative calculation, the time-dependent temperature and density can be supplied in file 'Time.Dep.Plasma.vs.t'. If a calculation is desired where the temperature and density are constant in time (such as when investigating how long it takes for a plasma to relax to steady-state for certain plasma conditions) the conditions can be specified in 'rt.inp' using namelist variables TEMPEL and DENSNN. The electron density can be held constant in time by setting $ISW(42)=1$.

For calculations involving high-Z materials, multigroup UTA opacities can be read in from files 'eos.dat.uw.NN', where NN is the atomic number of the material. Thus, NLTERT allows for computing the effects of the radiation field emitted by a high-Z region on a lower-Z material. The atomic level populations of the high-Z material are of course based on the assumption of LTE. However, non-LTE populations for the lower-Z

material can be computed using the collisional-radiative model, including photoexcitation and photoionization effects induced by the high-Z material.

Most of the useful output is written to 3 files: LUNs 6, 18, and 19. LUN 6 contains the descriptive output, including results for atomic level populations, ionization distributions, and line radiation power densities. LUN 18 contains plottable data for the flux vs. photon energy, while LUN 19 contains plot data for the optical depth vs. photon energy. The spectral properties are computed in subroutines SPECTn (n = 1 to 5), and written to LUNs 18 and 19 in subroutine RITFLX.

Several other output files provide results that can be used to analyze a problem. LUNs 41 and 42 contain transition rate information, which can be used to determine the most important transitions which populate and depopulate the various atomic levels. LUN 3 is used to write warning messages, the purpose of which is to warn the user of potential problems that may have occurred during the calculation without stopping the calculation. LUN 11 provides results for 2-level atom benchmark calculations. (A sample calculation involving a 2-level atom calculation is given in Section 10.)

Additional useful optical depth information can be written to files ‘opacs.regns’ and ‘optdep.contour.dat’. The former writes frequency-dependent optical depths for each plasma *region*. The latter writes data which can be used to generate optical depth contour data, with photon energy and spatial position being the dependent variables.

Table 6.1. Input/Output Files

Default Unit Number	Default Name (UNIX)	Type	Description
2	rt.inp	Input	Namelist input
3	rt.warnings	Output	Warning messages which occur during run time
4	rt.atom.dat.NN	Input	Atomic structure data (energy levels, oscillator strengths, collisional rate coefficients)
6	rt.out	Output	Standard output (level populations, ionization distributions, line radiation power densities)
7	eos.dat.uw.NN	Input	EOS/multigroup opacity file for high-Z materials
8	pixsec.dat.NN	Input	Photoionization cross sections
9	beam.AABB.xsec.NN	Input	Beam impact ionization cross sections
10	auger.atom.dat.NN	Input	Auger rate and fluorescence yields
11	2level.dat	Output	Results from 2-level atom benchmark calculations
18	rt.plot.08	Output	Plot file for frequency-dependent fluxes
19	rt.plot.09	Output	Plot file for frequency-dependent optical depths
20	TimeDep.Plasma.vs.t	Input	Time-dependent plasma conditions for t-dep. C-R calculation
41	rate1	Output	Transition rate tables
42	rate2	Output	Rate coefficient tables
43	rate.pop	Output	Level-dependent populating/depopulating rates
45	—	Input	Plasma conditions from hydrodynamic simulations
54	aul.scratch	Scratch	Scratch file
55	rt.scratch	Scratch	Scratch file
77	opac.regns	Output	Plot file for frequency-dependent optical depths by region
89	optdep.contour.dat	Output	Plot file for optical contours (vs. ν , position)

NN = atomic number of target plasma

AA = atomic element symbol of beam projectile

BB = ionization stage of beam projectile

(e.g., LUN 9 would be ‘beam.Hy02.xsec.13’ for Al irradiated by a proton beam)

7. Namelist Input Variables

The user defines the parameters of a problem with the namelist input file. Through it, the user specifies the plasma properties, atomic model, time step parameters, spectral grid, radiative transfer model, and hot electron and ion beam parameters (if necessary). In addition, the user can specify the types of plot output desired, and request the printing of various debugging output. Table 7.1 lists each of the namelist variable names, along with their type, dimensions, units, default values, and a brief description of their use. Comments can be inserted in the namelist input file to aid the user. Lines starting with ‘c’ in the namelist input file are considered comments. Note that the ‘c’ must be in the first column, and must be followed by a space.

The spatial grid is most easily set up using one of the automatic zoning algorithms. Subroutine ZONER uses IGEOM, NZONES, RADMIN, RADMAX, and DRADMN to define the grid. Subroutine ZONER3 provides the added capability of subdividing the plasma into multiple regions, which is useful for multilayer targets. This zoning method uses variables NREGNS, NZONRG, REGMAS, REGDM1, and IREGZN. For isothermal, isochoric plasmas, the user simply specifies the ion density and electron temperature for each zone. Note that the electron and ion temperatures are assumed to be equal. To use temperature and density distributions from hydrodynamics simulations, the user should set ISW(44) \neq 0, and set up input files in the proper format. (See subroutines DHYDRO, DHYDR1, or DHYDR2 for details of formatting and file specification; the user may wish to modify one of these routines to read other formatted temperature and density data.) The temperatures and densities for the radiative transfer grid are then determined by interpolation from the hydrodynamics grid. The parameter TDENDL can be used to specify the total “column density” ($n \cdot \Delta L$); this ensures, for example, that the total mass per unit area be conserved in an expanding foil calculation.

The atomic model parameters specify the distribution of atomic species in the plasma. Homogeneous mixtures as well as multilayer target plasmas can be modelled. Examples of this are shown in Table 7.1. Input files for each atomic species are automatically read in based on the atomic numbers specified (ATOMNM). MXIZCH can be used to limit the maximum change for transitions; e.g., multiple ionization effects from intense ion beams can be ignored by setting MXIZCH=1. IREADA is used to identify the format of file ‘rt.atom.dat.NN’. The most recent format has autoionization rates included in the file.

The selection of atomic levels included in the NLTE calculation is done through the variable ISELCT. This is a two-dimensional array arranged as [atomic level index, gas species]. By default, no levels are selected (all elements are zero). The user selects levels from the atomic data file (LUN 4) for each plasma species by setting the corresponding ISELCT array element to 1. For example, if one wishes to include level 85 from gas species 1, one simply sets ISELCT(85,1)=1. It is often useful to set up the selection process ion by ion. Thus, if level 85 were the ground state of some ion, the lowest 20 energy levels of that ion could be selected by setting ISELCT(85,1)=20*1. For a time-dependent C-R calculation, the initial population distribution is specified with ISELCT if ISW(6)=-1. In this case, the $t = 0$ populations are equally distributed about states which have an ISELCT value of 2. Examples of this are provided in Section 10.

The variable ILINEP (listed under Radiative Transfer Parameters) is used to set the line profile type. For laboratory plasmas, a Voigt profile should generally be used. Natural, Doppler, Stark, and Auger broadening effects are automatically included in the calculation. ISW(7) and ISW(8) are used to specify whether photoexcitation and photoionization be considered in the statistical equilibrium equations. ISW(4) and ISW(5) indicate the choice of radiative transfer model: angle- and frequency-averaged escape probability model or multiangle, multifrequency model. Variables NFPIZ0 through NCRAD listed under the Radiative Transfer Parameters heading are used in the multifrequency radiative transfer model. The default values should be sufficient for laboratory plasma calculations.

Recently, a new model has been added to include the effects of overlapping transitions and an external radiation source on the atomic level populations and emergent spectra. This model is invoked (instead of the escape probability or Feautrier radiative transfer models) by setting ISW(2)=1. Then if ISW(19)=0 both photoexcitation and photoionization are computed using this model. If ISW(19)=1, photoionization rates are computed using this model, but photoexcitation is computed using the escape probability or Feautrier models (depending on the value of ISW(5)). These radiation-dependent rates are computed in subroutine RRATE2, and use the short characteristics solution to the radiative transfer equation. Variables NFRQFR, HVMINR, and HVMAXR are used to define the frequency grid for the rate integrals, while TRADB1 and TRADBN can be used to specify a radiation temperature boundary condition. This model is considered to be more accurate than the other models, but it is more computationally expensive.

High-Z materials can also be included in NLTE calculations. As an example, one might want to study the influence of the radiation emitted by a high-Z hohlraum

wall on a low-Z material (such as an ablator or tracer). This model is invoked using the variable IHIGHZ, which is used to prescribe the material index of the high-Z material for each zone. If a zone is designated as a high-Z zone, opacities and source functions are determined using the multigroup opacity tables which are read in (these are the same EOS/opacity tables as those used by the BUCKY radiation-hydrodynamics code [53]). Atomic level populations of the high-Z zones need not be computed, as opacities and source functions are obtained from table look-up. (In most instances, the high-Z properties are computed using a UTA model in which LTE populations have been assumed.) The input parameter NMATRS defines the number of different high-Z materials to be considered. ATWMAT is the atomic weight of the material. IDEOS, IDOPAC, IZEOS, and NFG specify the properties of the EOS/opacity table (as they do in BUCKY).

The effects of an intense light ion beam can be modelled in NLTERT calculations. At present, this is done by setting ISW(37)=3. This model utilizes ATBASE atomic physics tables of ion beam impact ionization and excitation cross sections, as well as Auger rates and fluorescence yields. An option to model hot electrons (i.e., non-Maxwellian electron distributions) has also been added to the code. One application of this is the simulation of ion beam transport experiments, where energetic electrons and ions can play a significant role in affecting the ionization dynamics of the background medium [54,55]. This model is invoked by setting ISW(55)=1. Then input variables NBINHE, EMINHE, and EMAXHE define the electron (kinetic) energy grid. THOTEL can be used to define the hot component by a Maxwellian distribution of temperature THOTEL (thus prescribing a bi-Maxwellian distribution for the two-component electron model). FRACHE defines the fraction of electrons which are in the hot (non-Maxwellian) component.

By default, the calculation of atomic level populations is performed by solving multilevel statistical equilibrium equations which include both collisional and radiative terms. The user can specify that LTE populations be computed by setting ISW(6)=3. ISW(6) is also used to specify the initial guess at the populations (see Section 2 for a description of the iterative procedure). In addition, transition rates for each type of process can be adjusted (or set to zero) by redefining CON(42) through CON(49).

When a time-dependent collisional-radiative calculation (non-steady-state) is desired ISW(1) should be set to 1. NTIMES is the number of times on the simulation time grid, which is equal to the number of times LSODE is called. If ISW(11)=0, simulation times are specified by the array TIMSIM. If ISW(11)=1, a grid of uniformly spaced

times of time increment DELTAT is used. If ISW(11)=2, a uniform log-spaced time grid is used, which is prescribed using NTIMES, TCRMIN, and TCRMAX. If the simulation time exceeds TIMEND, the calculation is stopped. Several example namelist input files are shown in Section 10.

Table 7.1. Namelist Input Variables

PLASMA, GRID PARAMETERS

Variable Name	Type	Dimensions	Units	Default Value	Description
IGEOM	I*4	—	—	1	Coordinate index (1 – planar, 2 – cylindrical, 3 – spherical)
NZONES	I*4	—	—	0	Number of spatial zones (Maximum number = MXZONS)
RADMIN	R*8	—	cm	0.	Minimum radius or position
RADMAX	R*8	—	cm	0.	Maximum radius or position
DRADMN	R*8	—	cm	0.	Width of zone nearest the outer plasma boundary
DRAD	R*8	NZONES	cm	0.	Zone widths (not needed when using automatic zoning)
DENSNN	R*8	NZONES	cm ³	0.	Total ion density
TEMPEL	R*8	NZONES	eV	0.	Electron temperature
TDENDL	R*8	—	—	0.	Total column density ($\equiv \int_0^L n_{\text{ion}}(r) dr$) (Used to scale hydrodynamic density distributions to maintain correct target mass)
NREGNS	I*4	—	—	0	Number of plasma “regions” (used for zoning)
NZONRG	I*4	MXREGN	—	0	Number of spatial zones in each region
REGMAS	R*8	MXREGN	—	0.	Region mass (g/cm ² planar; g/cm cylindrical; g spherical)
REGDM1	R*8	MXREGN	—	0.	Mass in boundary zone (same units as REGMAS)
IREGZN	I*4	MXZONS	—	0	Region index for each zone

ATOMIC MODEL PARAMETERS

Variable Name	Type	Dimensions	Units	Default Value	Description
NGASES	I*4	—	—	1	Number of gas species (maximum number = MXGASS)
ATOMNM	R*8	NGASES	—	0.	Atomic number
ATOMWT	R*8	NGASES	amu	0.	Atomic weight
MXIZCH	I*4	—	—	999	Maximum ionization change considered for transitions
FRACSP	R*8	NZONES, NGASES	—	1 for igas=1 0 for igas>1	Fractional concentration of gases in each zone Example for homogeneous binary plasma with 20 zones: FRACSP(1,1) = 20*0.5 FRACSP(1,2) = 20*0.5 Example for layered plasma: FRACSP(1,1) = 10*1., 10*0. FRACSP(1,2) = 10*0., 10*1.
ISELCT	I*4	MXLVLI, MXGASS	—	0	Array to select atomic levels from atomic data files 1 ⇒ on (or select); 0 ⇒ off (default) 2 ⇒ ...
ICONTL	I*4	—	—	-1	Index for continuum lowering model 0 ⇒ compute occupation probabilities and continuum lowering 1 ⇒ compute occupation probabilities only 2 ⇒ compute continuum lowering only < 0 ⇒ neither
IREADA	I*4	MXGASS	—	2	Switch for format of atomic data files (rt.atom.dat.NN) 1 ⇒ contains autoionization rates 2 ⇒ does not contain autoionization rates
TELTE	R*4	—	eV	0.	Temperature below which LTE populations are assumed
IZONPQ	I*4	—	—	0	Index of zone for which a_{voigt} and P_Q are written out

SPECTRAL CALCULATION PARAMETERS

Variable Name	Type	Dimensions	Units	Default Value	Description
IPLOT	I*4	—	—	0	Select as follows IPLOT (1) = 1: compute spectral flux using escape probability radiative transfer model IPLOT (1) = 2: compute spectral flux using multiangle, multifrequency radiative transfer model IPLOT (1) = 3: compute spectral intensity along a specified line of sight defined by XMULOS using multiangle, multifrequency radiative transfer model IPLOT (8) = 1: print out photon energies and fluxes IPLOT (8) = 2: print out log ₁₀ values of photon energies and fluxes IPLOT (9) = 1: print out photon energies and optical depths IPLOT (9) = 2: print out log ₁₀ values of photon energies and optical depths
NFRQFF	I*4	—	—	100	Number of frequency points for continuum
NFRQBB	I*4	—	—	5	Number of frequency points for each line
HVMIN	R*8	—	eV	1.0	Minimum frequency for spectral grid
HVMAX	R*8	—	eV	5000.	Maximum frequency for spectral grid
XMULOS	R*8	—	—	1.0	Cosine of angle used for line of sight if IPLOT (1) = 3

RADIATIVE TRANSFER PARAMETERS

Variable Name	Type	Dimensions	Units	Default Value	Description
ILINEP	I*4	—	—	1	Line profile type (1 \Rightarrow Doppler; 2 \Rightarrow Lorentz; 3 \Rightarrow Voigt)
XMUBAR	R*8	—	—	0.51	Cosine of angle used for angle-averaged escape probability model
ISW (7)	I*4	100	—	0	Compute photoexcitation if equal to 1
ISW (8)	I*4	100	—	0	Compute photoionization if equal to 1
ISW (5)	I*4	100	—	0	If 0, use escape probability model for photoexcitation calculation; if 1, use multiangle, multifrequency model for photoexcitation calculation
ISW (4)	I*4	100	—	0	If 0, use escape probability model for photoionization calculation; if 1, use multiangle, multifrequency model for photoionization calculation
NFLINE	I*4	—	—	5	Number of frequency points for each line (sum for core and wings; used to compute photoexcitation rate)
NFPIZ0	I*4	—	—	5	Number of frequency points for each bound-free transition (used to compute photoionization rates)
NFCORE	I*4	—	—	10	Number of frequency points in core of line (for Voigt line profiles only)
BANDWD	R*8	—	Doppler widths	4.	Total bandwidth for each line
BWCORE	R*8	—	Doppler widths	5.	Bandwidth of line cores

RADIATIVE TRANSFER PARAMETERS (CONT.)

Variable Name	Type	Dimensions	Units	Default Value	Description
NANGLE	I*4	—	—	2	Number of angles
NCRAD	I*4	—	—	5	Number of impact parameter rays inside core (for spherical plasma with RADMIN > 0)
HVMINR	R*8	—	eV	0.1	Minimum photon energy used in -RRATE2- in computing photoexcitation and photoionization rates
HVMAXR	R*8	—	eV	5000.	Maximum photon energy used in -RRATE2- in computing photoexcitation and photoionization rates
NFRQFR	I*4	—	—	100	Number of frequency points for -RRATE2- photoexcitation/photoionization calculation
TRADB1	R*8	—	eV	0.	Radiation temperature applied to the boundary at zone 1
TRADBN	R*8	—	eV	0.	Radiation temperature applied to the boundary at zone NZONES

ION BEAM IONIZATION PARAMETERS

Variable Name	Type	Dimensions	Units	Default Value	Description
EBEAM	R*8	MXZONS	MeV	0.	Beam energy
CURDEN	R*8	MXZONS	MA cm ⁻²	0.	Beam current density (i.e., particle flux in 10 ⁶ MA/s/cm ²)
IZBEAM	I*4	—	—	0	Beam atomic number
ISTGBM	I*4	—	—	0	Beam ionization state (1 ⇒ neutral)
ISW (37)	I*4	100	—	0	If > 0, consider ion impact ionization

CALCULATED MULTIGROUP OPACITY PARAMETERS

Variable Name	Type	Dimensions	Units	Default Value	Description
NGRUPS	I*4	—	—	0	Number of photon energy groups
EGRPBD	R*8	MXGRPS+1	eV	0.0	Photon energy group boundaries

OTHER PARAMETERS

Variable Name	Type	Dimensions	Units	Default Value	Description
				See	
CON	R*8	100	—	Table 7.2	Array of constants (see Table 7.2)
ISW	I*4	100	—	0	Array of integer switches (see Table 7.3)
IEDIT	I*4	100	—	0	Array of edit (debugging) flags (see Table 7.4)
IBENCH	I*4	20	—	0	Array used for benchmark test calculations IBENCH(3) = 1: 2-level atom with $\kappa \propto r^{-2}$ 2: 2-level atom with $\kappa \propto r^{-2}$ and $B_\nu \propto r^{-2}$ (spherical case; see [56]) IBENCH(4) = 1,2: 2-level atom (planar case; see [57]) IBENCH(6) = 1: 2-level atom with continuum background (see [58])
				See	
FNAMES	C*55	100	—	Table 6.1	File names corresponding to logical unit number of same index FNAMES(45) = name of rad-hydro input file

CRE CONVERGENCE PARAMETERS

Variable Name	Type	Dimensions	Units	Default Value	Description
ERRMXF	R*8	—	—	1.e-3	Maximum error allowed in fractional populations during convergence procedure
IMAXSE	I*4	—	—	40	Maximum number of iterations during convergence procedure
NGCYCL	I*4	—	—	4	Apply Ng acceleration every NGCYCL'th cycle
NGORDR	I*4	—	—	2	Order of Ng acceleration
NGBEGN	I*4	—	—	0	Iteration cycle at which to begin Ng acceleration

HOT ELECTRON DISTRIBUTION PARAMETERS

Variable Name	Type	Dimensions	Units	Default Value	Description
NBINHE	I*4	—	—	0	Number of hot electron energy bins
EMINHE	R*8	—	eV	0.	Minimum energy in hot electron distribution
EMAXHE	R*8	—	eV	0.	Maximum energy in hot electron distribution
THOTEL	R*8	MXZONS	eV	0.	Temperature of hot electron component (when modeled as hot Maxwellian distribution)
FRACHE	R*8	MXZONS	—	0.	Fraction of electrons in non-Maxwellian component ($n_e^{\text{hot}}/n_e^{\text{thermal}}$)
ISW(55)	I*4	—	—	0	If ISW(55)=1, consider hot electrons in atomic rate equations

HIGH-Z MULTIGROUP OPACITY FILE PARAMETERS

Variable Name	Type	Dimensions	Units	Default Value	Description
NMATRS	I*4	—	—	0	Number of high-Z (i.e., EOS/opacity table look-up) materials
IDEOS	I*4	MXMATR	—	3	EOS table type: (3 \Rightarrow EOSOPA)
IDOPAC	I*4	MXMATR	—	3	Opacity table type: (3 \Rightarrow EOSOPA)
IZEOS	I*4	MXMATR	—	99	EOS/opacity file identifiers
IHIGHZ	I*4	MXZONS	—	0	Material index of high-Z species
ATWMAT	R*8	MXMATR	a.m.u.	0.	EOS material mean atomic weight
NFG	I*4	MXMATR	—	0	Number of frequency groups in opacity look-up tables

TIME-STEPPING PARAMETERS

Variable Name	Type	Dimensions	Units	Default Value	Description
NTIMES	I*4	—	—	0	Number of times on simulation time grid
TCRMIN	R*8	s	—	0.	Minimum simulation time
TCRMAX	R*8	s	—	0.	Maximum simulation time
TIMSIM	R*8	s	MXTIMS	0.	Grid of simulation times
DELTAT	R*8	s	—	0.	Δt , when using uniformly-spaced time grid
TIMEND	R*8	s	—	1.e10	End C-R simultion after TIMEND
ISW(11)	I*4	—	—	0	If ISW(11) = 0 \Rightarrow specify times using TIMSIM 1 \Rightarrow specify times using DELTA (constant linear time step) 2 \Rightarrow specify times using TCRMIN, TCRMAX (uniform log-spaced time grid)

O.D.E. SOLVER PARAMETERS

Variable Name	Type	Dimensions	Units	Default Value	Description
ATOLLS	R*8	—	—	10^{-16}	Absolute tolerance parameter for LSODE
RTOLLS	R*8	—	—	10^{-7}	Relative tolerance parameter for LSODE
MFLS	I*4	—	—	21	Method flag for LSODE

Table 7.2. Real Constants - CON

Array Element	Default Value	Description
6	1.e-30	Minimum value of fractional level population
12	0.1	Scaling parameter for statistical equilibrium matrix elements
19	1.e-7	Minimum fractional population used to test convergence
20	1.0	Multiplier for natural line width
21	1.0	Multiplier for Doppler line width
22	1.0	Multiplier for Stark line width
24	1.0	Multiplier for ion dynamic broadening (hydrogenic Lyman series)
25	0.0	Ratio of line-to-continuum opacity for benchmark calculation
26	1.0	Multiplier for bound-bound opacity
27	1.0	Multiplier for bound-free opacity
28	1.0	Multiplier for free-free opacity
29	0.	Multiplier for electron scattering opacity
42	1.0	Multiplier for collisional deexcitation/excitation rate
43	1.0	Multiplier for spontaneous emission rate
44	1.0	Multiplier for hot electron collisional excitation/deexcitation rate
45	1.0	Multiplier for collisional recombination/ionization rate
46	1.0	Multiplier for radiative recombination rate
47	1.0	Multiplier for dielectronic recombination rate
48	1.0	Multiplier for autoionization rate
49	1.0	Multiplier for hot electron ionization/recombination rate
50	1.0	Multiplier for ion beam-impact excitation cross section
51	1.0	Multiplier for ion beam-impact single ionization rate
52	1.0	Multiplier for ion beam-impact double ionization rate
53	1.0	Multiplier for ion beam-impact triple ionization rate
57	1.e-30	Minimum value of $\Delta E/T$ for ionization windowing
58	1.e-30	Minimum value of $\Delta E/T$ for ionization windowing
60	0.1	Value of occupation probability used to find continuum lowering ΔE
61	10^{-3}	Minimum value of oscillator strength for which frequency points are added to spectral calculation frequency grid
72	0.1	$\Delta E/E$ range for which a bound-bound transition contributes to overall opacity
76	1.0	Multiplier on densities read in from rad-hydro file
77	1.0	Multiplier on temperatures read in from rad-hydro files
88	0.0	Temperature of reference blackbody spectrum written to emission spectrum file
89	0.0	Minimum electron temperature to be used when reading plasma conditions from rad-hydro file or plasma file for time-dependent C-R calculation
90	-1.0	Simulation time corresponding to rad-hydro file

Table 7.3. Control Switches - ISW

Array Element	Value*	Description
1	0*	Perform CRE calculation
	1	Perform time-dependent collisional-radiative calculation
2	0*	Compute photoexcitation and photoionization rates using either escape probability model or Feautrier transport model (depending on ISW(4) and ISW(5))
	1	Compute photoionization using short characteristics transport model. Also compute photoexcitation using this model if ISW(19)=1
4	0*	Compute radiative transfer (RT) for bound-free (b-f) transitions using escape probability model
	1	Compute RT for b-f transitions using multiangle, multifrequency Feautrier model
5	0*	Compute RT for bound-bound (b-b) transitions using escape probability model
	1	Compute RT for b-b transitions using multiangle, multifrequency Feautrier model
6	-1	Start with user-specified populations (setting values of ISELCT=2)
	0	Start with coronal populations
	1*	Start with LTE populations
	2	Start with coronal populations
	3	Final populations are LTE
	4	Final populations are coronal
7	0*	Include photoexcitation effects in calculation of atomic level populations
8	0*	Include photoionization effects in calculation of atomic level populations
11	0*	For time-dependent C-R calculation, time grid is specified with TIMSIM
	1	For time-dependent C-R calculation, use uniform time step (defined using DELTAT)
	2	For time-dependent C-R calculation, use uniform LOG time step (defined using TCRMIN, TCRMAX)
An asterisk () indicates default value.		

Table 7.3. (Continued)

Array Element	Value*	Description
12	0*	Compute line radiation power densities (do not compute if nonzero)
14	0*	Neglect background continuum in escape probability line transport calculation
	1	Include background continuum
15	0*	Use automatic zoning procedure
	1	Specify grid by DRAD array in namelist input
	2	Use exact same zoning as hydro output (set ISW(44)=0)
16	0*	Write out bound-bound and bound-free transition information if zero (if non-zero, do not write)
17	0*	Use evenly spaced frequency grid in line core; logarithmically spaced grid in wings
	1	Use evenly spaced frequency grid for line transport calculation
18	0*	Use scaled values of source function and optical depth for photoionization calculation
	1	Use computed source functions and optical depths
19	0*	Used only if ISW(2)=1. Compute both photoexcitation and photoionization using subroutine RRATE2
	1	Used only if ISW(2)=1. Compute photoionization using RRATE2, photoexcitation using RRATES
20	0*	Non-LTE equation of state: $E = E_{\text{ion}} + E_e + E_{\text{iz}}$
	1	$E = E_{\text{ion}} + E_e + E_{\text{iz}} + E_{\text{degen}}$
	2	$E = E_{\text{ion}} + E_e + E_{\text{iz}} + E_{\text{DH}}$
	3	$E = E_{\text{ion}} + E_e + E_{\text{iz}} + E_{\text{degen}} + E_{\text{DH}}$
23	0*	Compute Voigt parameter
	1	Set Voigt parameter = CON (23)
	2	Estimate T and a_{voigt} from rate coefficients
An asterisk () indicates default value.		

Table 7.3. (Continued)

Array Element	Value*	Description
26	0*	For time-dependent C-R calculation, write out populations every time step (otherwise, do not)
27	0*	For time-dependent C-R calculation, write out transition rate tables every time step (otherwise, do not)
28	0*	For time-dependent C-R calculation, write out transition rate data every time step (otherwise, do not)
29	0*	Add frequency points near bound-free edges when computing photoionization rates using short characteristics model
30	0 1*	Compute \bar{g} in Stark width calculation Set $\bar{g} = 0.2$ in Stark width calculation
34	0* 1	Use LAPACK matrix scaling Use LAPACK + NLTERT matrix scaling
35	0*	Read in photoionization cross sections from 'pixsec.dat.NN' files (otherwise, do not)
36	0 1*	Read in autoionization rates and fluorescence yield from 'auger.atom.dat.NN' files Do not use auger.atom.dat.NN files
37	0* 3	Do not consider ion-impact ionization or excitation Read ion beam-impact ionization/excitation cross sections from 'beam.AABB.xsec.NN' files
38	0* 1	No equation of state calculation Compute internal energy and pressure
39	0* 1	No multigroup opacity calculation Compute multigroup opacities
41	0* 1	Do not read in time-dependent plasma conditions Read in time-dependent plasma conditions from file 'TimeDep.Plasma.vs.t'
An asterisk () indicates default value.		

Table 7.3. (Continued)

Array Element	Value*	Description
42	0*	Allow electron density to change during time-dependent C-R calculation
	1	Hold electron density constant during time-dependent C-R calculation
44	-1	Read in T(r), n(r) using -dhydr2-
	1	Read in T(r), n(r) using -dhydro-
45	0*	Parameter to indicate hydro simulation time for setting T(r), n(r)
46	0*	Low index zones of NLTERT correspond to low index zones of rad-hydro output
	1	Low index zones of NLTERT correspond to high index zones of rad-hydro output
51	0*	Use Hummer/Mihalas approximation in computing occupation probabilities
	1	Use Hummer/Mihalas exact formula in computing occupation probabilities
	<0	Use discrete cutoff of occupation probabilities at $n_{\max} = -\text{ISW}(51)$
55	0*	Do not consider hot electrons (non-Maxwellian electron distribution)
	1	Compute transition rates due to hot electrons
61	0*	Use dielectronic recombination “effective” DR values from ‘rt.atom.dat.NN’ files
	1	Model DR as an explicit electron capture into autoionization levels
71	0*	Use first order method (S linear) in short characteristics model
	1	Use second order method (S quadratic) in short characteristics model
72	0*	Computed spectra using -SPECT4- or -SPECT5- are fluxes
	1	Computed spectra using -SPECT4- or -SPECT5- are specific intensities along a specific line-of-sight
87	0*	Parameter used in 2-level atom benchmark calculations

An asterisk () indicates default value.

Table 7.4. Debugging Switches - IEDIT

<u>Array Element</u>	<u>Subroutine Writing Debug Output</u>
21	CLOWER
18	CLSLAB
18	CPLC1P
18	CPLC9P
18	CPLCFP
84	FESCAP
10	FORM1C
9	FORM1L
10	FORM3C
9	FORM3L
12	GETCFS
78	GPOPAC
17,93	INIT1
44	INIT2
28,29	INPUT
33	INPUT3
71	INPUT4
72	INPUT5
61	LINEPR
80	LINWID
11,27	LOPACS
48	LTEPOP
48	LTEPPZ
1,14,54,99	MATRX0
52	MESHF2
52	MESHHV

Table 7.4. Debugging Switches - IEDIT (Cont.)

<u>Array Element</u>	<u>Subroutine Writing Debug Output</u>
77	MESHMG
78	MGOPAC
34	NGACCL
22	OCPRB0
22	OCPRB1
22	OCPRB2
1,14	ODESOL
73	OPACS
73	OPACSZ
59	OUT3
25	PWRDEN
42	RATBEM
41	RATCOF
95	RDEOS0
47,81	READA1
47,81	READA2
85,87	RRATE2
12,55	RRATES
74	SHORTC
82,83,85,86	SPECT1
85	SPECT2
85	SPECT3
85	SPECT4
85	SPECT5
92	VOIGT
81	WSTARK

8. Subroutines

Table 8.1 lists the name of each subroutine in NLTERT, along with a brief description of its primary function. Flow diagrams showing the relation of the higher level subroutines are shown in Figs. 8.1 through 8.4. With the exception of using NAMELIST input, all subroutines are written in FORTRAN 77.

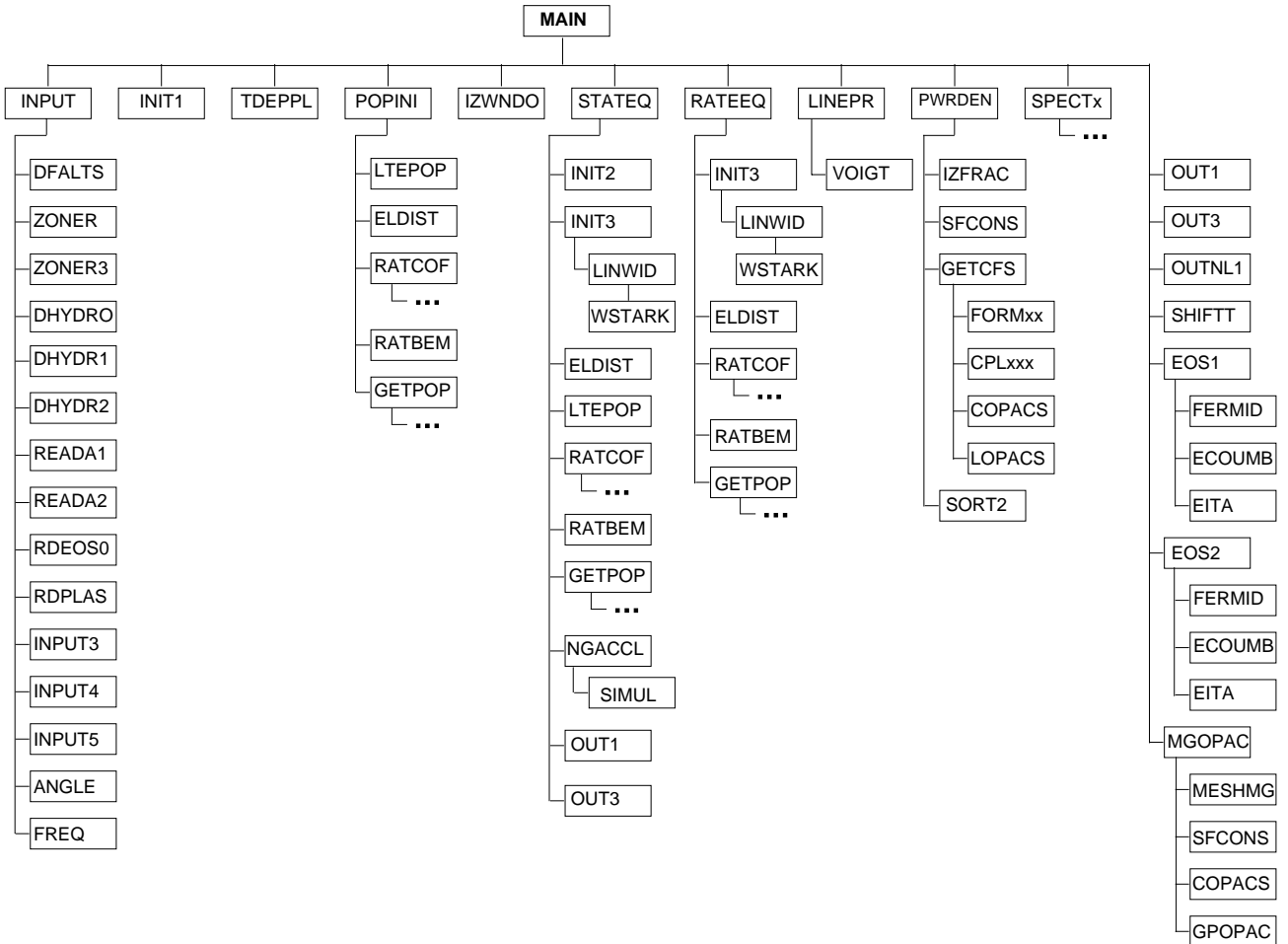


Figure 8.1. Flow diagram for top-level NLTERT subroutines.

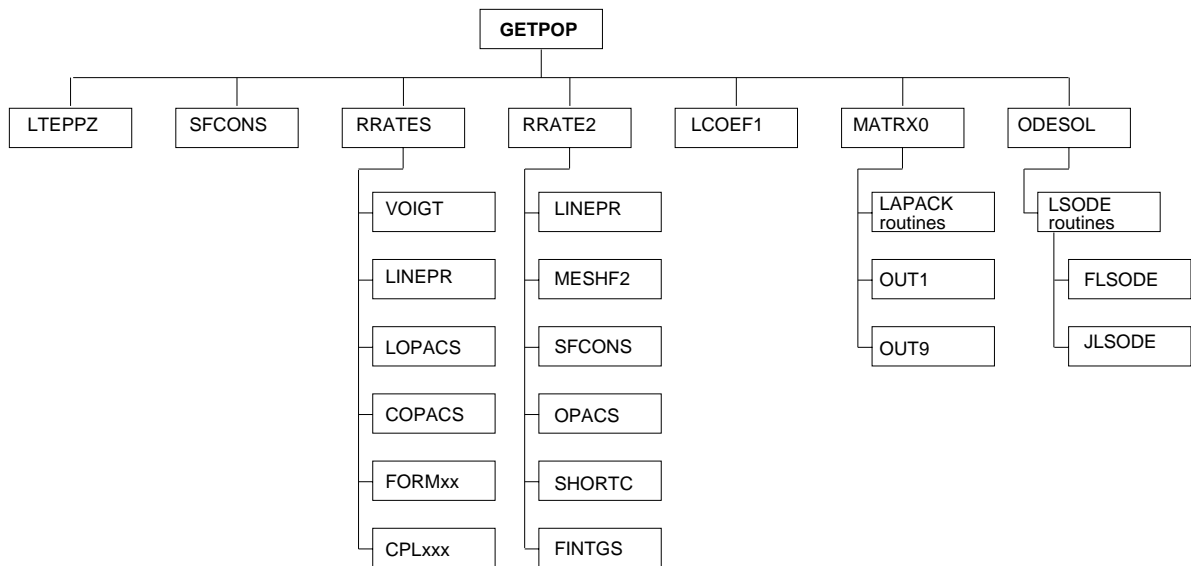


Figure 8.2. Flow diagram for subroutines in GETPOP branch.

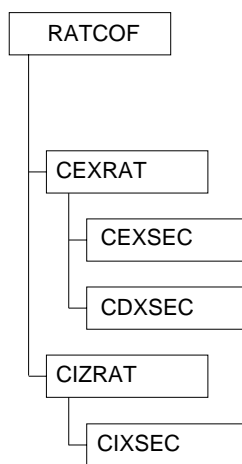


Figure 8.3. Flow diagram for subroutines in RATCOF branch.

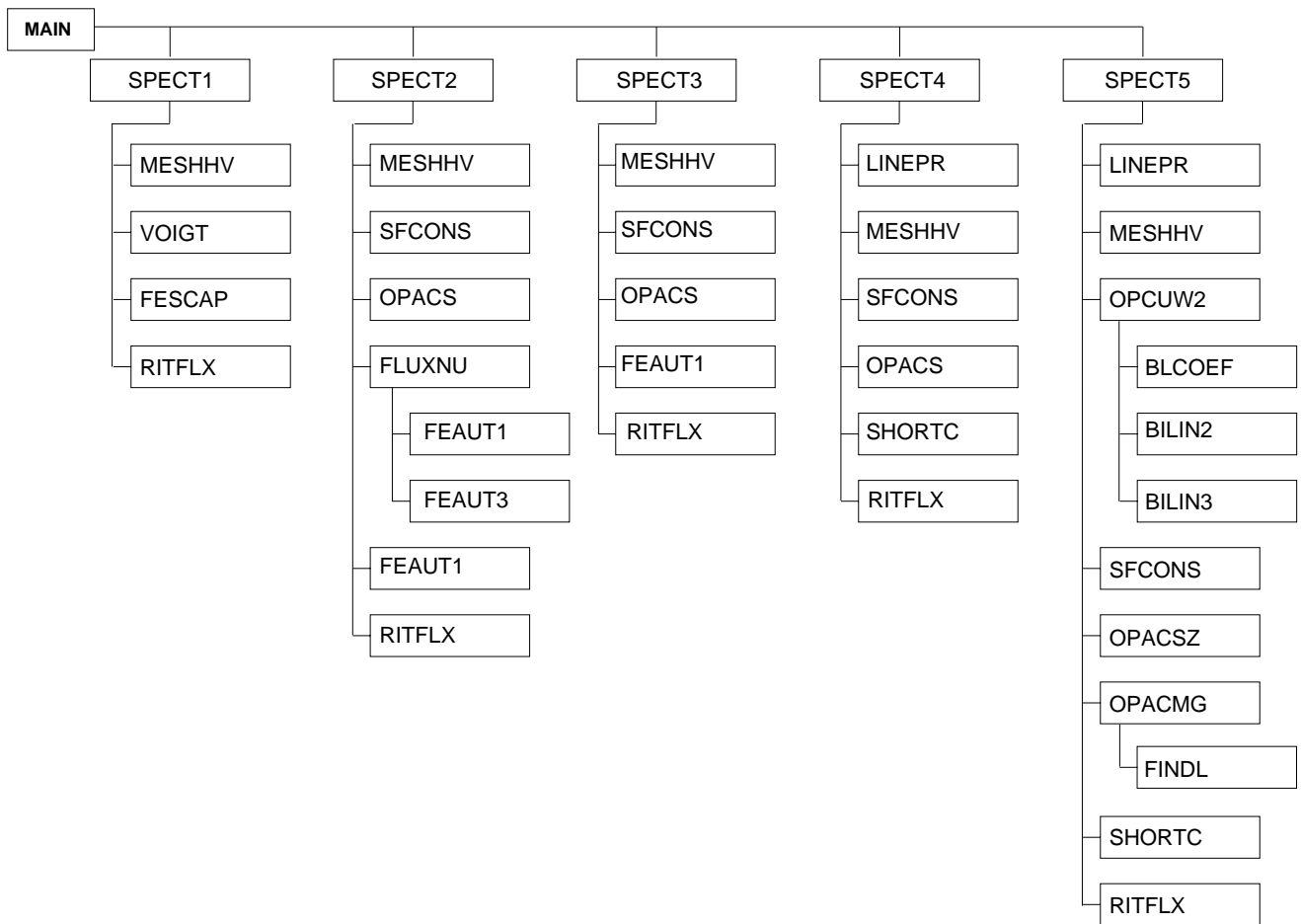


Figure 8.4. Flow diagram for spectral calculation subroutines.

Table 8.1. NLTERT Subroutines

Subroutine Name	Called By	Calls To	Description
MAIN	—	INPUT, INIT1, IZWNO, PWRDEN, LINEPR, SPECT1, SPECT2, SPECT3, SPECT4, SPECT5, RATEEQ, MGOPAC, STATEQ, OUT3, TDEPPL, OUT1, POPINI, EOS1, EOS2, OUTNL1, SHIFTT	Driver routine (main program).
BDATA	—	—	Block data routine for initializing constants.
ANGLE	INPUT	—	Sets up angles and integration weights for radiative transfer calculation.
AVG	WSTARK	EXTROP, YVALUE	Computes effective Gaunt factors for Stark broadening.
BFARGS	CPLCFS, CPLCFP, CPLCF9	—	Sets up bound-free escape probability parameters.
BILIN2	OPCUW2	—	Performs bi-linear interpolation for \bar{Z} .
BILIN3	OPCUW2	—	Performs bi-linear interpolation for multigroup opacities.
BLCOEF	OPCUW2	LOCATE	Sets coefficients for bi-linear interpolation of EOS/opacity tables.
CDXSEC	CEXRAT	—	Computes collisional deexcitation cross sections.
CEXRAT	RATCOF	—	Computes collisional excitation rates.
CEXSEC	CEXRAT	—	Computes collisional excitation cross sections.
CIXSEC	CIZRAT	—	Computes collisional ionization cross sections.
CIZRAT	RATCOF	—	Computes collisional ionization rates.
CLOWER	INIT3	—	Computes continuum lowering quantities.
CLSLAB	RRATES	—	Computes bound-bound escape probability coupling coefficients for slab geometry.
COPACS	FORM1C, FORM3C, GETCFS, MGOPAC, RRATES	—	Computes frequency-dependent continuum opacities and emissivities.

Table 8.1 (Continued)

Subroutine Name	Called By	Calls To	Description
CPLC1P	RRATES, GETCFS	EPINT1	Computes escape probability coupling coefficients for Doppler profiles in planar geometry.
CPLC9P	RRATES, GETCFS	EPINT9, BFARGS	Computes escape probability coupling coefficients for bound-free transitions in planar geometry.
CPLCFP	RRATES, GETCFS	EPINT2, EPINT3, BFARGS	Computes escape probability coupling coefficients for bound-bound transitions in planar geometry.
CPLCFS	RRATES, GETCFS	EPINT1, EPINT2, EPINT3, EPINT9, BFARGS	Compute escape probability coupling coefficients for bound-bound transitions in cylindrical and spherical geometry.
DFALTS	INPUT	—	Initialize variables and set default values.
DHYDRO	INPUT	DTABLE, FNEWT	Set up temperature and density distributions from hydrodynamics simulation output.
DHYDR1	INPUT	—	Set up temperature and density distributions from hydrodynamics simulation output.
DHYDR2	INPUT	DTABLE, FNEWT	Set up temperature and density distributions from hydrodynamics simulation output
DTABLE	DHYDRO, DHYDR2, RDPLAS	—	Sets up divided difference tables for interpolation.
ECOUMB	EOS1	FERMID	Calculates Debye-Huckel correction term to the plasma internal energy.
EITA	EOS1, EOS2	FERMID	Determines degeneracy factor for a partially degenerate electron gas.
ELDIST	POPINI, RATEEQ, STATEQ	—	Sets up arrays for non-Maxwellian electron distributions.
EOS1	MAIN	FERMID, ECOUMB, EITA	Computes plasma internal energy.
EOS2	MAIN	FERMID, PCOUMB, EITA	Computes plasma pressure.
EPINT1	CPLC1P, CPLCFS	—	Computes escape probability integral for a Doppler profile.

Table 8.1 (Continued)

Subroutine Name	Called By	Calls To	Description
EPINT2	CPLCFP, CPLCFS	—	Computes escape probability integral for a Lorentz profile.
EPINT3	CPLCFP, CPLCFS	—	Compute escape probability integral for a Voigt profile.
EPINT9	CPLC9P, CPLCFS	—	Compute escape probability integral for bound-free transitions.
FEAUT1	FLUXNU, SPECT2, SPECT3	—	Feautrier radiative transfer algorithm for planar geometry (spectral calculation).
FEAUT3	FLUXNU	—	Feautrier radiative transfer algorithm for spherical geometry (spectral calculation).
FEAUTP	FORM1C, FORM1L	—	Feautrier radiative transfer algorithm for planar geometry.
FEAUTX	FORM1C, FORM1L	—	Feautrier radiative transfer algorithm for spherical geometry.
FERMID	ECOUMB, EITA, EOS1, EOS2, PCOUMB	—	Computes Fermi-Dirac integrals.
FESCAP	SPECT1	—	Calculates escape probability factors.
FINDL	OPACMG	—	Finds index in photon energy grid of EOS/opacity tables
FINTGS	RRATE2	—	Updates frequency integrals for radiation field-dependent rate coefficients.
FLSODE	LSODE routines	—	Used by LSODE update atomic level populations
FLUXNU	SPECT2	FEAUT1, FEAUT3	Computes frequency-dependent flux using Feautrier radiative transfer model.
FNEWT	DHYDRO, DHYDR2, TDEPPL	—	Newton divided difference interpolation routine.
FORM1C	GETCFS, RRATES	COPACS, FEAUTP	Solves formal solution of transfer equation to obtain photoionization rate in planar geometry.

Table 8.1 (Continued)

Subroutine Name	Called By	Calls To	Description
FORM1L	GETCFS, RRATES	VOIGT, FEAUTP	Solves formal solution of transfer equation to obtain photoexcitation rate in planar geometry.
FORM3C	GETCFS, RRATES	COPACS, FEAUTX	Solves formal solution of transfer equation to obtain photoionization rate in spherical geometry.
FORM3L	GETCFS, RRATES	VOIGT, FEAUTX	Solves formal solution of transfer equation to obtain photoexcitation rate in spherical geometry.
FREQ	INPUT	—	Sets of frequency mesh and integration weights for bound-bound transitions.
GETCFS	PWRDEN	FORM1C, FORM1L, FORM3C, FORM3L, CPLC1P, CPLC9P, CPLCFP, CPLCFS, COPACS, LOPACS	Compute zone-to-zone coupling coefficients for all transitions.
GETPOP	STATEQ, POPINI, RATEEQ	LCOEF1, MATRX0, ODESOL, LTEPPZ, RRATES, RRATE2, SFCONS	Computes atomic level populations for all gas species.
GINT5	GPOPAC	—	Computes integrals used for evaluation of Planck opacities.
GINT6	GPOPAC	—	Computes integrals used for evaluation of Rosseland opacities.
GPOPAC	MGOPAC	GINT5, GINT6	Computes Planck and Rosseland opacities for a single group.
INIT1	MAIN	—	Initialize some atomic parameters and print out control switches and constants.
INIT2	STATEQ	—	Initialize radiative transfer parameters.
INIT3	STATEQ, RATEEQ	LINWID, OCPRB0, OCPRB1, OCPRB2, CLOWER	Initialize line profile parameters.

Table 8.1 (Continued)

Subroutine Name	Called By	Calls To	Description
INPUT	MAIN	INPUT3, INPUT4, INPUT5 ZONER, ZONER3 (DATE,) READA1, READA2, FREQ, DFALTS, ANGLE, DHYDRO DHYDR2, RDPLAS, RDEOS0	Input controller routine.
INPUT3	INPUT	NSHELL	Reads in photoionization data.
INPUT4	INPUT	—	Reads in ion beam impact ionization cross sections.
INPUT5	INPUT	—	Reads in Auger rates, fluorescence yields, and ion beam impact ionization cross sections.
IZFRAC	PWRDEN	—	Computes ionization fractions.
IZWNO	MAIN	—	Sets range of ionization stages to be considered for each spatial zone.
JLSODE	LSODE routines	—	Used by LSODE. Computes Jacobian for rate equations.
LCOEF1	GETPOP	—	Sets up statistical equilibrium matrix coefficients.
LINEPR	MAIN, RRATE2, RRATES, SPECT4, SPECT5	VOIGT	Computes line profile parameters.
LINWID	RRATES	WSTARK, OCWITH	Sets up line broadening parameters.
LOCATE	BLCOEF	—	Finds index j such that $x_j < x \leq x_{j+1}$.
LOPACS	GETCFS, RRATES	VOIGT	Computes source functions and opacities for a given line.
LTEPOP	POPINI, STATEQ	—	Computes LTE populations for each zone.
LTEPPZ	GETPOP	—	Computes LTE populations for a single zone
MATRX0	GETPOP	LAPACK routines, OUT3, OUT9	Inverts statistical equilibrium matrix to get atomic level populations for 1 spatial zone.
MESHF2	RRATE2	SORT	Sets up photon energy grid for calculation of detailed photoionization/photoexcitation rates

Table 8.1 (Continued)

Subroutine Name	Called By	Calls To	Description
MESHV	SPECT1, SPECT2, SPECT3	SORT	Sets up photon energy grid for spectral calculations.
MESHMG	MGOPAC	SORT	Sets up photon energy groups for multigroup opacity calculations.
MGOPAC	MAIN	MESHMG, SFCONS, COPACS, GPOPAC	Computes Planck and Rosseland multigroup opacities.
NGACCL	STATEQ	SIMUL	Ng acceleration algorithm.
NSHELL	INPUT3, OCPRB0, OCPRB1, OCPRB2	—	Finds the number of subshells in an atomic configuration.
OCPRB0	INIT3	NSHELL	Determines survival probability for Hummer-Mihalas model.
OCPRB1	INIT3	NSHELL, OCPRFN	Determines survival probability for Hummer-Mihalas model.
OCPRB2	INIT3	NSHELL	Sets occupation probabilities for each level using a cutoff at n_{\max} .
OCPRFN	OCPRB1	—	Used for evaluating the function Q used in occupation probability formalism
OCWITH	LINWID	—	Sets up line broadening parameters for H-like ions at high density.
ODESOL	GETPOP	LSODE subroutines	Solves time-dependent collisional-radiative rate equations.
OPACMG	SPECT5	FINDL	Sets of optical depth and source function grid for high-Z materials.
OPACS	RRATE2, SPECT2, SPECT3, SPECT4, SPECT5	VOIGT	Computes total source function and opacity at each spatial point.
OPACSZ	SPECT5	—	Computes opacities and source functions for a single zone
OPCUW 2	SPECT5	BLCOEF, BILIN2, BILIN3	Does table look-up of high-Z multigroup opacities
OUT1	MAIN, STATEQ	—	Prints out population distributions.

Table 8.1 (Continued)

Subroutine Name	Called By	Calls To	Description
OUT3	MAIN, STATEQ, MATRX0	—	Prints out transition rates.
OUT9	MATRX0	—	Writes out total populating and depopulating rates for each level.
OUTNL1	MAIN	—	Writes out a summary of atomic rates (used for NLTE Kinetics Workshop).
POPINI	MAIN	LTEPOP, ELDIST, RATCOF, RATBEM, GETPOP	Initializes atomic level populations.
PCOUMB	EOS2	—	Calculates Debye-Huckel correction term to plasma pressure.
PWRDEN	MAIN	IZFRAC, SFCONS, GETCFS, SORT2	Computes line and bound-free power densities for radiation escaping the plasma.
RATBEM	STATEQ, POPINI, RATEEQ	—	Calculates ion beam impact ionization rate coefficients.
RATCOF	STATEQ, POPINI, RATEEQ	CEXRAT, CIZRAT	Calculates collisional and radiative rate coefficients.
RATEEQ	MAIN	INIT3, ELDIST, RATCOF, RATBEM, GETPOP	Computes atomic level populations by solving time-dependent rate equations.
RDEOS0	INPUT	—	Reads in EOS/multigroup opacity tables for high-Z materials.
RDPLAS	INPUT	—	Reads in atomic data.
READA1	INPUT	DTABLE	Reads in time-dependent plasma conditions.
READA2	INPUT	—	Reads in atomic data.
RITFLX	SPECT1, SPECT2, SPECT3,	—	Writes spectral fluxes, intensities, and optical depths to plot files.

Table 8.1 (Continued)

Subroutine Name	Called By	Calls To	Description
RRATE2	GETPOP	LINEPR, MESHF2, SFCONS, OPACS, SHORTC, FINTGS	Computes radiation field-dependent rate coefficients; includes overlapping transitions and external radiation sources (b.c.).
RRATES	GETPOP	FORM1C, FORM1L, FORM3C, FORM3L, CPLC1P, CPLC9P, CPLCFP, CPLCFS, CLSLAB, COPACS, LOPACS, VOIGT, LINEPR	Computes radiation-dependent rate coefficients.
SFCONS	MGOPAC, PWRDEN, GETPOP, RRATE2, SPECT2, SPECT3, SPECT4, SPECT5	—	Sets up parameters for source function calculations.
SHIFTT	MAIN	—	Updates arrays for collisional-radiative calculation at next simulation time.
SHORTC	RRATE2, SPECT4, SPECT5	—	Solves radiative transfer equation using method of short characteristics
SIMUL	NGACCL	—	Solves a set of linear equations (for small matrices only).
SORT	MESHHV, MESHMG, MESHF2	—	Sorting algorithm.
SORT2	PWRDEN	—	Sorting algorithm.
SPECT1	MAIN	VOIGT, MESHHV, FESCAP, RITFLX	Computes spectrum using escape probability radiative transfer model.
SPECT2	MAIN	MESHHV, SFCONS, OPACS, FLUXNU, FEAUT1, RITFLX	Computes spectrum using multiangle, multifrequency radiative transfer model.

Table 8.1 (Continued)

Subroutine Name	Called By	Calls To	Description
SPECT3	MAIN	MESHHV, SFCONS, OPACS, FEAUT1, RITFLX	Computes emission spectrum along specified line of sight.
SPECT4	MAIN	LINEPR, MESHHV, SFCONS, OPACS, SHORTC, RITFLX	Computes spectrum using method of short characteristics
SPECT5	MAIN	LINEPR, MESHHV, OPCUW2, SFCONS, OPACSZ, OPACMG, SHORTC, RITFLX	Computes spectrum using method of short characteristics; includes option for high-Z multigroup opacities.
STATEQ	MAIN	INIT2, INIT3, RATCOF, ELDIST, RATBEM, GETPOP, NGACCL, OUT1, OUT3, LTEPOP	Determines distribution of atomic populations from self-consistent solution of statistical equilibrium equations and radiation field.
TDEPPL	MAIN	—	Sets up time-dependent, space-dependent plasma conditions.
VOIGT	FORM1L, FORM3L, LINEPR, LOPACS, OPACS, OPACSZ, RRATES, SPECT1	—	Compute Voigt line profile.
WSTARK	LINWID	AVG	Computes Stark width for a given line.
YVALUE	AVG	Several internal routines	Routines used to compute Gaunt factors for Stark broadening.
ZONER	INPUT	—	Sets up spatial zoning.
ZONER3	INPUT	—	Sets up region-based spatial zoning.

9. Common Blocks

Listed in Table 9.1 are the common blocks used in NLTE. For each common block, the variable name, type, dimensions, and a brief description of each variable is provided. In most cases, the dimensions of variables are specified by quantities defined in parameter statements. These parameters are:

Parameter	Description
MXLVLS	Maximum number of atomic levels
MXTRNS	Maximum number of atomic transitions
MXGASS	Maximum number of gas species
MXIONZ	Maximum number of ionization stages (per gas species)
MXLVLI	Maximum number of levels in atomic data file
MXPHOT	Maximum number of frequency points in spectral calculation
MXZONS	Maximum number of spatial zones
MXREGN	Maximum number of regions used for zoning
MXDATT	Maximum number of temperatures in rate coefficient tables
MXDATD	Maximum number of electron densities in rate coefficient tables
MXDATE	Maximum number of beam energies in ion impact cross section table
MXANGL	Maximum number of angles in radiative transfer calculation
MXFREQ	Maximum number of frequency points per line
MXIMPS	Maximum number of impact parameter rays in spherical radiative transfer calculation
MXSSHL	Maximum number of atomic subshells
MXGRPS	Maximum number of groups for multigroup opacity calculation.
MXTTAB	Maximum number of temperatures in EOS tables
MXDTAB	Maximum number of densities in EOS tables
MXMATR	Maximum number of materials in EOS/opacity tables
MXTTBO	Maximum number of temperatures in multigroup opacity tables
MXDTBO	Maximum number of densities in multigroup opacity tables
MXGTAB	Maximum number of frequency groups in opacity look-up tables
MXTIMS	Maximum number of time steps
MXHEBN	Maximum number of hot electron energy bins
MXMGFS	Maximum number of groups for computed multigroup opacities

Table 9.1. Common Blocks

COMMON/ATDATA/

Variable	Type	Dimensions	Units	Description
TEMIN	R*8	MXGASS	eV	Minimum electron temperature for rate coefficient grid
DLOGTE	R*8	MXGASS	—	Logarithmic increment (base 10) of electron temperature for rate coefficient grid
DEMIN	R*8	MXGASS	cm ⁻³	Minimum electron density for rate coefficient grid
DLOGDE	R*8	MXGASS	—	Logarithmic increment (base 10) of electron density for rate coefficient grid
CLDEXA	R*4	MXDATT, MXTRNS	cm ³ s ⁻¹	Collision excitation rate coefficient due to thermalized electrons
SPNEMA	R*8	MXTRNS	s ⁻¹	Spontaneous emission rate
CLRECA	R*4	MXDATT, MXTRNS	cm ⁶ s ⁻¹	Collisional recombination rate coefficient due to thermalized electrons
RDRECA	R*4	MXDATT, MXTRNS	cm ³ s ⁻¹	Radiative recombination rate coefficient
DIELRA	R*4	MXDATT, MXDATD, MXTRNS	cm ³ s ⁻¹	Dielectronic recombination rate coefficient
AUTIZA	R*4	MXTRNS	s ⁻¹	Autoionization rate coefficient
AUTOTT	R*8	MXLVLS,	s ⁻¹	Total autoionization rate from a given level
FLOYLD	R*8	MXLVLS	—	Fluorescence yield
NDATTE	I*4	MXGASS	—	Number of points in temperature grid of atomic data file
NDATDE	I*4	MXGASS	—	Number of points in electron density grid of atomic data file

Values for the above variables are read in from ATBASE files and stored.

COMMON/ATOMIC/

Variable	Type	Dimensions	Units	Description
ATOMWT	R*8	MXGASS	amu	Atomic weight
FRACSP	R*8	MXZONS, MXGASS	—	Fractional abundance (by number density) of each gas species
STATWT	R*8	MXLVLS	—	Statistical weight
ENERGY	R*8	MXLVLS	eV	Atomic level energy measured relative to fully ionized
EREFER	R*8	MXGASS	eV	Reference energy for equation of state calculation
ENBIND	R*8	MXLVLS, MXSHEL	a.u. (=27.2 eV)	Electron binding energy used for Stark width calculation
ELRADM	R*8	MXLVLS, MXSSHL	a.u.	Mean orbital radius
STRKR2	R*8	MXLVLS, MXSSHL	a.u. (= a_0)	Electron mean squared orbital radius for Stark width calculation
STRKDE	R*8	MXLVLS	a.u.	Energy to nearest level for Stark width calculation
STARKF	R*8	MXLVLS	—	Gaunt factor parameter for Stark width calculation
STKRI	R*8	MXLVLS	a.u.	Orbital radius of level of interest for Stark width calculation
STKRIP	R*8	MXLVLS	a.u.	Orbital radius of nearest level for Stark width calculation
XJQN	R*8	MXLVLS	—	“J” quantum number
GTOTCF	R*8	MXLVLS	—	Total statistical weight for a configuration
NLEVLS	I*4	—	—	Total number of atomic levels
IONSTG	I*4	MXLVLS	—	Ionization stage (1 \Rightarrow neutral)
IGROUN	I*4	MXGASS, MXIONZ	—	Level index of ground state for each ion
NGASES	I*4	—	—	Number of gas species

COMMON/ATOMIC/ (Continued)

Variable	Type	Dimensions	Units	Description
LKMIN	I*4	MXGASS	—	Index of first (lowest) energy level for each gas species
LKMAX	I*4	MXGASS	—	Index of last (highest) energy level for each gas species
NLEVLK	I*4	MXGASS	—	Number of energy levels for each gas species
IREADA	I*4	MXGASS	—	Flag indicating format of atomic data file
LKJMIN	I*4	MXGASS, MXIONZ	—	Index for first (lowest) energy level for each ion
LKJMAX	I*4	MXGASS, MXIONZ	—	Index of last (highest) energy level for each ion
IZGAS	I*4	MXGASS,	—	Atomic number of each gas
KGAS	I*4	MXLVLS	—	Gas species index
LCONFIG	I*4	MXLVLS	—	Index of electronic configuration
LMINZN	I*4	MXZONS, MXGASS	—	Index of lowest energy level for each gas in each zone
LMAXZN	I*4	MXZONS, MXGASS	—	Index of highest energy level for each gas in each zone
NLEVZN	I*4	MXZONS, MXGASS	—	Index of energy levels for each gas in each zone
ICONTL	I*4	—	—	Flag for continuum lowering model

COMMON/ATRANS/

Variable	Type	Dimensions	Units	Description
ETRANS	R*8	MXTRNS	eV	Transition energy
OSCSTR	R*8	MXTRNS	—	Oscillator strength
PROFLC	R*8	MXZONS, MXTRNS	Hz ⁻¹	Value of line profile at line center ($\int \phi_\nu d\nu = 1$)
AVOIGT	R*8	MXZONS, MXTRNS	—	Voigt profile damping parameter
PHINU0	R*4	MXZONS,	—	Value of Voigt function $H(a, v)$ at line center
TAUTOT	R*8	MXTRNS	—	Total optical depth for each transition
EFFCHG	R*8	MXTRNS	—	Effective charge of target ion undergoing excitation
WIDNAT	R*8	MXTRNS	eV	Natural line width
WIDDOP	R*8	MXTRNS	eV ^{3/2}	Doppler line width
WIDSTK	R*8	MXZONS, MXTRNS	eV ^{3/2} cm ³	Stark line width
WIDION	R*8	MXZONS, MXTRNS	eV	Stark ion dynamic broadening
ILINEP	I*4	—	—	Line profile type (1 ⇒ Doppler; 2 ⇒ Lorentz; 3 ⇒ Voigt)
ITTYPE	I*4	MXTRNS	—	Transition type (1 ⇒ bound-bound; 6-10 ⇒ bound-free)
LUPPER	I*4	MXTRNS	—	Upper level index of transition
LLOWER	I*4	MXTRNS	—	Lower level index of transition
NSUBSH	I*4	MXTRNS	—	Number of electrons in lower-state subshell undergoing excitation
NTRANS	I*4	—	—	Total number of transitions
MINTRN	I*4	MXGASS	—	Minimum transition index of gas
MAXTRN	I*4	MXGASS	—	Maximum transition index of gas
MXIZCH	I*4	—	—	Maximum change in ionization state considered for bound-free transitions
LTRANS	I*2	MXLVLS, MXLVLS	—	Transition index for (upper, lower) levels

COMMON/CLOCAL/

Variable	Type	Dimensions	Units	Description
AMATF	R*8	MXLVLS+1, MXLVLS+1	—	Coefficients for statistical equilibrium matrix

COMMON/CMATRIX/

AMAT1	R*8	MXLVLS+1, MXLVLS+1	—	Coefficients for statistical equilibrium matrix
-------	-----	-----------------------	---	---

COMMON/CONSTS/

Variable	Type	Dimensions	Units	Description
HPLANK	R*8	—	eV s	Planck's constant
BOLTZK	R*8	—	—	Boltzmann's constant
CLIGHT	R*8	—	cm s ⁻¹	Speed of light
AMUMAS	R*8	—	g	Atomic mass unit
ELMASS	R*8	—	g	Electron mass
SIGMSB	R*8	—	erg cm ⁻² s ⁻¹ eV ⁻⁴	Stefan-Boltzmann constant
ERG2EV	R*8	—	eV erg ⁻¹	erg-to-eV conversion constant
EV2ANG	R*8	—	Å eV ⁻¹	eV-to-angstrom conversion constant
XSECES	R*8	—	cm ²	Electron (Thomson) scattering cross section
RYDBRG	R*8	—	eV	Rydberg (= 13.6 eV)
AVGDRO	R*8	—	—	Avogadro's number
ZERO	R*8	—	—	Zero
ONE	R*8	—	—	One
TWO	R*8	—	—	Two
HALF	R*8	—	—	One-half
THIRD	R*8	—	—	One-third
SIXTH	R*8	—	—	One-sixth
PI	R*8	—	—	π
FOURPI	R*8	—	—	4π
SQRTPI	R*8	—	—	$\pi^{1/2}$
SPIINV	R*8	—	—	$\pi^{-1/2}$

COMMON/CONTRL/

Variable	Type	Dimensions	Units	Description
CON	R*8	100	—	Array of constants (see Table 6.2)
XMUBAR	R*8	—	—	Mean cosine angle for escape probability model
XMULOS	R*8	—	—	Cosine angle of line-of-sight for emergent flux calculation
ERRMXF	R*8	—	—	Maximum fractional error in atomic level populations
RATMIN	R*8	—	—	Minimum value for rate coefficients (≈ 0)
TELTE	R*8	—	eV	Temperature below which LTE populations are assumed
RTOLLS	R*8	—	—	Relative tolerance parameter for LSODE
ATOLLS	R*8	—	—	Absolute tolerance parameter for LSODE
NGCYCL	I*4	—	—	Apply Ng acceleration every NGCYCL'th cycle
NGORDR	I*4	—	—	Order of Ng acceleration
NGBEGN	I*4	—	—	Iteration cycle to begin Ng acceleration
IZONPQ	I*4	—	—	Zone index used when printing out Voigt parameter and quenching coefficient
MFLS	I*4	—	—	Method flag for LSODE
IMAXSE	I*4	—	—	Maximum number of iterations for statistical equilibrium cycle
ISW	I*4	100	—	Array of switches (see Table 6.3)
IPLOT	I*4	30	—	Array of switches (see Section 6)
IEDIT	I*4	100	—	Array of debug switches (see Table 6.4)
IBENCH	I*4	20	—	Switch for benchmarking calculations

COMMON/ELHOT/

Variable	Type	Dimensions	Units	Description
EMINHE	R*8	—	eV	Minimum energy of hot electron distribution
EMAXHE	R*8	—	eV	Maximum energy of hot electron distribution
FRACHE	R*8	MXZONS	—	Hot electron fraction (n_e^{hot}/n_e)
THOTEL	R*8	MXZONS	eV	Hot electron temperature (when using Maxwellian distribution for hot component)
EBINBD	R*8	MXHEBN+1	eV	Hot electron energy bin boundaries
VBINBD	R*8	MXHEBN+1	cm/s	Hot electron velocity bin boundaries
HEDENS	R*8	MXHEBN, MXZONS	cm ⁻³	Hot electron density
NBINHE	I*4	—	—	Number of hot electron energy bins

COMMON/EOSCOM/

Variable	Type	Dimensions	Units	Description
ZTAB	R*8	MXTTAB, MXDTAB, MXMATR	esu	EOS table for mean charge state
DZDTAB	R*8	same as above	esu/eV	EOS table for (dZ/dT)
ENTAB	R*8	same as above	J/g	EOS table for specific ion internal energy
ENTTAB	R*8	same as above	J/g/eV	EOS table for $(\partial E_{\text{ion}}/\partial T)$
ENNTAB	R*8	same as above	eV ⁻¹	EOS table for scaled $(\partial E_{\text{ion}}/\partial \rho)$
EETAB	R*8	same as above	J/g	EOS table for specific electron internal energy
EETTAB	R*8	same as above	J/g/eV	EOS table for $(\partial E_e/\partial T)$
PNTAB	R*8	same as above	J/cm ³	EOS table for ion pressure
PNTTAB	R*8	same as above	J/cm ³ /eV	EOS table for $(\partial E_{\text{ion}}/\partial T)$
PETAB	R*8	same as above	J/cm ³	EOS table for electron pressure
PETTAB	R*8	same as above	J/cm ³ /eV	EOS table for $(\partial P_e/\partial T)$
RRTAB	R*8	MXGTAB, MXTTAB, MXDTAB, MXMATR	cm ² /g	Rosseland opacity table
RPTAB	R*8	same as above	cm ² /g	Planck opacity table (absorption)
RPETAB	R*8	same as above	cm ² /g	Planck opacity table (emission)

COMMON/EOSCOM/

Variable	Type	Dimensions	Units	Description
ADTAB	R*8	MXMATR	—	ρ -increment for EOS table
ATTAB	R*8	MXMATR	—	T -increment for EOS table
BDTAB	R*8	MXMATR	—	\log_{10} of ρ_{\min} in EOS table
BTTAB	R*8	MXMATR	—	\log_{10} of T_{\min} in EOS table
RADTAB	R*8	MXMATR	—	ρ -increment for opacity table
RATTAB	R*8	MXMATR	—	T -increment for opacity table
RBDTAB	R*8	MXMATR	—	\log_{10} of ρ_{\min} in opacity table
RBTTAB	R*8	MXMATR	—	\log_{10} of T_{\min} in opacity table
TMPTAB	R*8	MXTTAB, MXMATR,5	eV	Temperature grid for SESAME EOS table
RHOTAB	R*8	MXTTAB, MXMATR,5	g/cm ³	Density grid for SESAME EOS table
RADCON	R*8	MXMATR,3	—	Multiplier for opacities
TTBEOS	R*8	MXTTAB, MXMATR	eV	Temperature grid for EOSOPA EOS table
DTBEOS	R*8	MXDTAB, MXMATR	cm ⁻³	Ion density grid for EOSOPA EOS table
TTBOPC	R*8	MXTTAB, MXMATR	eV	Temperature grid for EOSOPA opacity table
DTBOPC	R*8	MXDTAB, MXMATR	cm ⁻³	Ion density grid for EOSOPA opacity table

COMMON/EOSCOM/

Variable	Type	Dimensions	Units	Description
HNUEOS	R*8	MXGTAB	eV	Photon energies at mid-points of multigroup opacity bins
ATWMAT	R*8	MXMATR	amu	Mean atomic weight of EOS material
NTTAB	I*4	MXMATR	—	Number of temperatures in EOS table
NDTAB	I*4	MXMATR	—	Number of densities in EOS table
NTTABO	I*4	MXMATR	—	Number of temperatures in opacity table
NDTABO	I*4	MXMATR	—	Number of densities in opacity table
NTMPTB	I*4	MXMATR,5	—	Number of temperatures in SESAME EOS table
NRHOTB	I*4	MXMATR,5	—	Number of densities in SESAME EOS table
IZEOS	I*4	MXMATR	—	File identifier for EOS/opacity tables
IDEOS	I*4	MXMATR	—	Flag indicating format of EOS look-up table
IDOPAC	I*4	MXMATR	—	Flag indicating format of opacity look-up table
NMATRS	I*4	—	—	Number of EOS/opacity materials to read in
NFG	I*4	—	—	Number of frequency groups in opacity look-up table

COMMON/FILUNS/

LUN	I*4	100	—	Logical unit numbers of input and output files
FNAMES	C*16	100	—	File names of input and output files

COMMON/GRID/

Variable	Type	Dimensions	Units*	Description
RADIUS	R*8	MXZONS+1	cm	Spatial zone boundaries
DRAD	R*8	MXZONS	cm	Zone width
RBAR	R*8	MXZONS	cm	Position of zone midpoint
DRAY	R*8	MXZONS, MXZONS	—	Parameters used in escape probability model
DDRAY	R*8	MXZONS, MXZONS	—	Parameters used in escape probability model
DRAYS	R*8	MXZONS, MXZONS	—	Parameters used in escape probability model
DDRAYS	R*8	MXZONS, MXZONS	—	Parameters used in escape probability model
XNEONA	R*8	MXZONS, MXZONS MXGASS	—	Ratio of number of atoms in emitting zone to that in absorbing zone
VOLZON	R*8	MXZONS	cm ^α	Volume in each spatial zone
VOLTOT	R*8	—	cm ^α	Total volume of plasma
GEOMA	R*8	3	—	(1,2π,4π) for IGEOM = (1,2,3)
GEOMV	R*8	3	—	(1,π,4π/3) for IGEOM = (1,2,3)
DELROZ	R*8	MXZONS, MXIMPS	—	(Δr/Δz) for spherical radiative transfer calculation
BMURAD	R*8	MXZONS+1, MXIMPS	—	Cosine angle for flux calculation

COMMON/GRID/ (Continued)

Variable	Type	Dimensions	Units*	Description
WTINT0	R*8	MXIMPS, MXZONS	—	Angle integration weights for mean intensity calculation
WTFLX0	R*8	MXIMPS, MXZONS+1	—	Angle integration weights for flux calculation
NZONES	I*4	—	—	Number of spatial zones
IGEOM	I*4	—	—	Geometry index*
KMINCP	I*4	MXZONS	—	Zone indexing parameters for coupling coefficient calculation
KMINCS	I*4	MXZONS	—	Zone indexing parameters for coupling coefficient spectral calculation
NREGNS	I*4	—	—	Number of zoning regions
NZONRG	I*4	MXREGN	—	Number of zones in each region
IREGZN	I*4	MXZONS	—	Region index of each zone
IHIGHZ	I*4	MXZONS	—	Material index of EOS/opacity look-up table
NCRAD	I*4	—	—	Number of impact parameters within “core”
NDRAD	I*4	—	—	Number of impact parameters outside “core” (= NZONES+1)
NPRAD	I*4	—	—	Total number of impact parameters (for spherical RT calculation)
NIRAD	I*4	MXIMPS	—	Number of points along each impact parameter

$$*\alpha = \text{IGEOM} = \begin{cases} 1 & \text{planar} \\ 2 & \text{cylindrical} \\ 3 & \text{spherical} \end{cases}$$

COMMON/GRIDF/

Variable	Type	Dimensions	Units	Description
XFREQ	R*8	MXFREQ	—	Frequency mesh for line transport calculation (in Doppler widths)
WTFREQ	R*8	MXFREQ	—	Weights for frequency integration
WTANGL	R*8	MXANGL	—	Weights for angle integration
XMU	R*8	MXANGL	—	Angle mesh for radiative transfer calculation
TRADB1	R*8	—	eV	Radiation boundary temperature (first zone) when using <code>-RRATE2-</code>
TRADBN	R*8	—	eV	Radiation boundary temperature (last zone) when using <code>-RRATE2-</code>
HVMINR	R*8	—	eV	Minimum photon energy used in computing detailed photoexcitation/photoionization rates
HVMAXR	R*8	—	eV	Maximum photon energy used in computing detailed photoexcitation/photoionization rates
NFLINE	I*4	—	—	Number of frequency points for line transport calculation
NFCORE	I*4	—	—	Number of frequency points in line “core” of Voigt profile
NFPIZ0	I*4	—	—	Number of frequency points for photoionization rate calculation
NANGLE	I*4	—	—	Number of angle points for radiative transfer calculation
NFRQFR	I*4	—	—	Number of frequency points used in computing photoexcitation/photoionization rates with <code>-RRATE2-</code>

COMMON/IBEAM/

Variable	Type	Dimensions	Units	Description
EBEAM	R*8	MXZONS	MeV	Ion beam energy (velocity)
CURDEN	R*8	MXZONS	MA cm ⁻²	Ion beam current density
BIXSEC	R*4	MXDATE, MXTRNS	cm ²	Beam impact ionization cross section
EBMMIN	R*8	MXGASS	MeV	Minimum beam energy for beam ionization cross section grid
DLOGEB	R*8	MXGASS	—	Logarithmic increment (base 10) of beam energy for cross section grid
IZBEAM	I*4	—	—	Beam atomic number
ISTGBM	I*4	—	—	Beam ionization stage (1 ⇒ neutral)
NDATEB	I*4	MXGASS	—	Number of beam energy points in beam ionization cross section grid

COMMON/OPACMG/

EGRPBD	R*8	MXGRPS+1	eV	Photon energy group boundaries for multigroup opacity calculation
NGRUPS	I*4	—	—	Number of photon energy groups

COMMON/PIXSEC/

HVEDGE	R*4	MXTRNS	eV	Energy of photoionization edge ($h\nu_1$)
PIXS0	R*4	MXTRNS	cm ²	Photoionization cross section at threshold
PIBETA	R*4	MXTRNS	—	“ β ” in cross section fit*
PISEXP	R*4	MXTRNS	—	“s” in cross section fit*
MNHVPI	I*4	MXTRNS	—	Minimum photon energy index such that $\nu \geq \nu_1$

*Photoionization cross sections are fit to:

$$\alpha(\nu) = \alpha(\nu_1) \left\{ \beta \left(\frac{\nu_1}{\nu} \right)^s + (1 - \beta) \left(\frac{\nu_1}{\nu} \right)^{s+1} \right\}, \quad \nu \geq \nu_1.$$

COMMON/POPULS/

Variable	Type	Dimensions	Units	Description
POPSAV	R*4	MXLVLS, MXZONS, 6	—	Saved values of fractional level populations from previous (up to 6) iterations
POPLTE	R*8	MXLVLS, MXZONS	—	LTE populations
POPBEQ	R*8	MXLVLS	—	Initial populations in time-dependent collisional-radiative calculation
OCPROB	R*8	MXLVLS, MXZONS	—	Level-dependent occupation probability
DECLOW	R*4	MXLVLS, MXZONS	eV	Effective ΔE due to continuum lowering

COMMON/RADCFS/

CCCFS	R*8	MXZONS, MXTRNS	—	“Residual” of Λ -operator
CCFS1	R*8	MXZONS, MXTRNS	—	“Diagonal” of Λ -operator
PHOTUP	R*8	MXZONS, MXTRNS	s ⁻¹	Photoexcitation or photoionization rate
PHOTDN	R*8	MXZONS, MXTRNS	s ⁻¹	Stimulated emission or recombination rate
SPONRC	R*8	MXZONS, MXTRNS	cm ³ s ⁻¹	Spontaneous recombination rate coefficient

COMMON/RADTRN/

CCOEFS	R*8	MXZONS, MXZONS	—	Zone-to-zone coupling coefficients
TAU	R*8	MXZONS+1	—	Optical depth integrated from plasma surface
DTAU	R*8	MXZONS	—	Optical depth for each zone

COMMON/RATCFS/

COLLUP	R*8	MXZONS, MXTRNS	$\text{cm}^3 \text{s}^{-1}$	Collisional excitation or ionization rate coefficient
COLLDN	R*8	MXZONS, MXTRNS	$\text{cm}^3 \text{s}^{-1}$	Collisional deexcitation or recombination rate coefficient
RADREC	R*8	MXZONS, MXTRNS	$\text{cm}^3 \text{s}^{-1}$	Radiative recombination rate coefficient
DIELRC	R*8	MXZONS, MXTRNS	$\text{cm}^3 \text{s}^{-1}$	Dielectronic recombination rate coefficient
ELCAPT	R*8	MXZONS, MXTRNS	$\text{cm}^3 \text{s}^{-1}$	Electron capture rate coefficient
BIMPUP	R*8	MXZONS, MXTRNS	s^{-1}	Ion beam impact ionization or excitation rate
CLUPHE	R*8	MXZONS, MXTRNS	s^{-1}	Collisional ionization or excitation rate coefficient due to hot electrons
CLDNHE	R*8	MXZONS, MXTRNS	s^{-1}	Collisional recombination or deexcitation due to hot electrons
SPONEM	R*8	MXTRNS	s^{-1}	Spontaneous emission rate
EINBLU	R*8	MXTRNS,	$\text{cm}^2 \text{eV}^{-1} \text{s}^{-1}$	Einstein coefficient B_{lu}
EINBUL	R*8	MXTRNS,	$\text{cm}^2 \text{eV}^{-1} \text{s}^{-1}$	Einstein coefficient B_{ul}
AUTOIZ	R*8	MXTRNS,	s^{-1}	Autoionization rate

COMMON/SFNCON/

Variable	Type	Dimensions	Units	Description
CONABS	R*8	MXZONS, MXTRNS	cm ⁻³	Source function absorption constant
CONEMS	R*8	MXZONS, MXTRNS	eV ⁻² cm ⁻⁵	Source function emission constant
FFCONA	R*8	MXZONS	cm ⁻¹	Free-free absorption constant
FFCONE	R*8	MXZONS	eV ⁻² cm ⁻³	Free-free emission constant
CONLTE	R*8	MXZONS	—	Bound-free constant

COMMON/SPECTR/

HVMIN	R*8	—	eV	Minimum photon energy of spectral calculation
HVMAX	R*8	—	eV	Maximum photon energy of spectral calculation
NFRQFF	I*4	—	—	Number of continuum photon energy points in spectral grid

COMMON/STRING/

CONFIG	C*130	MXLVLS	—	Atomic configuration
TRMSYM	C*10	MXLVLS	—	Atomic term symbol

COMMON/TDPLAS/

TIMSIM	R*8	MXTIMS	s	Simulation time array for time-dependent collisional-radiative calculation
TIMEND	R*8	—	s	End time of time-dependent collisional-radiative calculation
TEMPTB	R*8	MXTIMS	eV	Time-dependent electron temperatures read in from file
EDENTB	R*8	MXTIMS	cm ⁻³	Time-dependent electron densities read in from file
TIMETB	R*8	MXTIMS	s	Time grid for T_e , n_e read in from file
DTIMTB	R*8	MXTIMS	s	Δt based on TIMSIM
TETABL	R*8	MXTIMS, 5	—	T_e divided-difference table
EDTABL	R*8	MXTIMS, 5	—	n_e divided-difference table
NTIMTB	I*4	—	—	Number of times for T_e , n_e read in from file
NTIMES	I*4	—	—	Number of simulation times for time-dependent collisional-radiative model.

COMMON/THERMO/

TEMPEL	R*8	MXZONS	eV	Electron temperature
TMPION	R*8	MXZONS	eV	Ion temperature
DENSNN	R*8	MXZONS	cm ⁻³	Ion number density
DENSNE	R*8	MXZONS	cm ⁻³	Electron density
AVGATW	R*8	MXZONS	—	Average atomic weight

10. Sample Calculations

10.1. Example 1: Thermal Spectrum for Aluminum

The first example is for a planar Al plasma with an ion density of $n = 10^{20} \text{ cm}^{-3}$, a temperature of $T = 30 \text{ eV}$, and a slab width of 0.012 cm . This corresponds to a $0.2 \text{ }\mu\text{m}$ -thick solid density foil which has expanded by a factor of 600. Under these conditions, the plasma populations are close to LTE (within about a factor of 2), but the plasma is not thick enough for the spectrum to be that of a blackbody. (If the plasma were optically thick ($\tau_\nu \gg 1$) at all frequencies the spectrum of an LTE plasma would be a blackbody spectrum.) The input file is shown in Fig. 10.1, while the calculated emission spectrum is shown in Fig. 10.2. The frequency-dependence of the optical depth is shown in Fig. 10.3.

10.2. Example 2: 2-Level Atom

Figure 10.4 shows the input file for a 2-level atom calculation in spherical geometry. The bound-bound transition corresponds to the Ly_α line of Al ($h\nu = 1.728 \text{ keV}$). The plasma temperature, density, and radius were chosen to give a value of the scattering (or “quenching”) parameter of $\varepsilon = 10^{-4}$ and line center optical depth of 5.64×10^1 . The line is specified to have a Doppler profile. The multifrequency radiative transfer model is used in this case (ISW(5) = 1). The number of spatial grid points is 40.

The spatial distribution of the source function is shown in Fig. 10.5 for 2 cases: $\tau_{\text{max}} = 5.64 \times 10^3$ and 56.4 . The results are in good agreement with previously published calculations [56].

10.3. Example 3: K_α Absorption Spectrum for Aluminum

The input file for calculation of an Al K_α absorption spectrum is shown in Fig. 10.6. The plasma conditions are: $T = 58 \text{ eV}$, $\rho = 0.02 \text{ g/cm}^3$, and the plasma thickness is $6.75 \text{ }\mu\text{m}$ (which correspond to a 500 \AA foil which has expanded by a factor of 135). The atomic level populations are calculated in the LTE approximation (ISW(6) = 3). The calculated absorption spectrum (transmission $\equiv \exp(-\tau_\nu)$) is shown in Fig. 10.7. Results from calculations of this type are in good agreement with experimental data for laser-produced plasmas [7].

10.4. Example 4: Time-Dependent Carbon Recombination

Figure 10.8 shows the input file for a time-dependent collisional-radiative calculation of the recombination of fully ionized carbon. ISW(1)=1 specifies this is a time-dependent C-R calculation. The time grid is uniformly spaced (logarithmically), and runs up to 10 ns. ICONTL=0 specifies the default occupation probability continuum lowering model is to be used. There is one zone, no radiative transfer effects, and a constant temperature of 2 eV and ion density of 10^{19} ions/cm³. The initial state of the carbon is fully ionized (ISELCT(512,1)=2). Figure 10.9 shows the mean charge state as a function of time, which was written to file ‘Zbar.vs.time’.

10.5. Example 5: Time-Dependent Argon Plasma With Hot Electrons

The input file for this problem is shown in Figure 10.10. The argon plasma has a constant temperature of 2 eV and ion density of 7×10^{16} ions/cm³. At the start of the simulation, all argon is in the Ar I ground state (ISELCT(1,1)=2). There is only one zone and no radiative transfer effects (ISW(7)=ISW(8)=1). Ion-impact excitation and ionization due to a 9 MeV Li beam with a current density of 0.02 MA/cm² are considered. One percent of the free electrons are in a “hot” component (99% have a thermal, Maxwellian distribution with $T = 2$ eV). The energy distribution of the hot electron component is defined in subroutine ELDIST. For this problem, $f(\varepsilon) = 1/\varepsilon^2$, where ε is the electron kinetic energy. The low energy endpoint is 100 eV, while the high energy endpoint is 2,500 eV. The time-dependent electron density from this simulation is shown in Figure 10.11.

10.6. Example 6: A SiO₂ Cylindrical Plasma Surrounded by Tungsten

Figure 10.12 shows the namelist input file a Z-pinch-related simulation in which a W wire array implodes on a Si aerogel foam. To treat the W radiative properties, multigroup UTA opacities are read in from file ‘eos.dat.us.74’ (IZEOS(1)=74). The emission intensity (resultant spectra) is computed along a single line of sight (ISW(72)=1) which is perpendicular (XMULOS=1) to the cylindrical plasma grid; i.e., it goes through the axis of symmetry). The line spectrum of the Si and O is treated in detail, but in this calculation we assume they have LTE population distributions (ISW(6)=3). There are 12 spatial zones: the inner 6 containing SiO₂, and the outer 6 containing W. The IHIGHZ array specifies that for zones 7 through 12 the opacities will be obtained by table look-up from the file corresponding to high-Z material index 1. The temperature and ion density

in all zones is 100 eV and 2×10^{20} ions/cm³. Subroutine ZONER3 is used (ISW(15)=1) to set up the spatial zoning by region. There are 0.628 mg/cm of SiO₂ and 0.470 mg/cm of W in this cylindrical calculation. The emergent spectrum is shown in Figure 10.13. Figure 10.14 shows the frequency-dependent optical depth for the individual SiO₂ and W regions (along a line-of-sight normal to the plasma grid).

10.7. Example 7: Al K_α Satellite Emission and Absorption Spectra Based on Radiation-Hydrodynamics Output

Figure 10.15 shows the namelist input file for a CRE simulation in which we post-process the output of a radiation-hydrodynamics simulation of a Li beam-heated planar target. The radiation-hydrodynamics results are contained in file ‘bk.CRE.5851-...’. Rad-hydro results for the space-dependent temperature, density, Li beam current, and Li beam kinetic energy at simulation time $t = 20$ ns (con(90)=20) are utilized. In this non-LTE calculation, photoionization rates for the Al are computed using subroutine RRATE2 (ISW(2)=1, ISW(19)=1). A detailed atomic energy level model is used (see ISELCT) to compute the emission and absorption due to K_α satellite transitions ($2p \rightarrow 1s$) and K_β satellite transitions ($3p \rightarrow 1s$). Resultant emission and absorption spectra are shown in Figure 10.16.

```

$input1
c ...                               PLOTTING SWITCHES
    iplot(1) = 1
    iplot(8) = 1, 1
c ...                               SPECTRAL GRID PARAMETERS (energies in eV)
    hvmin = 1.
    hvmax = 2000.
    nflin = 3
    nfrqff = 500
c ...                               MEAN DIFFUSIVITY ANGLE FOR SPECTRAL CALCULATION
    xmulos = .51
c ...                               SPATIAL GRID INFO
    igeom = 1
    nzones = 6
    radmin = 0.
    radmax = 1.2e-2
    dradmn = 1.2e-4
c ...                               TEMPERATURES AND ION DENSITIES
    tempel(1) = 6*30.
    densnn(1) = 6*1.e20
c ...                               ATOMIC DATA PARAMETERS
    ireada(1) = 1
    atomnm = 13.
    atomwt = 27.
    ilinep = 3
c ...                               SELECT LEVELS
c
c ... thermal states                exc.d states to n=2    exc.d states to n=3 (spectator in M-shell)
c -----
c Al I                               iselct( 1,1) = 10*1
c Al II                              iselct( 35,1) = 10*1
c Al III                             iselct( 90,1) = 7*1
c Al IV   Ne-like                    iselct(167,1) = 15*1
c Al V     F-like                     iselct(301,1) = 28*1
c   n=4                               iselct(329,1) = 10*1
c Al VI    O-like                     iselct(536,1) = 48*1
c   n=4                               iselct(586,1) = 40*1
c Al VII   N-like                     iselct(771,1) = 41*1
c   n=4                               iselct(812,1) = 33*1
c Al VIII  C-like                     iselct(921,1) = 34*1
c   n=4                               iselct(955,1) = 12*1
c Al IX    B-like                     iselct(1050,1) = 30*1
c Al X     Be-like                    iselct(1152,1) = 30*1
c Al XI    Li-like                    iselct(1269,1) = 6*1
c Al XII   He-like                    iselct(1327,1) = 13*1
c Al XIII  H-like                     iselct(1362,1) = 1
c Al XIV   Fully Ionized              iselct(1382,1) = 0
$end

```

Figure 10.1. Namelist input for Example 1.

Aluminum Emission Spectrum
 $T = 30 \text{ eV}$, $n = 10^{20} \text{ cm}^{-3}$, $L_{\text{orig}} = 0.2 \mu\text{m}$

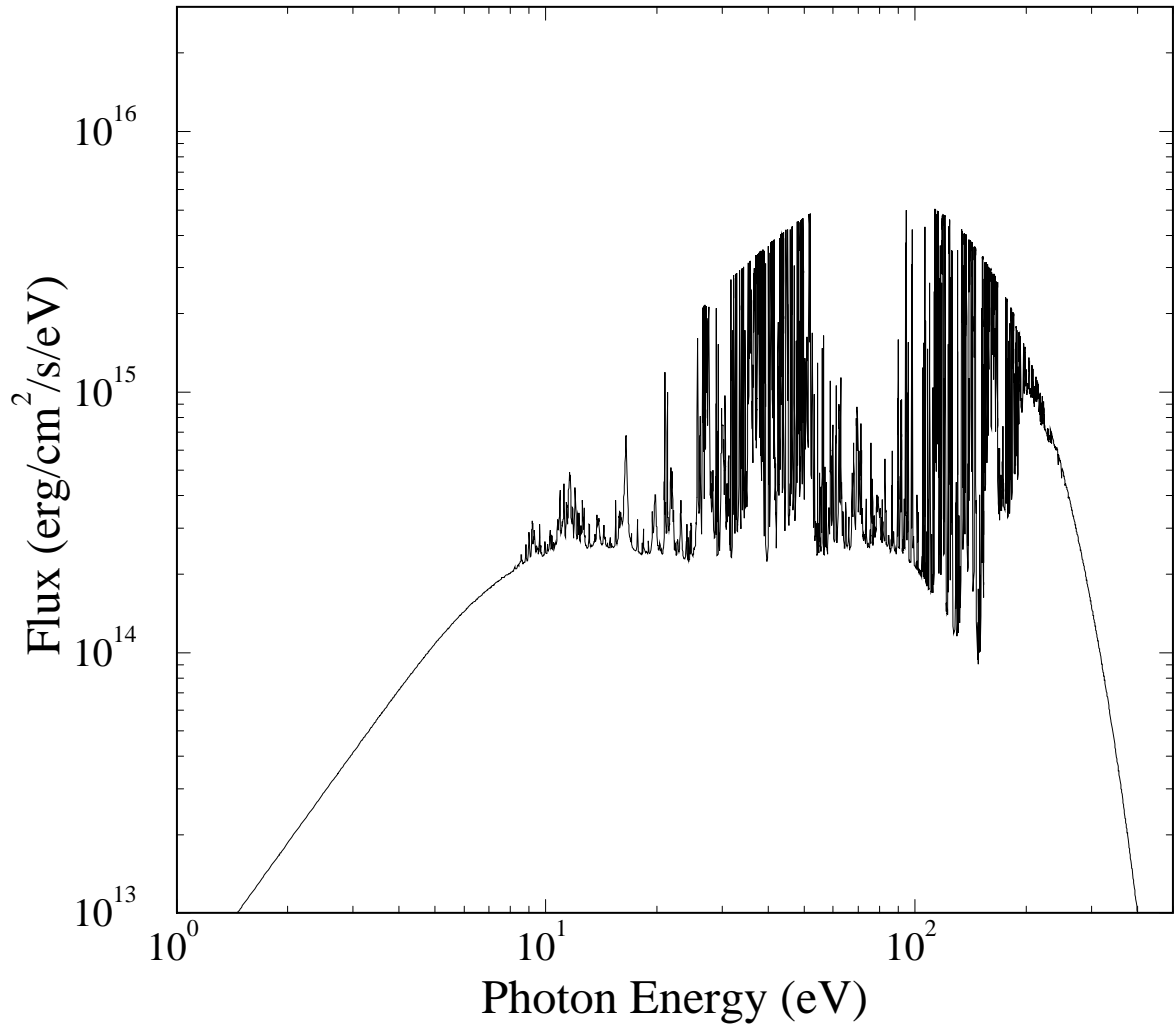


Figure 10.2. Emission spectrum for Example 1.

Aluminum Optical Depth vs. Frequency
 $T = 30 \text{ eV}$, $n = 10^{20} \text{ cm}^{-3}$, $L_{\text{orig}} = 0.2 \mu\text{m}$

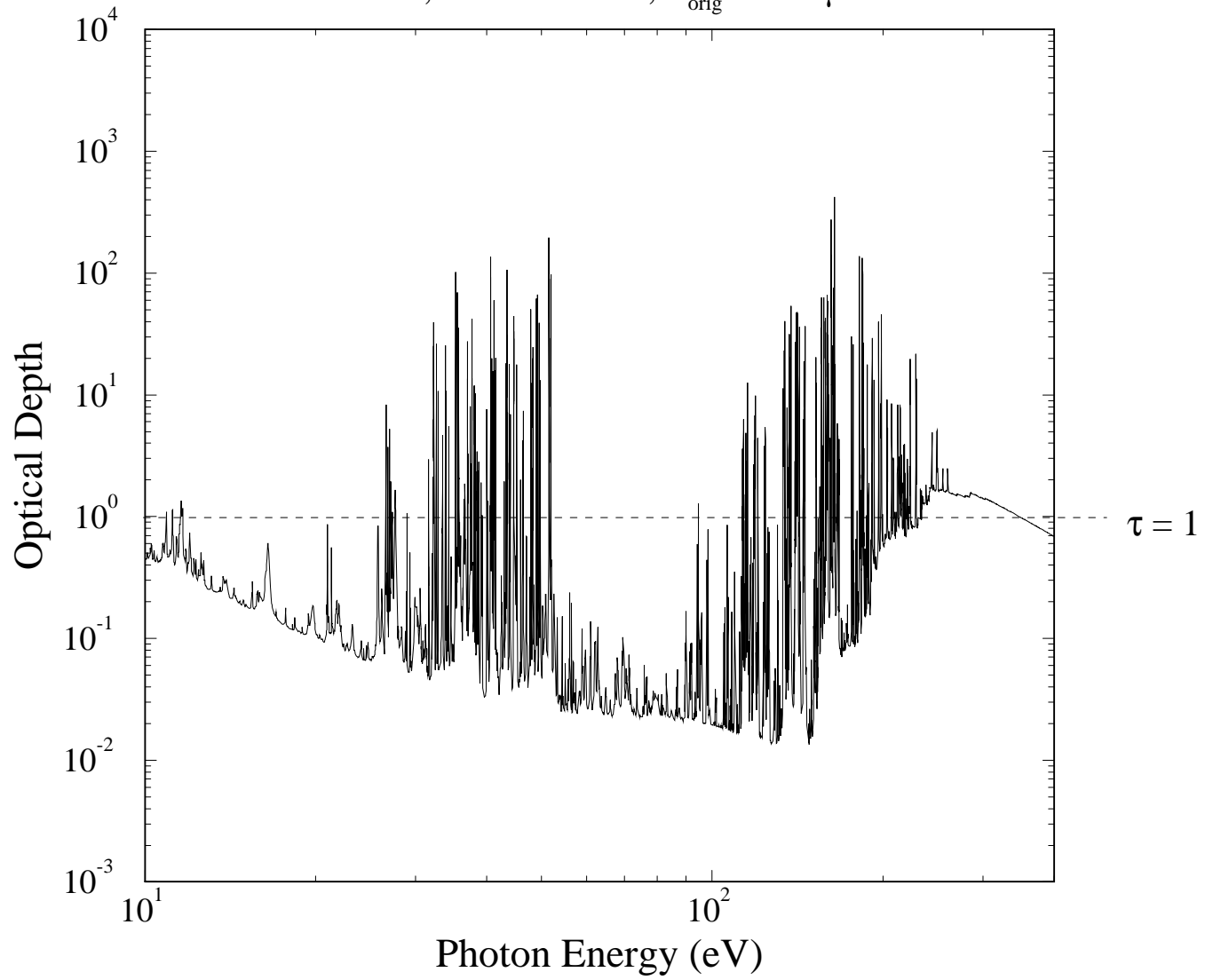


Figure 10.3. Frequency-dependent optical depths for Example 1.

```

$input1
c ...
      isw(5) = 1
c
      imaxse = 200
      errmxfl = 1.e-4
c ...
      isw(6) = 1
c ...
      iplot(1) = 3
      iplot(8) = 1, 1,
c ...
      hvmin = 1.
      hvmax = 10000.
      nflines = 11
      nfrqff = 100
c ...
      igeom = 3
      nzones = 40
      radmin = 0.
      radmax = 6.496e-3
      dradmn = 5.e-8
c ...
      tempel(1) = 40*300.
      densnn(1) = 40*0.8958e20
c ...
      ireada(1) = 1
      atomnm = 13.
      atomwt = 27.
      ilinep = 1
c ...
c Al XIII H-like
      iselct(1362,1) = 2*1
c
$end

```

RADIATIVE TRANSFER PARAMETERS

isw6=1 => start with LTE populations
isw6=2 => start with coronal populations
isw6=3 => set populations to LTE values
isw6=4 => set populations to coronal values

plot file switch (=2 for log-log plots)

SPECTRAL GRID PARAMETERS (energies in eV)

GRID PARAMETERS

TEMPERATURES AND ION DENSITIES

ATOMIC DATA PARAMETERS

SELECT LEVELS

Figure 10.4. Namelist input for Example 2.

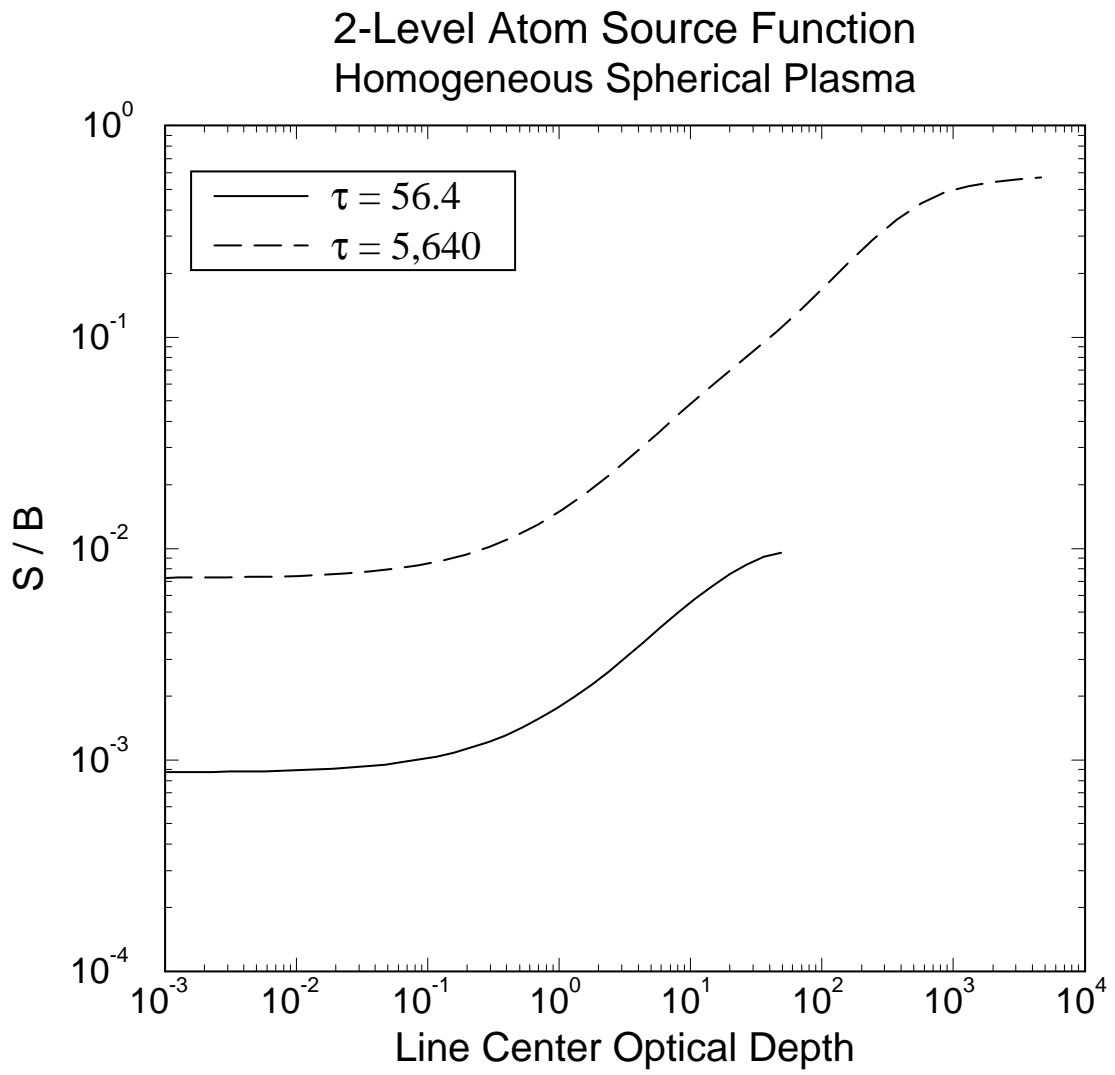


Figure 10.5. Two-level atom source function vs. line center optical depth for Example 2.

```

$input1
c ...
c ... INITIAL POPULATIONS
c ... isw6=1 => start with LTE populations
c ... isw6=2 => start with coronal populations
c ... isw6=3 => set populations to LTE values
c ... isw6=4 => set populations to coronal values
c ... isw(6) = 3
c ... PLOTTING SWITCHES
c ... iplot(1) = 1
c ... iplot(8) = 4, 4
c ... SPECTRAL GRID PARAMETERS (energies in eV)
c ... hvmin = 1480.
c ... hvmax = 1920.
c ... nflines = 3
c ... nfrqff = 1000
c ... GRID PARAMETERS
c ... igeom = 1
c ... nzones = 1
c ... radmin = 0.
c ... radmax = 6.75e-4
c ... dradmn = 2.e-6
c ... TEMPERATURES AND ION DENSITIES
c ... tempel(1) = 1*58.
c ... densnn(1) = 1*4.4e20
c ... ATOMIC DATA PARAMETERS
c ... ireada(1) = 1
c ... atomnm = 13.
c ... atomwt = 27.
c ... ilinep = 3
c ... SELECT LEVELS
c ... thermal states autoionizing states (n=2) autoionizing states (n=3)
c ... -----
c Al I iselct( 1,1) = 0
c Al II iselct( 35,1) = 0
c Al III iselct( 90,1) = 7*1 iselct(147,1) = 20*1
c Al IV Ne-like iselct(167,1) = 15*1
c Al V F-like iselct(301,1) = 28*1 iselct(449,1) = 1*1 iselct(450,1) = 10*1
c Al VI O-like iselct(536,1) = 48*1 iselct(693,1) = 6*1 iselct(699,1) = 10*1
c Al VII N-like iselct(771,1) = 41*1 iselct(845,1) = 16*1 iselct(861,1) = 10*1
c Al VIII C-like iselct(921,1) = 34*1 iselct(967,1) = 30*1 iselct(997,1) = 10*1
c Al IX B-like iselct(1050,1) = 30*1 iselct(1096,1) = 35*1 iselct(1131,1) = 10*1
c Al X Be-like iselct(1152,1) = 30*1 iselct(1197,1) = 30*1 iselct(1227,1) = 10*1
c Al XI Li-like iselct(1269,1) = 6*1 iselct(1287,1) = 17*1 iselct(1303,1) = 10*1
c Al XII He-like iselct(1327,1) = 13*1 iselct(1352,1) = 10*0
c Al XIII H-like iselct(1362,1) = 1
c Al XIV Fully Ionized iselct(1382,1) = 0
$end

```

Figure 10.6. Namelist input for Example 3.

Al K_{α} Absorption Spectrum
 $T = 58 \text{ eV}$, $\rho = 0.02 \text{ g/cm}^{-3}$, $L_0 = 500 \text{ \AA}$

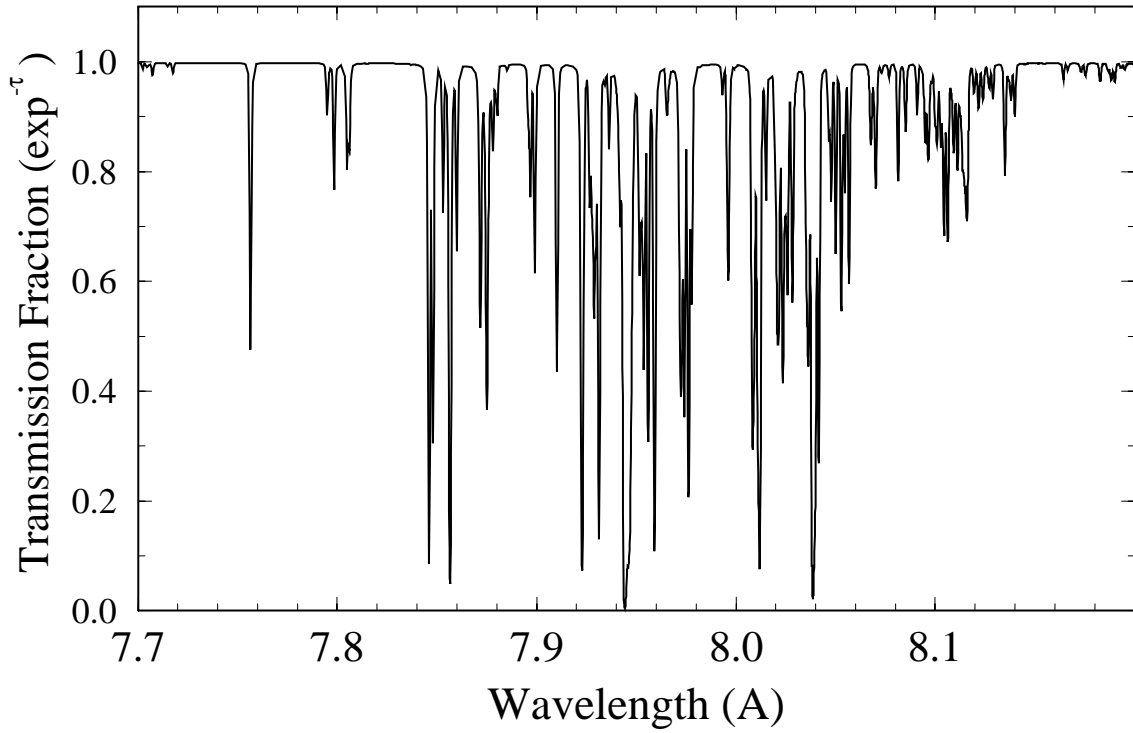


Figure 10.7. Al K_{α} absorption spectrum for Example 3.

Time-Dependent Carbon Recombination Problem

$T = 2 \text{ eV}$, $n = 10^{19} \text{ ions/cm}^3$, Initial state: fully stripped C

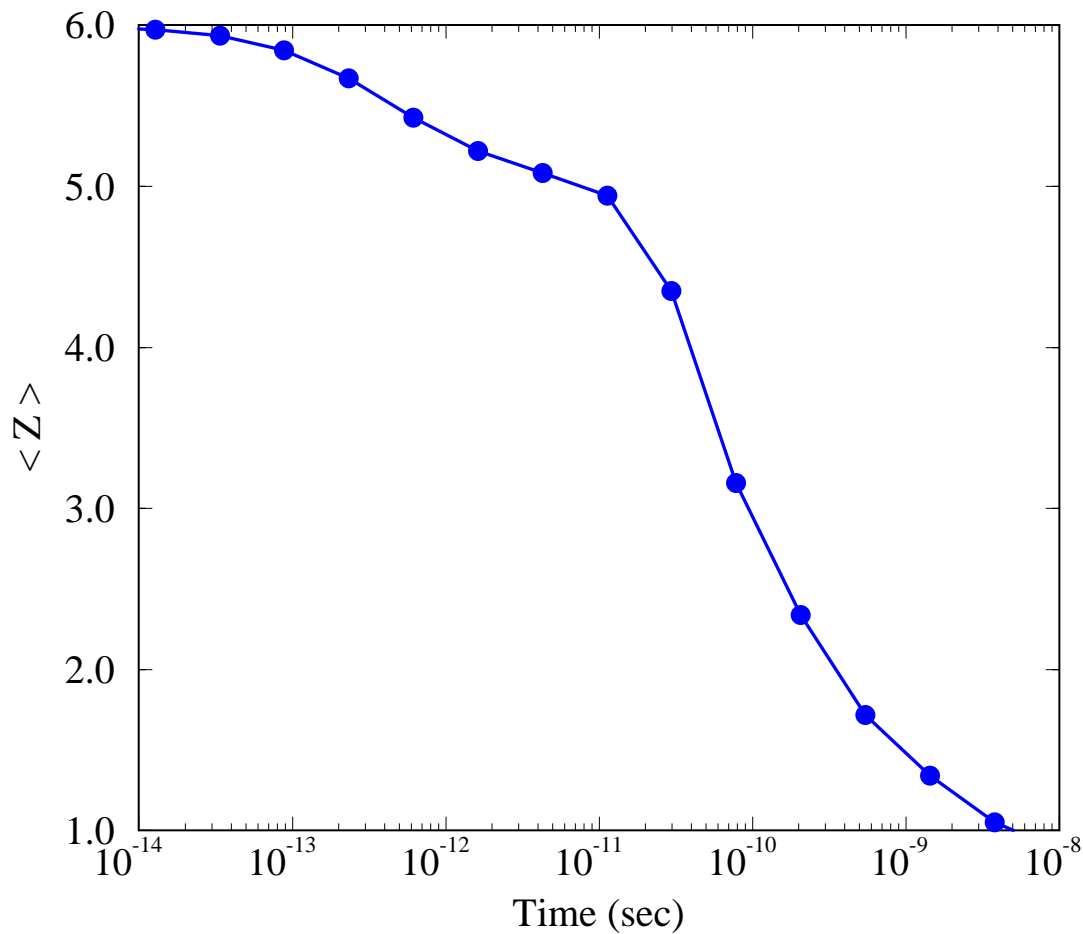


Figure 10.9. Average charge state of carbon versus time for Example 4.

Time-Dependent Collisional-Radiative Simulation
Ar at $T = 2$ eV ; 1% Hot Electrons

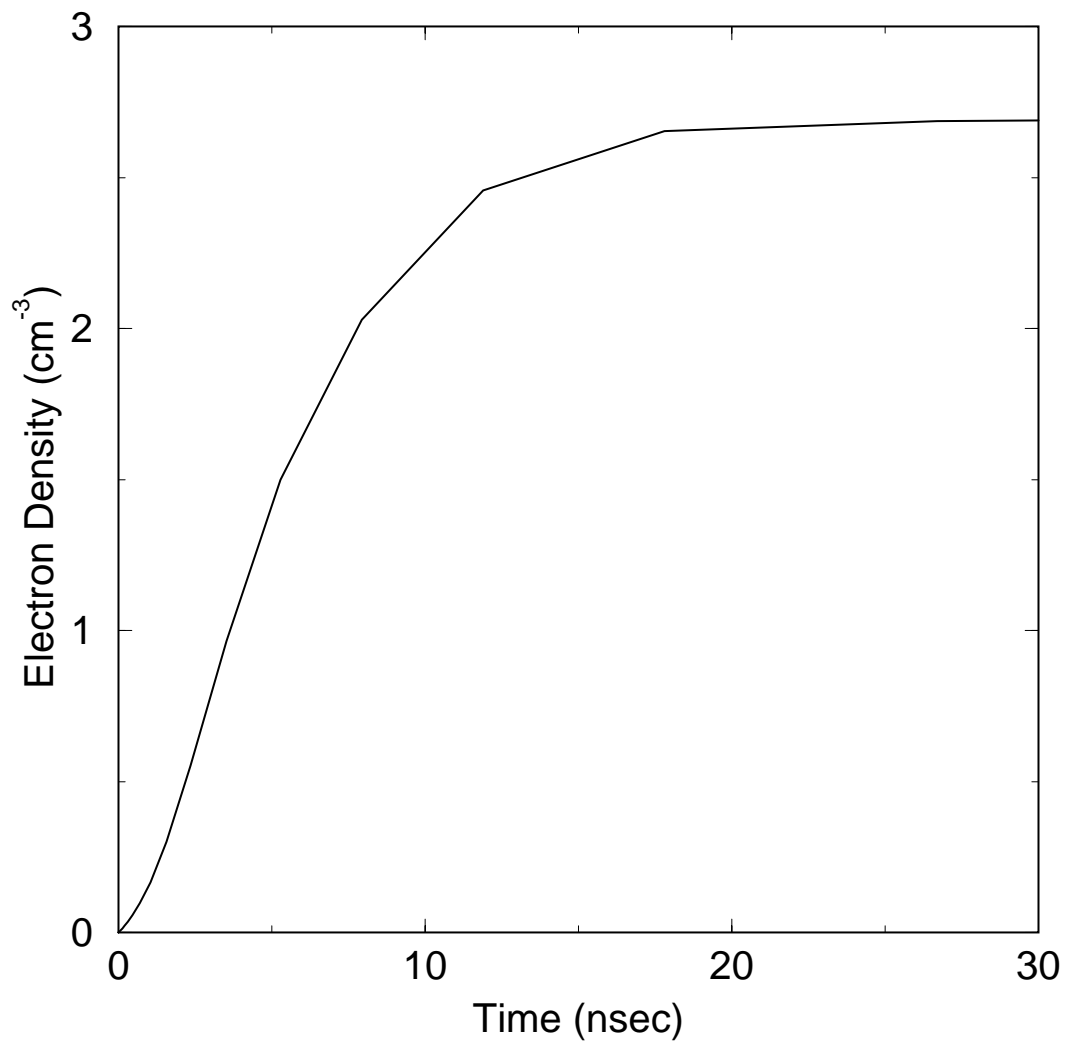


Figure 10.11. Time-dependent electron density for Example 5.

```

$input1
c ... HIGH-Z EOS parameters
      nmatrs = 1
      izeos(1) = 74
      ideos(1) = 3
      idopac(1) = 3
      nfg = 500
      atwmat(1) = 184.
c ... line-of-sight angle for emission spectra calculation;
c use in -spect4- if isw72=1
c if isw72=0, flux (angle-integrated) is computed
      isw(72) = 1
      xmulos = 1.
c ... use new RT model if isw(2) = 1
      isw(2) = 0
c ... SPECTRAL GRID PARAMETERS (energies in eV)
      hvmin = 0.1
      hvmax = 1.e4
      nfrqff = 1000
      nfline = 6
c ... line freq grid params
      con(61) = 1.e-2
      bandwd = 1.e2
      nfcore = 4
      bwcore = 4.
c ... ZONING SCHEME
      isw(44) = 0
      isw(15) = 1
c ... isw16<>0=> do NOT print out trans. table (save space)
      isw(16) = 1
c ... if isw61<>0 compute ELECTRON CAPTURE rate from autoiz rate
      isw(61) = 1
c ... start with LTE (isw(6)=1) or cor. pops
c 1 => start with LTE
c 3 => start & finish with LTE
      isw(6) = 3
c ... thick (isw7=0) or thin (isw7=1) for b-b
c ... thick (isw8=0) or thin (isw8=1) for b-f
      isw(7) = 0, 0
c ... plot file switch (=2 for log-log plots)
c *****
      iplot(1) = 5
      iplot(8) = 5, 6
c *****
c ... iplot5=1 => optical depth contour plot
      iplot(5) = 1
c
c ... GRID PARAMETERS
      igeom = 2
      radmin = 0.
c
c ... min. T for NLTE populations
      con(89) = 0.3
c ... min. T for NLTE populations
      telte = 10.
c
c ... print out P_Q, a_voigt for zone "izonpq"
      izonpq = 8
c
      nzones = 12
      nregns = 2
c
c ... NOTE: flux computed at IZON = NZONES
      nzonrg(1) = 6, 6
c
      tempel(1) = 6*100., 6*100.
      densnn(1) = 6*2.e20, 6*2.e20
      fracsp(1,1) = 6*0.33, 6*1.e-10
      fracsp(1,2) = 6*0.67, 6*1.e-10
c
      ihighz(1) = 6*0, 6*1
c
c ... Region masses in g/cm (cyl geom)
c
c ... SiO2 foam: 6.28e-4 g/cm (5 mg/cc at R=.2)
c ... W wires: 4.70e-4 g/cm
      regmas(1) = 6.28e-4, 4.70e-4
      regdml(1) = 0.3e-4, 0.1e-4
c
c ... ATOMIC DATA PARAMETERS
      ngases = 2
c ... use NEW atomic data files (post-Mar. 1995) if ireada=1
      ireada(1) = 1, 1
      atomnm(1) = 14., 8.
      atomwt(1) = 28., 16.
      ilinep = 3
c
c ... =====
c ... SELECT LEVELS FOR SILICON
c ... =====
      iselct( 1,1) = 1
      :
      :
c
c ... =====
c ... SELECT LEVELS FOR OXYGEN
c ... =====
      iselct( 1,2) = 1
      :
      :
$end

```

Figure 10.12. Namelist input for Example 6.

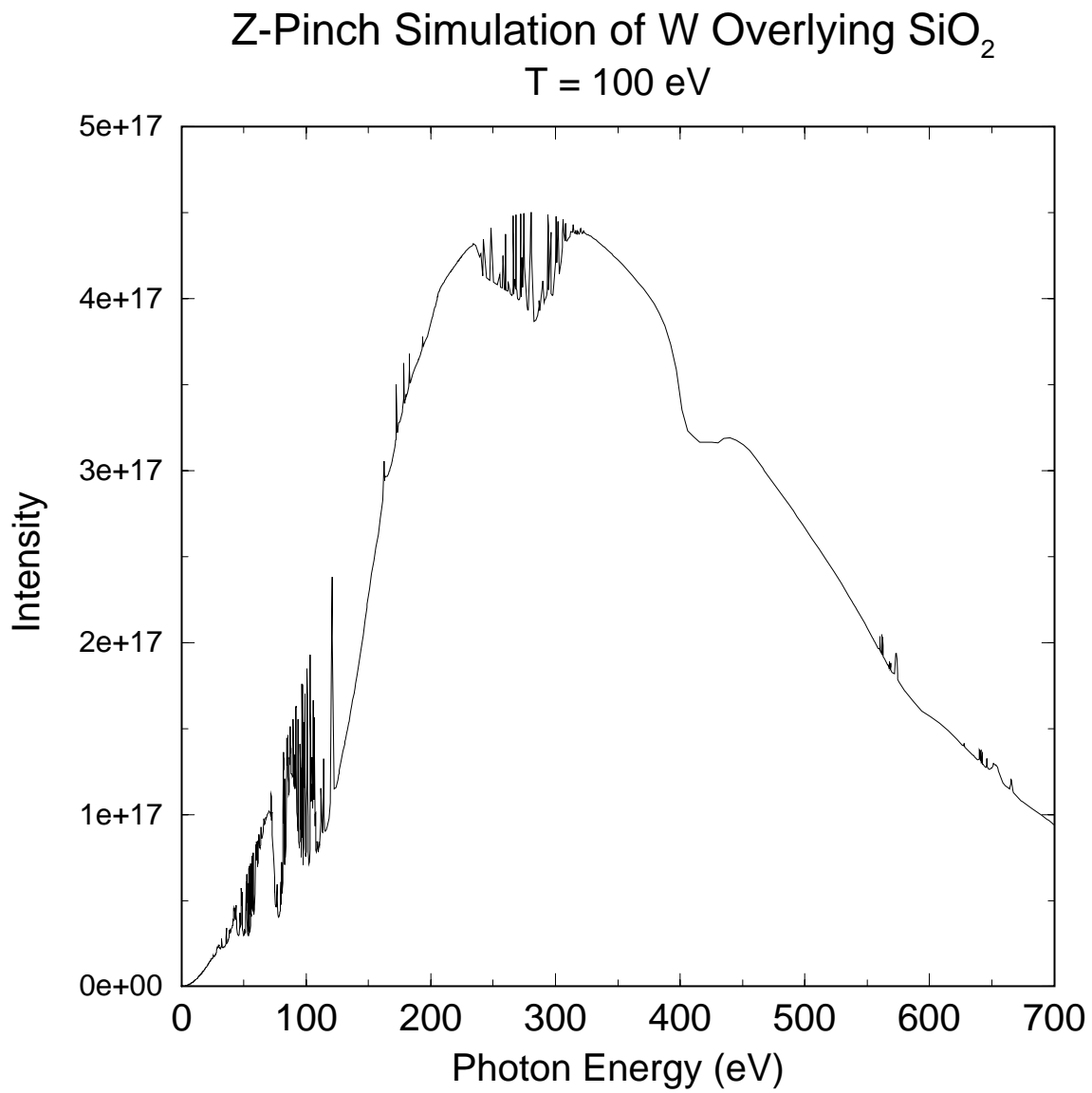


Figure 10.13. W/SiO₂ emission spectrum for Example 6.

Optical Depths for W and SiO₂ Regions

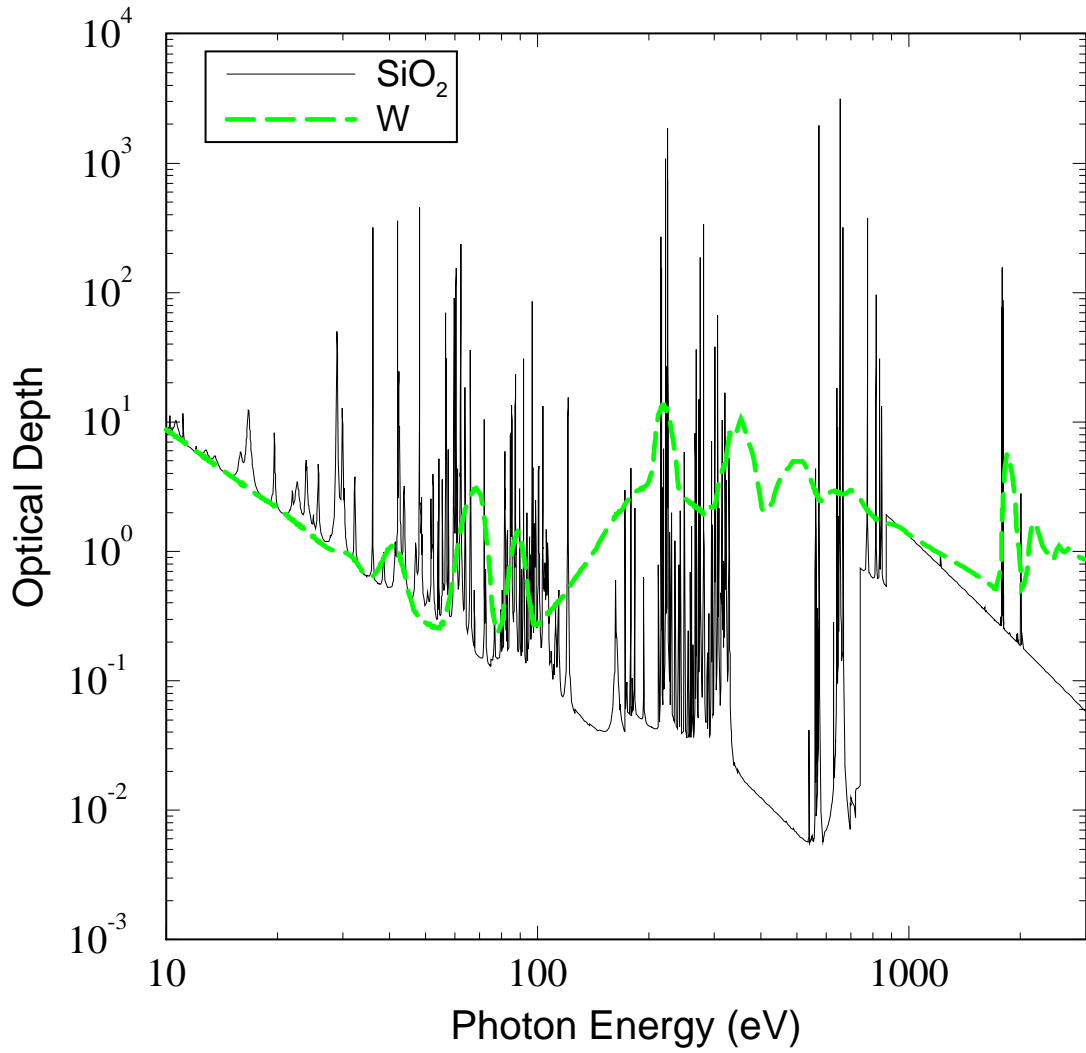


Figure 10.14. W region and SiO₂ region optical depths for Example 6.

```

$input1
c ...
c NEW GRIDDING SCHEME
c isw44<0 => interpolate hydro data by mass
c isw15=0 and isw44<>-1 => use -zoner- zoning
c isw(44) = -1
c isw(15) = 0
c if isw46<>0, compute flux at lowest index hydro zone
c isw(46) = 0
c HYDRO FILE
c fnames(45) = 'bk.CRE.5851_area_A.Jmult_1.50.Final'
c HYDRO TIME
c con(90) = 20.
c ... isw16<>0=> do NOT print out trans. table (save space)
c isw(16) = 1
c ionization windowing
c ...
c con(57) = 0.005
c con(58) = 2000.
c ...
c ***
c isw(6) = 1
c ***
c BEAM PARAMETERS
c -----
c ... consider ion-impact ioniz. if isw37 > 0
c isw(37) = 3
c izbeam = 3
c istgbm = 4
c ...
c RADIATIVE TRANSFER MODEL OPTIONS
c -----
c radiation field-dependent rates can include the
c effects of overlapping transitions and an external
c radiation field.
c ... if isw(2)=1 and isw(19)=0, both photoexcitation and
c photoionization are computed using this model
c if isw(2)=0, both photoexcitation and photoionization are
c computed in -rrates- (EP)
c if isw(2)=1 and isw(19)=1, photoionization is
c computed using this model; photoexcitation is
c computed using the EP model
c isw(2) = 1
c isw(19) = 1
c ... T_rad at boundaries (tradbm is on "drive" side)
c tradbl = 0.
c tradbn = 0.
c nfrqfr = 100
c if isw29.ne.0 do not add hv pts at b-f edges for rrate2
c isw(29) = 1
c hvminr = 1.
c hvmaxr = 1000.
c ... thick (isw7=0) or thin (isw7=1) for b-b
c ... thick (isw8=0) or thin (isw8=1) for b-f
c isw(7) = 0, 0
c if isw5=1, use multifreq. RT model
c isw(5) = 0
c PARAMETERS FOR PLOTTING SPECTRA
c -----
c ... plot file switch
c iplot(1) = 4
c iplot(8) = 4, 4
c ... line-of-sight angle for emission spectra calculation;
c use in -spect4- if isw72=1
c isw(72) = 1
c xmulos = 0.5
c ... spectral grid parameters (energies in eV)
c hvmin = 1480.
c hvmax = 2000.
c nfln = 3
c nfrqff = 1000
c ... line freq grid params
c (add only 1 freq-pt if osc str < con61)
c con(61) = 1.e-2
c nfln = 3
c bandwd = 5.
c nfcors = 3
c bwcore = 5.
c ... CONVERGENCE PARAMETERS
c -----
c imaxse = 40
c errmxf = 1.e-3
c ngordr = 2
c ngcycl = 4
c con(7) = 0.
c ... SPATIAL GRID PARAMETERS
c -----
c igeom = 1
c radmin = 0.
c nzones = 4
c nregns = 1
c nzonrg(1) = 4
c regmas(1) = 0.513e-4
c regdml(1) = 0.1e-4
c ... fracsp(1,1) = 4*1.
c NOTE: flux computed at IZON = NZONES
c print out P_Q, a_voigt for zone "izonpq"
c izonpq = 1
c ... ATOMIC DATA PARAMETERS
c -----
c ngases = 1
c use NEW atomic data files (post-Mar. 1995) if ireada=1

```

Figure 10.15. Namelist input for Example 7.

```

        ireada(1) = 1
        atommm(1) = 13.
        atomwt(1) = 27.
        ilinep = 3
c ...
c                                     SELECT LEVELS
c ... thermal states          exc.d states to n=2  exc.d states to n=3 (spectator in M-shell)
c -----
c Al I
c   iselct( 1,1) = 1
c Al II
c   iselct( 35,1) = 1
c Al III
c   iselct( 90,1) = 7*1
c Al IV   Ne-like
c   iselct(167,1) = 15*1
c   n=4
c     iselct(182,1) = 32*0
c   double M-shell
c     iselct(214,1) = 5*1
c   triple M-shell
c     iselct(219,1) = 5*1
c                                     iselct(253,1) = 28*1
c Al V     F-like
c   iselct(301,1) = 28*1
c   n=4
c     iselct(329,1) = 10*0
c   double M-shell
c     iselct(408,1) = 10*1
c                                     iselct(449,1) = 1*1
c                                     iselct(450,1) = 0
c   double M-shell
c                                     iselct(474,1) = 0
c   triple M-shell
c                                     iselct(481,1) = 0
c Al VI    O-like
c   iselct(536,1) = 30*1
c   n=4
c     iselct(586,1) = 98*0
c   double M-shell
c     iselct(684,1) = 9*1
c                                     iselct(693,1) = 6*1
c                                     iselct(699,1) = 0
c   double M-shell
c                                     iselct(757,1) = 0
c Al VII   N-like
c   iselct(771,1) = 30*1
c   n=4
c     iselct(812,1) = 33*0
c                                     iselct(845,1) = 16*1
c                                     iselct(861,1) = 0
c Al VIII  C-like
c   iselct(921,1) = 34*1
c   n=4
c     iselct(955,1) = 12*0
c                                     iselct(967,1) = 30*1
c                                     iselct(997,1) = 0
c Al IX    B-like
c   iselct(1050,1) = 30*1
c   n=4
c     iselct(1080,1) = 16*0
c                                     iselct(1096,1) = 35*1
c                                     iselct(1131,1) = 0
c Al X     Be-like
c   iselct(1152,1) = 30*1
c   n=4
c     iselct(1182,1) = 15*0
c                                     iselct(1197,1) = 30*1
c                                     iselct(1227,1) = 0
c Al XI    Li-like
c   iselct(1269,1) = 6*1
c   n=4
c     iselct(1275,1) = 12*0
c                                     iselct(1287,1) = 17*1
c                                     iselct(1303,1) = 0
c Al XII   He-like
c   iselct(1327,1) = 13*1
c   n=4
c     iselct(1340,1) = 12*0
c                                     iselct(1352,1) = 10*0
c Al XIII  H-like
c   iselct(1362,1) = 1
c Al XIV   Fully Ionized
c   iselct(1382,1) = 0
$end

```

Figure 10.15. Namelist input for Example 7 (continued).

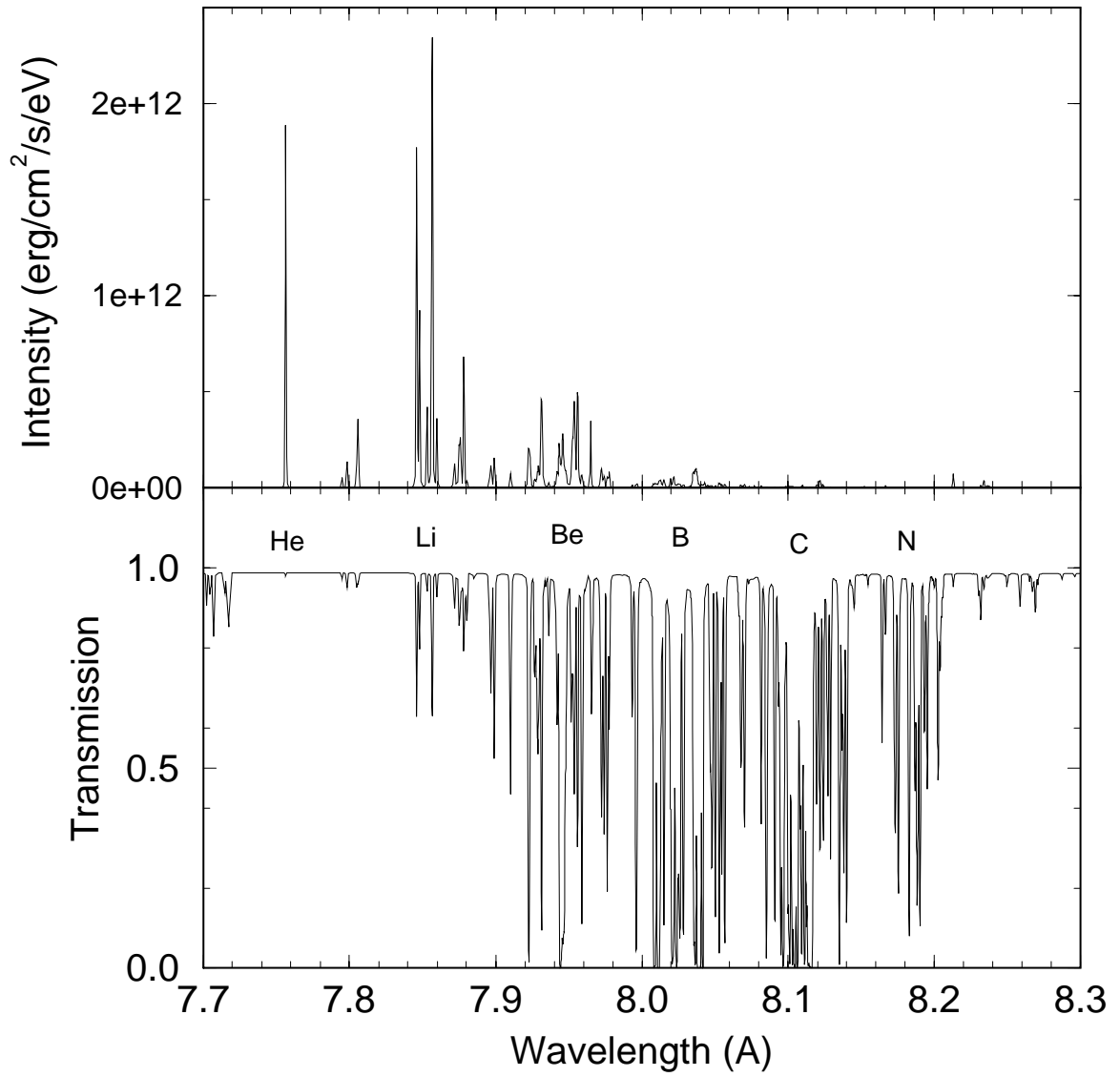


Figure 10.16. Al K_{α} satellite emission and absorption spectra based on radiation-hydrodynamics output (Example 7).

Acknowledgments

This work has been supported by Forschungszentrum Karlsruhe through Fusion Power Associates.

References

- [1] A. Hauer, R.D. Cowan, B. Yaakobi, O. Barnouin, and R. Epstein, *Phys. Rev. A* **34**, 411 (1986).
- [2] C. Chenais-Popovics, C. Fievet, J.P. Geindre, J.C. Gauthier, E. Luc-Koenig, J.F. Wyart, H. Pepin, and M. Chaker, *Phys. Rev. A* **40**, 3194 (1989).
- [3] J. Bruneau, C. Chenais-Opoovics, D. Desenne, J.-C. Gauthier, J.-P. Geindre, M. Klapisch, J.-P. Le Breton, M. Louis-Jacquet, D. Naccache, and J.-P. Perrine, *Phys. Rev. Lett. Phys. Rev. Lett.* **65**, 1435 (1990).
- [4] S.J. Davidson, J.M. Foster, C.C. Smith, K.A. Warbutron, and S.J. Rose, *Appl. Phys. Lett.* **52**, 847 (1988).
- [5] D.M. O'Neil, C.L.S. Lewis, D. Neely, and S.J. Davidson, *Phys. Rev. A* **44**, 2641 (1991).
- [6] J. Abdallah, Jr., R.E.H. Clark, and J.M. Peek, *Phys. Rev. A* **44**, 4072 (1991).
- [7] T.S. Perry, S.J. Davidson, F.J.D. Serduke, D.R. Bach, C.C. Smith, J.M. Foster, R.J. Doyas, R.A. Ward, C.A. Iglesias, F.J. Rogers, J. Abdallah, Jr., R.E. Steward, J.D. Kilkenny, and R.W. Lee, *Phys. Rev. Lett.* **67**, 3784 (1991).
- [8] T. S. Perry, et al., *J.Q.S.R.T.* **54**, 317 (1995).
- [9] T.S. Perry, et al., *Phys. Rev. E* **54**, 5617 (1996).
- [10] C.J. Keane, B.A. Hammel, D.R. Kania, J.D. Kilkenny, R.W. Lee, A.L. Osterheld, L.J. Suter, R.C. Mancini, C.F. Hooper, and N.D. Delameter, *Phys. Fluids B* **5**, 3328 (1993).
- [11] D. Duston and J. Davis, *Phys. Rev. A* **21**, 1664 (1980).
- [12] A. Demir, et al., *Phys. Rev. E* **55**, 1827 (1997).
- [13] T.J. Nash, et al., *Rev. Sci. Instrum.* **68**, 1083 (1997).

- [14] J. J. MacFarlane, et al., *Rev. Sci. Instrum.* **68**, 1069 (1997).
- [15] J. Bailey, A.L. Carlson, G. Chandler, M.S. Derzon, R.J. Dukart, B.A. Hammel, D.J. Johnson, R.R. Lockner, J. Maenchen, E.J. McGuire, T.A. Mehlhorn, W.E. Nelson, L.E. Ruggles, W.A. Stygar, and D.F. Wenger, *Lasers Part. Beams* **8**, 555 (1990).
- [16] J. Bailey, 6th International Workshop on Atomic Physics for Ion-Driven Fusion, Santa Fe, NM, November 1993.
- [17] J.J. MacFarlane, P. Wang, J. Bailey, T.A. Mehlhorn, R.J. Dukart, and R.C. Mancini, *Phys. Rev.* **E 47**, 2748 (1993).
- [18] J.J. MacFarlane, P. Wang, T.A. Mehlhorn, J. Bailey, and R.J. Dukart, *Rev. Sci. Instrum.* **63**, 5062 (1992).
- [19] J.J. MacFarlane, P. Wang, J.E. Bailey and T.A. Mehlhorn, submitted to *Phys. Rev. E* (1997).
- [20] J.J. MacFarlane, P. Wang, and G.A. Moses, Fusion Power Associates Report FPA-90-1, January 1990.
- [21] J.J. MacFarlane, P. Wang, and D.L. Henderson, Fusion Power Associates Report FPA-91-1, January 1991.
- [22] J.J. MacFarlane, P. Wang, and D.L. Henderson, Fusion Power Associates Report FPA-92-1, January 1992.
- [23] J.J. MacFarlane, P. Wang, D.L. Henderson, and O. Yasar, Fusion Power Associates Report FPA-93-1, January 1993.
- [24] P. Wang, ATBASE Users' Guide, Fusion Power Associates Report FPA-93-7, December 1993.
- [25] D.G. Hummer, *J.Q.S.R.T.* **36**, 1 (1986).
- [26] D.G. Hummer and D. Mihalas, *Astrophys. J.* **331**, 794 (1988).
- [27] G.L. Olson and P.B. Kunasz, *J.Q.S.R.T.* **38**, 325 (1987).
- [28] P. WANG, "EOSOPA — A Code for Computing the Equations of State and Opacities of High Temperature Plasmas with Detailed Atomic Models," University of Wisconsin Fusion Technology Institute Report UWFD-933, December 1993.

- [29] P. Wang, J.J. MacFarlane and T.J. Orzechowski, *Rev. Sci. Instrum.* **68**, 1107 (1997).
- [30] E. Anderson et al., LAPACK Users' Guide (SIAM, Philadelphia, 1992).
- [31] K. Werner and D. Husfield, *Astron. Astrophys.* **148**, 417 (1985).
- [32] J.J. MacFarlane, *Astron. Astrophys.* **264**, 153 (1992).
- [33] K.C. Ng, *J. Chem. Phys.* **61**, 2680 (1974).
- [34] L. Auer, in Numerical Radiative Transfer, edited by W. Kalkoten, Cambridge University Press, Cambridge, U.K. (1987), p. 101.
- [35] A.C. Hindmarsh, "LSODE and LSODI, Two-Initial Value Ordinary Differential Equation Solvers," ACM SIG NUM Newsletter, Vol. 15, No. 4, 10 (1980).
- [36] J.P. Apruzese, J. Davis, D. Duston, and K.G. Whitney, *J.Q.S.R.T.* **23**, 479 (1980).
- [37] J.P. Apruzese, *J.Q.S.R.T.* **25**, 419 (1981).
- [38] J.P. Apruzese, *J.Q.S.R.T.* **34**, 447 (1985).
- [39] D. Mihalas, Stellar Atmospheres, Second Edition, Freeman and Company, New York (1978).
- [40] W.J. Karzus and R. Latter, *Ap. J. Suppl. Ser.* **6**, 167 (1961).
- [41] G.B. Rybicki and D.G. Hummer, *Astron. Astrophys.* **245**, 171 (1991).
- [42] M. Abramowitz and I.A. Stegun, Handbook of Mathematical Functions, Dover Press, New York (1972).
- [43] D. Mihalas, P.B. Kunacz, and D.G. Hummer, *Astrophys. J.* **202**, 465 (1975).
- [44] P. Wang, Ph.D. Dissertation, Dept. of Nuclear Engineering and Engineering Physics, University of Wisconsin, Madison, WI (1991).
- [45] A. Burgess and M.C. Chidichimo, *Mon. Not. R. Astron. Soc.* **203**, 1269 (1983).
- [46] M.J. Seaton, in Atomic and Molecular Processes, edited by D.R. Bates, Academic, New York (1962) p. 374.
- [47] I.I. Sobelman, L.A. Vainshtein, and E.A. Yukov, Excitation of Atoms and Broadening of Spectral Lines, Springer-Verlag, New York (1981).

- [48] D.E. Post, R.V. Jensen, C.B. Tarter, W.H. Grasberger, and W.A. Lokke, *At. Data Nucl. Data Tables* **20**, 397 (1977).
- [49] E. Merzbacher and H.W. Lewis, in Corpuscles and Radiation in Matter II, edited by S. Flugge, *Handbuch der Physik*, Vol. 34, Springer-Verlag, Berlin (1958).
- [50] P. Wang, J.J. MacFarlane, and G. Moses, *Laser Part. Beams* **13**, 191 (1995).
- [51] D.A. Leiberman, D.T. Cromer, and J.T. Waber, *Comput. Phys. Commun.* **2**, 107 (1971).
- [52] D.H. Sampson, H.L. Zhang, A.K. Mohanty, and R.E. Clark, *Phys. Rev. A* **40**, 604 (1989).
- [53] J.J. MacFarlane, G.A. Moses, and R.R. Peterson, “BUCKY-1 — A 1-D Radiation-Hydrodynamics Code for Simulating Inertial Confinement Fusion High Energy Density Plasmas,” University of Wisconsin Fusion Technology Institute Report UWFD-984, August 1995.
- [54] D.R. Welch, C.L. Olson, and T. Sanford, *Phys. Plasmas* **1**, 763 (1994).
- [55] H.K. Chung, J.J. MacFarlane, P. Wang, G.A. Moses, J.E. Bailey, C.L. Olson, and D.R. Welch, *Rev. Sci. Instrum.* **68**, 350 (1997).
- [56] P.B. Kunacz and D.G. Hummer, *Mon. Not. Royal Astr. Soc.* **166**, 19 (1974).
- [57] G. Athay, Radiation Transport in Spectral Lines, Reidel Publishing, Dordrecht (1972).
- [58] D.G. Hummer, *Mon. Not. Royal Astr. Soc.* **138**, 73 (1968).